Artificial Muscle Technology Applied Towards Treating Ischemic Mitral Regurgitation Caused by Left Ventricular Remodeling

By

Nicaulas A. Sabourin

Bachelor's of Science, Biomedical Physics, Laurentian University, 1999
Bachelor's of Applied Science, Electrical Engineering, University of Ottawa, 2002

Submitted to the Department of Mechanical Engineering in Partial Fulfillment of the Requirements for the Degree of

Master of Science

at the

MASSACHUSETTS INSTITUTE OF TECHNOLOGY

June 2004

Signature of Author: .....

Department of Mechanical Engineering
May 7th, 2004

Certified by: .....

Ian W. Hunter
Hatsopoulos Professor of Mechanical Engineering and Professor of Biological Engineering
Thesis Supervisor

Accepted by: .....

Ain A. Sonin
Professor of Mechanical Engineering
Chairman, Department Committee on Graduate Students

Artificial Muscle Technology Applied Towards Treating Ischemic Mitral Regurgitation Caused by Left Ventricular Remodeling

By

NICAULAS A. SABOURIN

Submitted to the Department of Mechanical Engineering on
May7th, 2004 in Partial Fulfillment of the Requirements
for the Degree of Master of Science

Abstract

Ischemic Mitral Regurgitation (MR) affects a large portion of patients suffering from ischemic heart disease. Significant MR develops in one quarter to one third of patients who suffer from ischemic heart disease and doubles their late mortality rate after a myocardial infarction or revascularization. MR is most often caused by the bulging, or remodeling, of the heart's left ventricle. This remodeling displaces the papillary muscles inside of the ventricle and tethers the mitral valve, preventing it from closing properly. Current treatments attempt to either repair or replace the valve. These treatments require the heart be stopped and the patient be placed on a cardiopulmonary bypass pump for many hours. Both treatment approaches have serious side-effects, including relapse of the MR as quickly as six months post-operatively.

This thesis concerns the development of an active artificial muscle patch (AMP) for application to the exterior of the heart. The AMP constructively remodels the heart in order to alleviate MR. Two in-vivo experiments were conducted with a heart-gated fluid pumping apparatus connected to a balloon patch that successfully proofed the concept that an active patch can relieve MR. These experiments also established data on the mechanical requirements of such a patch. An in-vitro heart model was created to test iterations of AMP devices before undergoing further in-vivo studies. Development of an AMP using Nickel-Titanium shape memory alloy was begun and iterations of this device have had early success in in-vitro tests.

Thesis Supervisor: Ian W. Hunter
Title: Hatsopoulos Professor of Mechanical Engineering and Professor of Biological Engineering

Acknowledgements

I would first like to thank Professor Ian Hunter for giving me the opportunity to work in the Bioinstrumentation Laboratory and for creating a research atmosphere that encourages the mind to overcome its limits.

I would like to thank all of my colleagues in the Bioinstrumentation Laboratory for their help, guidance and input. Special thanks go to Patrick Anquetil and Peter Madden for sharing their experience with me, to Bryan Crane for helping me learn how to machine and to Michael Garcia-Webb for his help with programming.

I would like to thank our collaborators from the Cardiac Ultrasound Laboratory at Massachusetts General Hospital, especially Dr. Robert Levine, Dr. Judy Hung and Dr. Mordehay Vatury. Their input over the course of my research and the opportunity that I had to participate in the in-vivo procedures was invaluable. I also extend thanks to the NIH and CIMIT for their generous support of this research.

Many thanks go to the Fondation Baxter & Alma Ricard, most especially to the late Madame Alma Ricard. Her generosity is without measure and her contributions to the academic achievements of students such as myself is an incredible legacy.

I would like to thank Dr. Anny Usheva of Harvard Medical School who helped shape my approach to research and pushed me to both sharpen and broaden my skills as a researcher.

Many thanks go to Jennifer Johnson whose company made the many long hours and late nights spent on this document more enjoyable and whose assistance, both technical and otherwise, was invaluable.

I would also like to thank Tintin for always being there to help me unwind and enjoy the simple pleasures in life.

Above all, I'd like to thank my parents. Merci beaucoup pour votre support et patience. Je ne serais pas ici sans vous.

Table of Contents

List of Figures

List of Tables

1 Introduction

1.1 Addressing Problems of Heart Disease: The Case of Ischemic Mitral Regurgitation

Ischemic mitral regurgitation (MR) is a common complication of ischemic heart disease. A patient suffering from ischemic heart disease will often develop a region of weakened tissue where the heart is deprived of oxygen. This weakened area tends to bulge outwards under normal bio-mechanical stress. When this bulging area is located on the left ventricle (LV), the papillary muscles (PM) on the LV's endocardium are displaced and will often tether the leaflets of the mitral valve, preventing them from coapting and causing regurgitation back into the left atrium (LA)[1]. The physiology of the mitral valve is shown in Figure 1. This process of LV remodeling can lead to serious complications. Significant MR develops in one quarter to one third of patients who suffer from ischemic heart disease and doubles their late mortality rate after a myocardial infarction or revascularization[2,3,4].

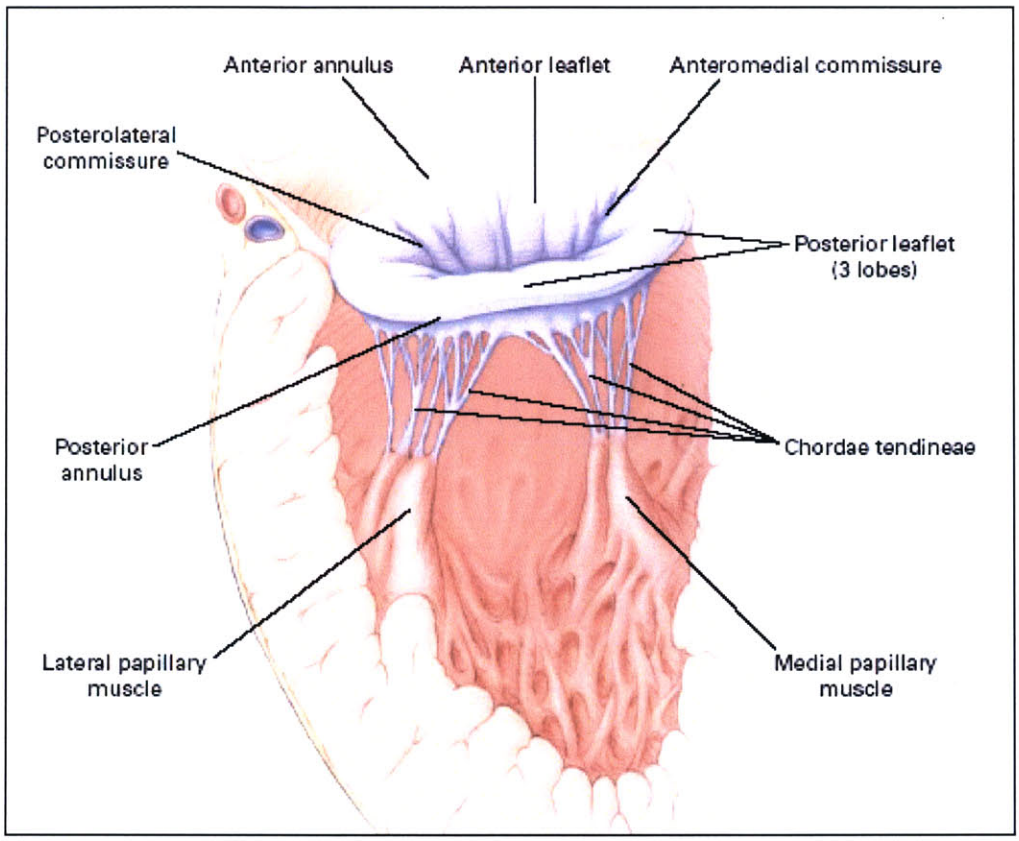

Figure 1: The mitral valve.[1]

Figure 2 shows an image taken with an echocardiograph of a sheep suffering from MR.[2] The echocardiograph assigns colors to blood flow vectors. In Figure 2, the red color indicates a flow towards the echo probe while a blue color indicates a flow away from the probe. This makes it very easy to visualize any backflow through the mitral valve. The tenting of the valve's leaflets caused by PM displacement can also be seen.

[1] Illustration source: [5].

[2] Echocardiography is the staple observation technique for MR.

Figure 2: Echocardiograph of MR in a sheep's heart[1].

1.2 Current Approaches to Treatment

Approximately 18,000 patients have mitral valve surgery per year[5]. The current treatments for MR are mitral ring annuloplasty or mitral valve replacement. Mitral ring annuloplasty involves installing an oval plastic ring around the mitral annulus.[3] This plastic ring has an outer diameter slightly smaller than that of the valve. By suturing the annulus to this ring, the annulus is reduced in size, bringing the valve's leaflets closer together which allows them to coapt and prevent further MR. The problem with this treatment is two-fold. First, any valve surgery is both major and relatively high risk. During surgery, the heart must be stopped and the patient must be placed on a cardiopulmonary bypass pump[4] for several hours (average valve

[3] Mitral valve's base.

[4] Referred to as being placed "on-pump." The cardiopulmonary bypass pump oxygenates the blood and provides blood flow throughout the body to keep the body alive while the operation is on-going.

repair surgery duration is four hours)[6]. Most importantly however, MR often recurs within a year if LV remodeling persists[7,8,9,10].

Mitral valve replacement involves replacing the entire valve with a mechanical or xeno-biological[5] substitute. To treat ischemic MR, a mechanical valve is generally used since the new valve can function independently of any remodeling of the LV. Major drawbacks of this procedure are that it also requires the patient to be placed on a cardiopulmonary bypass pump during the surgery. There are also long-term drawbacks such as the patient needing to take anti-coagulant medication for life to prevent blood clots forming in and around the new valve[11]. Both of these procedures are targeted towards the symptoms of ischemic MR. Both disregard the fact that the mitral valve itself is almost always in excellent health. It is simply being tethered open by PMs displaced due to ventricular remodeling.

1.3 Proposed New Treatment

A new approach to MR treatment would be a major contribution to this field of research. Experiments performed at the Cardiac Ultrasound Laboratory at the Massachusetts General Hospital (MGH) point to a new type of therapy for LV remodeling[1]. The idea of correcting ventricular remodeling with the application of an external mechanical device was tested. A Dacron[6] mesh was sutured onto a sheep's LV and a balloon was inserted under the mesh. The balloon was then filled with water, creating an indentation in the LV at the location of the PMs. This realigned the PMs with the mitral valve which allowed it to close more completely and had

[5] Usually a pig's or cow's valve is used as a replacement.

[6] Dacron is a brand of polyester fiber with high tensile strength, and is resistant to stretching and degradation by chemicals or abrasion.

a significant impact on MR. The problem with this static mechanical solution is that it increases the stiffness of the LV wall and also reduces the LV's blood intake volume. This countered some of the improvement in overall heart-pumping efficiency achieved by the MR reduction.

The MGH experiments highlight the need for an active device to compensate for pumping inefficiencies due to MR. Ideally an active mechanical device on the heart's epicardium would be able to create an indentation to displace the PMs during cardiac systole and then retract during diastole so as not to obstruct the LV's inflation. The ultimate goal would be to create a "patch" made from an artificial muscle technology. Such a patch could be applied directly to the epicardium and would both relieve MR and also increase the pumping force that a damaged LV can generate.

1.4 Study Purpose and Scope

This thesis presents the design and early development of an artificial muscle patch (AMP) device to treat MR. Chapter 2 covers the development of an AMP simulation device designed for use during a series of in-vivo experiments to proof the concept of an AMP. Data gathered during these experiments concerning the pressure and motion requirements of an AMP device is also presented. Chapter 3 discusses the development of an in-vitro model to test present and future AMP device iterations. Chapter 4 covers the development of an AMP device based on shape memory alloy, an artificial muscle technology. The final chapter summarizes progress made toward AMP development and discusses future possibilities for research in this area.

2 AMP Device Simulation

2.1 Background

While a static patch had been shown to alleviate ischemic MR and was a relatively simple device to construct, the function of this patch was not very complex. Data from the Cardiac Ultrasound Laboratory experiments with static patches also focused on the qualitative analysis of the static patches' effects on the MR under observation. Few data exist on the extent of myocardial displacement that the static patch was effecting or the force required to do so. Furthermore, no data were available on the timing and speed of actuation that an active patch should have relative to LV systole. Attempts to design an artificial muscle-based device from these incomplete data would have required too much guess-work to establish the device's operating parameters, leading to many failed attempts that would be both time consuming and require the needless use of test animals. It was therefore decided that an artificial muscle patch simulation device should be constructed in order to proof the concept of active patch therapy and to gather as much quantitative data as possible to develop the missing design criteria required for the creation of an AMP device.

2.2 AMP Simulation Apparatus

In order to make the data gathering results as reliable as possible, a mechanism for effecting change to the LV wall having the least amount of variables was selected. Continuing along the same lines as the Cardiac Ultrasound Lab's previous method[1], a fluid-filled balloon held against the LV's exterior wall was chosen as the on-heart displacement element. The active

portion of the device would be a fluid pumping system (FPS) capable of receiving gated signals from the test animal's heart and of filling and emptying the balloon at very high rates.[7] An electronics package also had to be developed to receive a signal either from an electrocardiogram taken directly from the test animal's heart or from an internal LV pressure monitor already in place in the operating room, and transform this signal into a digital triggering pulse recognizable by the fluid pump. The final element of the instrument was a series of sensors to measure the pressure applied by the balloon to ensure sufficient displacement of the myocardium to relieve MR.

2.2.1 On-Heart Elements

The Cardiac Ultrasound Laboratory's original balloon patch device was held in place using a Dacron mesh sutured to the LV wall. This setup was satisfactory for a static device but unsuitable for an active device, where its constant motion would cause location shifts. This would not have provided good results since the effect of the patch observed in the Levine experiments was very dependant on its location[1]. In order to solve this problem it was necessary to build a frame, referred to as a base ring, which attached to the balloon and would be in turn sutured onto the epicardial wall of the LV. A balloon that could be connected to the fluid line coming from the pumping system would then have to be designed to properly fit into the base ring.

[7] Systolic contraction of the LV lasts approximately 180 ms for a heart rate of 2Hz (120 bpm) (standard heart rate for a sheep during an in-vivo procedure)[12].

2.2.2 Base Ring Version 1

The first iteration of this base ring was designed to hold a circular-shaped balloon. Its parts were modeled in CAD (Figure 3a) then machined on a HAAS 3-axis CNC mill from 1.5 mm thick stainless steel sheet stock. Figure 3b shows the machined bottom two layers of the ring assembly. Dimensional schematics can be seen in Appendix A, Figure 49.

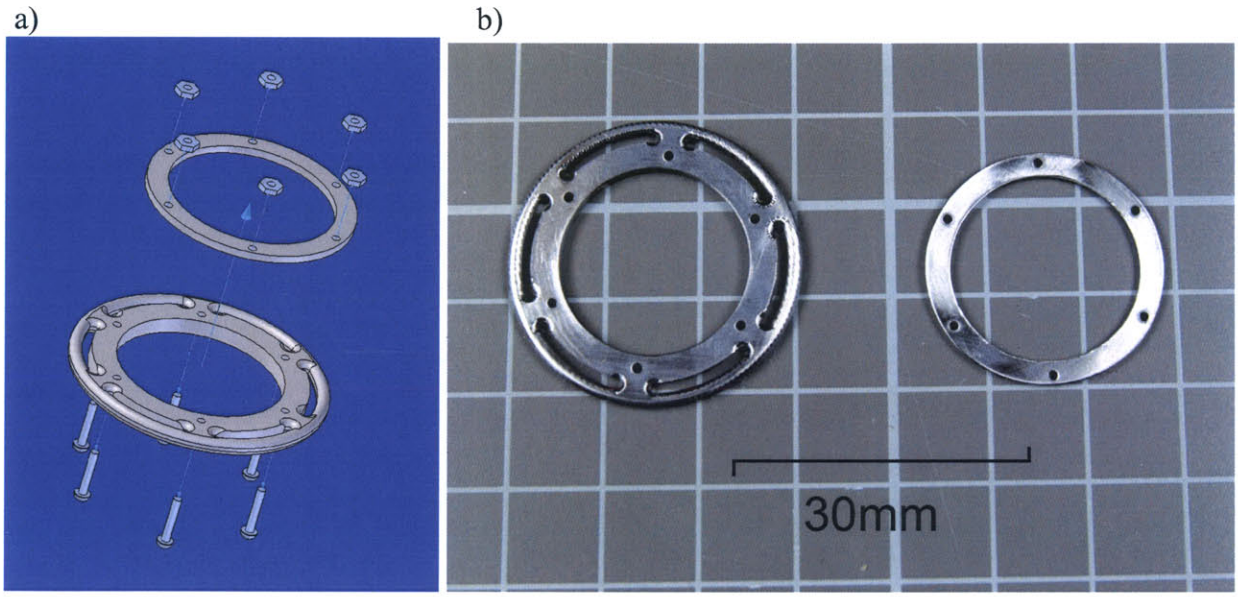

Figure 3: a) CAD assembly of Base Ring Version 1; b) Photo of machined main components of Base Ring Version 1.

Based on the design and preliminary machining, and in consultation with the cardiologists at the Cardiac Ultrasound Laboratory, it was decided that an oval-shaped balloon would be more successful.[8] As a result, further development of this iteration was halted before completing any other element of this base ring design.

[8] This decision was based on the Cardiac Ultrasound Laboratory's previous experiments using a static patch[1]. The longer oval balloon covers a greater area of the LV's epicardium thus reducing the difficulty in trying to align the balloon precisely with the PMs. It also does not deform a single point of the epicardium as much as a smaller round balloon would which would put less stress on the base ring's sutures.

2.2.3 Base Ring Version 2

In order to accommodate an oval-shaped balloon, a new base ring was constructed with the appropriate shape. This iteration used a design and method similar to that used for version 1. This oval base ring was designed as a three-layered device held together by M1 screws. Slots were machined into the bottom layer's periphery to provide an easily accessible edge. This edge could then be used to suture the assembly to the heart. The top layer was an oval 2.5 mm wider than the periphery of the bottom layer's cutout. Its center was also partially milled out to provide extra space for the balloon. The middle layer consisted of an oval ring segmented in two to allow the balloon to be fitted and clamped between the top and bottom layers. Figure 4a shows the CAD assembly of the oval base ring. Figure 4b shows each individual machined part while Figure 4c shows the final machined assembly. Dimensional schematics can be seen in Appendix A, Figure 50.

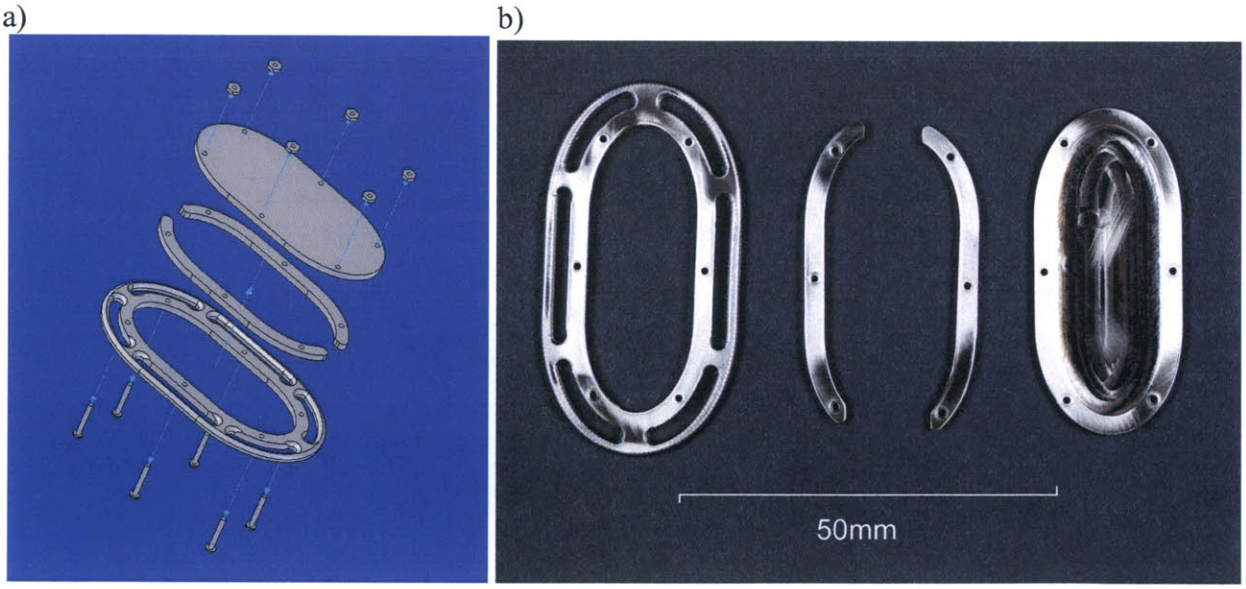

Figure 4: a) CAD assembly of Base Ring Version 2; b) Individual machined parts of Base Ring Version 2.

2.2.4 Balloon

Once the oval base ring was complete, a balloon of the same dimension as the ring's inner cutout was assembled. The insert of the balloon was a nylon tube fitting that was ground down to fit inside of the Teflon PFA tube coming from the FPS. The balloon material was taken from two intra-aortic balloons provided by the Cardiac Ultrasound Laboratory. The intra-aortic balloons measured 200 mm in length but only 85 mm from the tips down were used. Wet Surface Gap Filling epoxy was applied to the threaded end of the nylon fitting, which was then inserted into the open base of the balloon section. 250 μm wire was then wrapped tightly around the portion of the balloon mated to the nylon fitting. Finally, flexible urethane epoxy was generously applied on top of the wire and on the edges of the mated balloon section to cover any sharp edges or wire endings. Figure 5 shows the assembled balloon. Two were built to ensure that at least one of the assembled balloons would work properly.

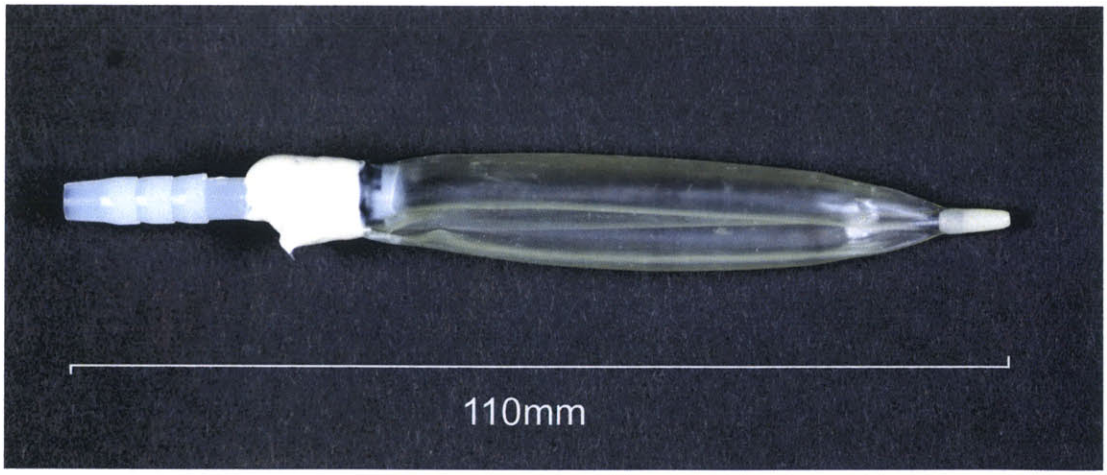

Figure 5: Fabricated balloon for on-heart assembly.

2.2.5 Assembly

Once the oval base ring and balloon were completed they were assembled in two steps. The balloon was inserted between the two middle sections of the oval ring, and then the ring's top layer was placed into position and secured by tightening the nuts on the M1 screws. Figure 6 shows the assembled on-heart portion of the simulation device.

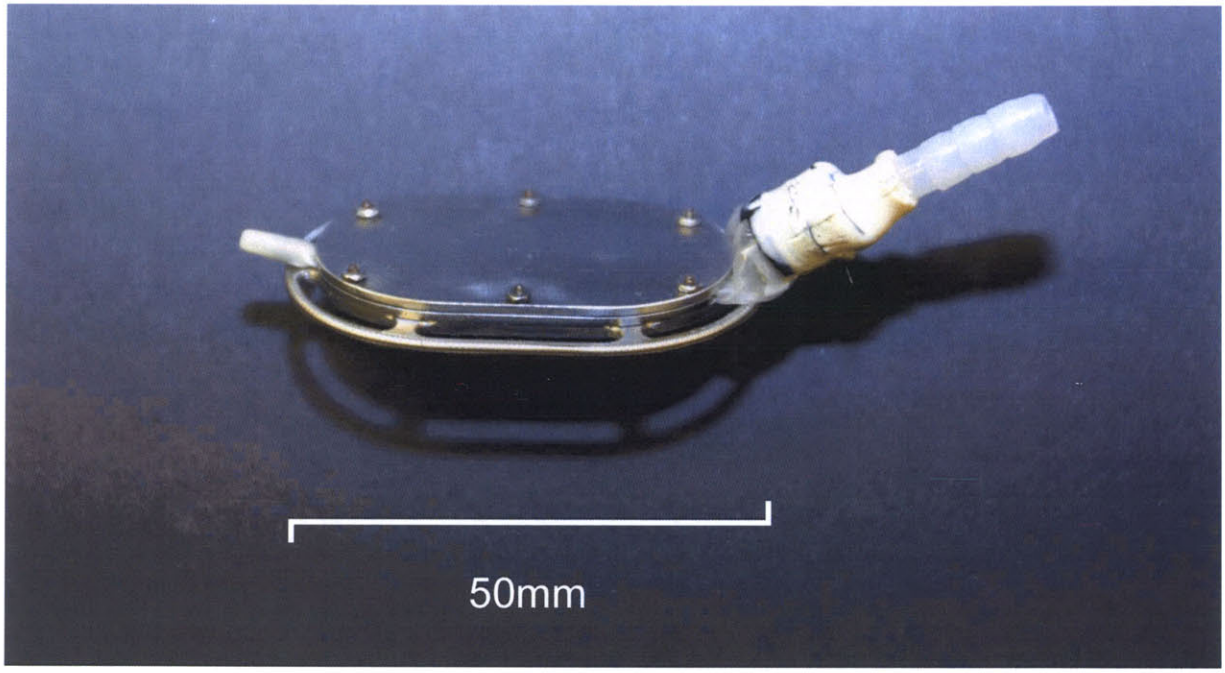

Figure 6: Photos of the fully assembled on-heart assembly.

2.2.6 Fluid Pumping System (FPS)

In order for the system to function properly, the fluid pumping system would have to be gated to the systolic portion of the LV's contractile cycle. As previously mentioned, systole occurs over a 180 ms period in a test animal with a 2 Hz (120 bpm) pulse[12]. This meant that the balloon needed to be filled and emptied in approximately 200 ms. This placed very high force and velocity requirements on the pumping apparatus and limited the possible choices of

mechanisms. The combination of a linear actuator pushing a syringe was chosen as the best option given these requirements.

2.2.7 Linear Actuator

In order to select a linear actuator, calculations of force and velocity requirements had to be performed. The volume required to fill the balloon that would be attached to the heart was taken from the Cardiac Ultrasound Laboratory's prior in-vivo experiment using a similar-sized balloon. On average, a balloon filled with 11 mL was successful at relieving MR[1]. Assuming a syringe inner diameter of 20 mm,[9] the linear actuator needed to have a travel of approximately 40 mm in order to displace the proper amount of fluid.[10] This number was increased to 150 mm in order to have the option of using a syringe of a different diameter at a later time. Using these assumptions, calculations were performed based on an estimate of the maximum pressure required to displace the LV and on the Poiseuille Flow equation for the pressure drop across each section of tube (Equation (1)) to determine the maximum force that the linear actuator would need to produce to meet the requirements of this application. The entire calculation is shown in Appendix B.

$$\Delta P := \frac{12 \cdot \mu \cdot Q \cdot L}{\pi \cdot R^4} + a \cdot \rho \cdot L \tag{1}$$

A summary of the linear actuator requirements is shown in Table 1. All values were obtained from calculations shown in Appendix B.

[9] Estimate based on available syringes.
[10] Based on experiments conducted by the Cardiac Ultrasound Laboratory[1]

REQUIREMENTS	VALUE
Length of Travel	150 mm
Force Output	~110 N
Acceleration (under 110 N load)	>10.84 m/s2

Table 1: Performance requirements for linear actuator.

Possibilities were narrowed down to three manufacturers: Parker Daedal[13], Aerotech[14] and Linmot[15]. The Linmot actuator was selected because of its superior price/performance ratio. Although its positional resolution of 100 μm was inferior to its competitors, it was still well within the tolerances for this application. Figure 7 shows the Linmot PS01-37x240 linear actuator.

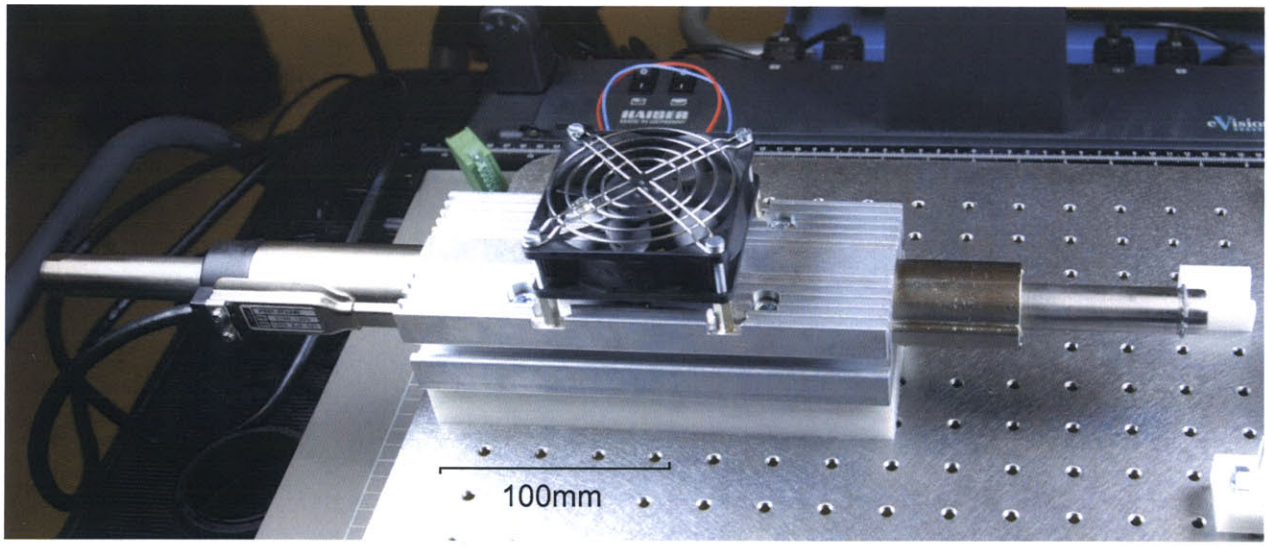

Figure 7: Photo of the Linmot PS01-37x240 linear actuator used in simulation apparatus.

Another interesting feature of the Linmot actuator's controller is that it allows the user to create custom-shaped position versus time waveforms for the Linmot linear actuator to execute. These waveforms can be easily modified within the Linmot controller's software interface, permitting modifications during the in-vivo procedure. This was especially useful since the LV's

systolic and diastolic cycles are not of the same duration.[11] This feature made it possible to adjust the position of the actuator at any given time to better match the characteristics of the test animal's LV cycle characteristics.

Finally, the Linmot controller directly accepts a TTL[12] triggering signal. This meant that a substantial amount of programming could be bypassed by simply creating a hardware electronic trigger[13] connected to a heart monitoring instrument.

2.2.8 Syringe and Mounts

A Popper & Sons Perfektum 50 mL glass syringe[16] was chosen for the water handling portion of the pumping system. Its smooth action provided very little friction resistance and it was rated for high-pressure applications.[14] The syringe needed to be seated within an immobilizing mount to ensure that the Linmot actuator did not apply any significant off-axis force to the syringe's plunger. Otherwise the actuator accelerating at $50m/s^2$ would quite easily have shattered the syringe. Because the life expectancy of the syringe in this system was also unknown an all-encasing mount was built to contain any critical failure. The syringe body was measured and the mount was machined from two pieces of 25.4 mm thick Delrin. Since there was a significant amount of variability in the syringe's exterior dimensions a certain amount of sanding and filing was necessary for the mount to accommodate more than a single syringe. Figure 8a shows the CAD assembly of the syringe mount. Figure 8b shows one of the machined halves of the mount. See Appendix A, Figure 51 for dimensional schematics.

---

[11] Systole occurs over approximately 80 ms, diastole over approximately 130 ms for a 2 Hz (120 bpm) heart rate.

[12] Transistor-Transistor Logic (TTL) – A circuit element characterized by its ability to switch between high on-state to a low off-state.

[13] Details covered in the Electronic Gating System section on page 25.

[14] No data were available on its maximum pressure capacity.

a) b)

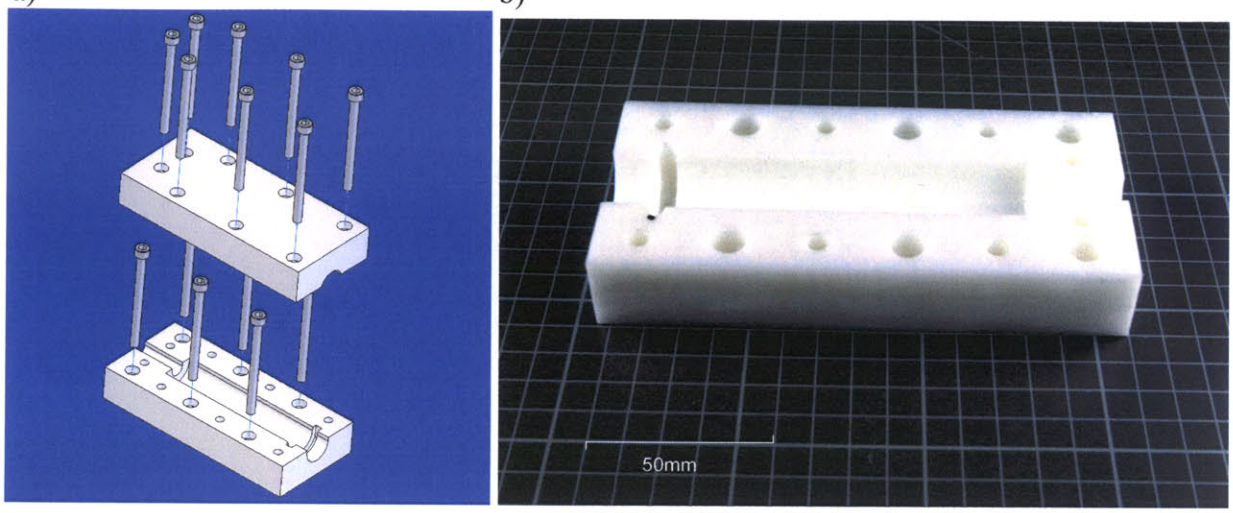

Figure 8: a) CAD assembly of Perfektum 50 mL syringe mounts; b) Machined Delrin component of Perfektum syringe mounts.

Once the mount was completed, a coupler also needed to be machined to join the syringe plunger to the Linmot actuator. The coupler was built in the same style as the mount. Figure 9a shows the CAD assembly of the syringe-actuator coupler. Figure 9b shows the machined top and bottom halves of the coupler. Dimensional schematics are available in Appendix A, Figure 52.

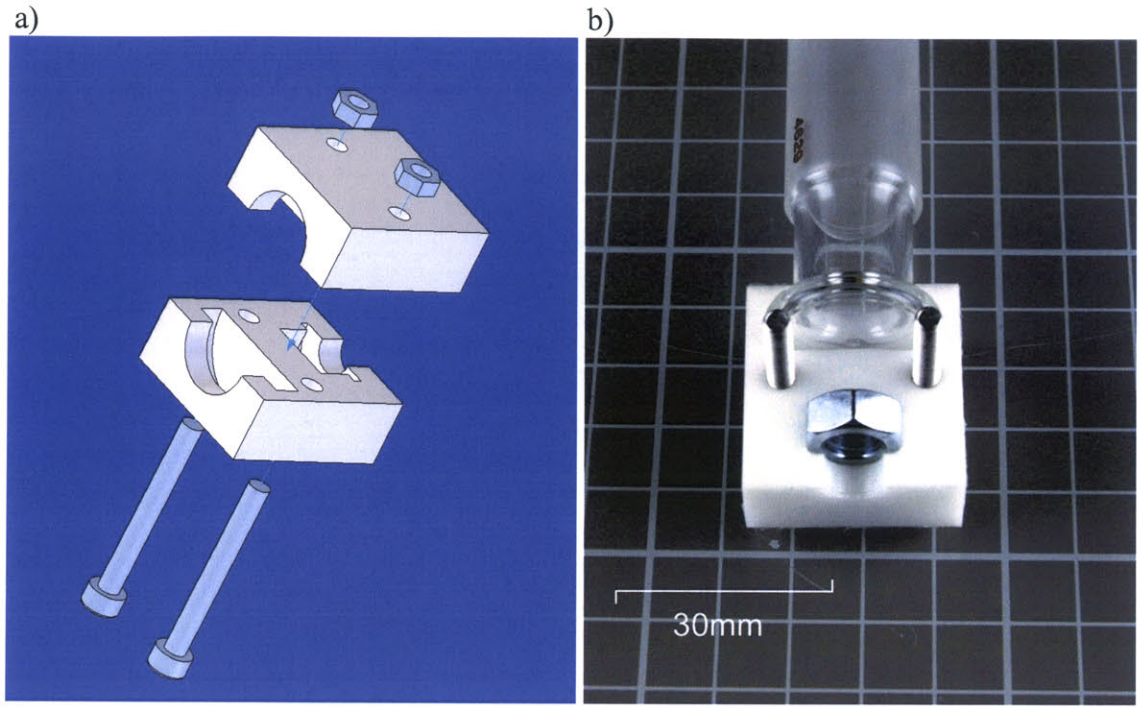

Figure 9: a) CAD Assembly of syringe-actuator coupler; b) Machined Delrin components of syringe-actuator coupler.

2.2.9 Electronic Gating System (EGS)

The next requirement was that the fluid pump be "gated" to the LV's systolic cycle. Since the Linmot controller was capable of accepting a 10 V TTL triggering signal, a hardware-based electronic trigger was constructed to produce this signal from a heart monitoring instrument's output.

The electronic gating system (EGS) was constructed around an MC14106BCP Hex Schmitt trigger, an integrated circuit (IC) that produces a high output signal in its rest state but switches to a low output state once the input signal passes the trigger's threshold.[15] Since the input signal would be relatively small, a non-inverting amplifier was placed in front of the trigger to boost the signal's voltage. A potentiometer was placed in this amplifier to enable it to accept a

[15] The exact threshold depends on the Schmitt trigger's supply voltage. In this case, a supply voltage of 10 V was used making the triggering threshold 5.9 volts.

wide range of input signals and also to adjust the triggering sensitivity of the EGS. An inverter was placed after the trigger to provide a positive output signal and an amplifier was placed after the inverter to adjust the output signal's voltage to 10 V. Figure 10 shows a circuit diagram of the EGS.

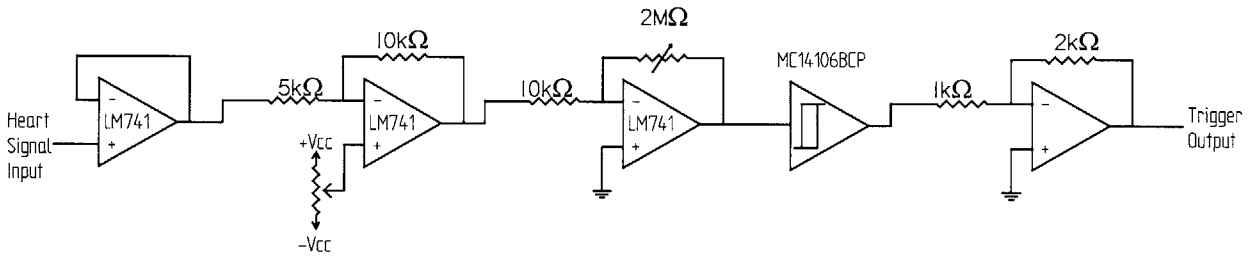

Figure 10: EGS circuit diagram.

The circuit was soldered together onto a 45 mm by 45 mm prototype board and placed into a custom circuit box machined from Delrin. Female BNC connectors were installed in the Delrin box and connected to the input and output of the circuit. Female banana jacks were also installed on the box to accept the power supply lines for the circuit elements. Finally, a threaded bolt was inserted in the bottom of the box to allow it to be screwed down into an optical table. Figure 11 shows the EGS circuit box.

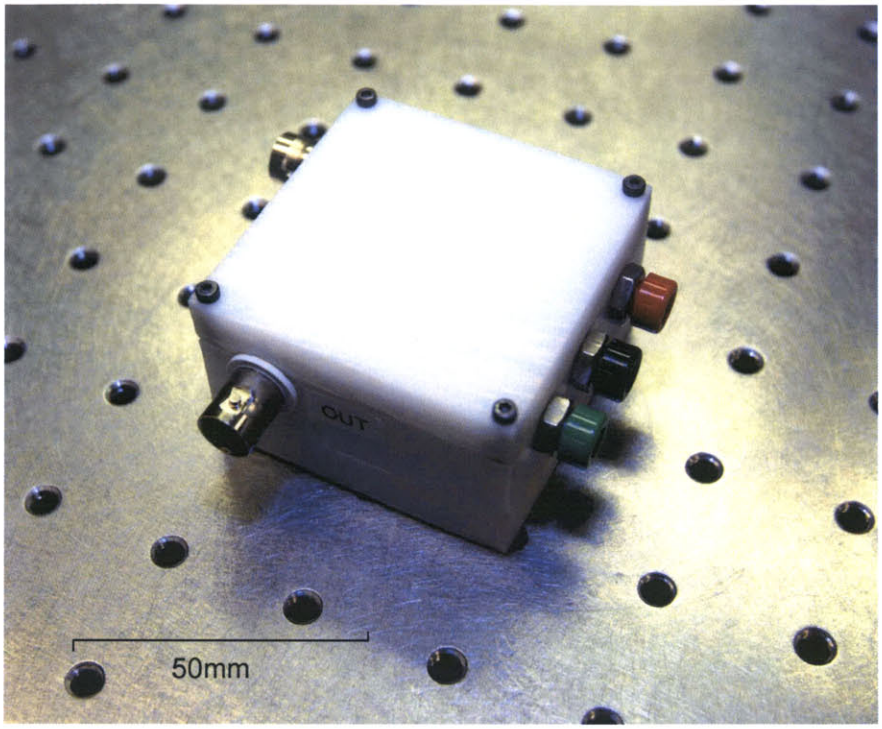

Figure 11: Machined Delrin EGS circuit box.

2.2.10 Sensors and Data Acquisition

Finally, sensors were added to the AMP simulation apparatus in order to gather data on the active patch's force and extent of displacement. Two sensors were inserted into the path of the fluid line between the fluid pump and the balloon. A flow meter was placed in series at the syringe's output to measure the flow of water while the FPS was pumping. A pressure transducer was placed in parallel with the pump-to-balloon line to measure the pressure inside of the fluid line. The internal line pressure varied cyclically when the FPS was active but the pressure transducer would pick up any external pressure applied to the balloon. During the in-vivo procedure, this rise in internal line pressure corresponded to the pressure required to displace the LV wall. This last could be calculated from the recorded pressure using the Poiseuille flow equation (Equation (1)).

The two sensors' outputs were in the form of a voltage signal on a 0 to 5 V scale. Both were connected through a BNC-2110 connection box to a National Instruments 6062E Data Acquisition (DAQ) card in a laptop computer. A Visual Basic interface[16] developed in Visual Studio .NET[17] was used to control the DAQ card's recording functions.

2.2.11 Apparatus Assembly

Each element of the simulation apparatus was mounted onto a 900 mm by 600 mm optical table and the elements connected together. Tube sections between the syringe and sensors were kept to a minimum length, Teflon tape was applied to all threaded sections of NPT-tube connectors and gap-filling epoxy was applied to all tube connections to ensure that no air would infiltrate the line. Finally, a 1m length of Teflon-PFA tube was used to connect the apparatus to the on-heart assembly. Figure 12 shows the simulation apparatus fully assembled.

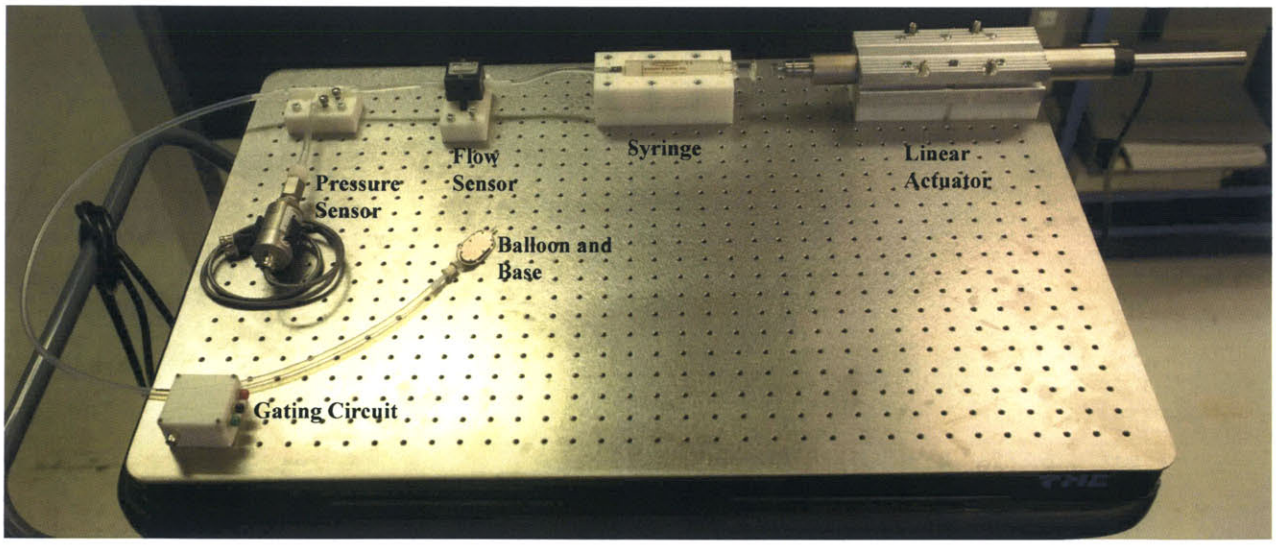

Figure 12: Simulation apparatus mounted onto its optical table.

[16] VB interface was created by Michael Garcia-Webb of the Bioinstrumentation Laboratory.

2.3 *In-Vivo Experiment 1 (Performed June 15th, 2003)*

2.3.1 Background and Preparation

Preparation for the in-vivo procedure began 12 weeks prior to the procedure date.[17] The sheep under observation had certain coronary arteries ligated to obstruct blood flow to the LV and create an infracted area. The sutures used to ligate the coronaries were left in until the in-vivo procedure so as to better reproduce the characteristics of a chronically infracted LV. This preparation was conducted by Dr. Luis Guerrero of the Cardiac Ultrasound Laboratory.

In the days prior to the in-vivo procedure, a series of tests were carried out to gauge the FPS's performance under various conditions that might be encountered during the upcoming in-vivo procedure. It was decided to use a $\lambda/2$ sine wave as the position versus time output waveform for all tests. The amplitude of the waveform was used to modify the volume pushed into the balloon by the actuator while the speed of each pumping action was controlled by the period of the sine wave. The Linmot controller's software was especially useful for testing the FPS's limits this since the actuator possessed internal encoders that the software used to plot the output waveform against the actual position of the actuator. This made it possible to detect what maximum heart rate and volume displacement were possible without the actuator lagging or the fluid lines taking in air bubbles.[18] Most importantly, baseline pressure variations for the system pumping at different volume displacements were recorded. It was necessary to do this prior to the experiment since the balloon device would immediately be sutured to the sheep's LV once the procedure began. These baseline data would be used in post-procedural data analysis to

[17] While the standard preparation time for a chronic model infarct study procedure is eight weeks, due to difficulty in obtaining all of the simulation apparatus equipment, a four-week delay was incurred. This delay would not have affected results.

[18] All fluid line connections were sealed with silicone and/or water-rated gap-filling epoxy, but it was discovered that when the actuator passed a certain operating frequency the integrity of the connections was compromised by the intense pressure variations and air would infiltrate into the fluid lines. Below this frequency, no significant air infiltration was detectable.

compare baseline pressure variations in the fluid line with the pressure variation when the balloon was applied against the LV.

The wiring and equipment of the simulation apparatus was simplified as much as possible as the entire setup needed to be brought to the Cardiac Ultrasound Laboratory at MGH for the procedure. The optical table where the pumping system was bolted was placed on top of a cart with all of the support equipment (power supplies, Linmot controller and oscilloscope) placed on the carts lower shelf.

2.3.2 Summary of Procedure

The actual procedure lasted approximately six hours. The equipment described above was transported to MGH, all electrical connections were made and the fluid line was filled with water to remove all air from the system. During this time, the sheep was brought into the operating room, sedated, prepped and its thoracic cage was opened to expose the heart. At this point the sheep's heart required two hours of preparation (discussed in the following section). The cart was then brought into the OR, the EGS was connected to an EKG monitor and the balloon device was sutured onto the sheep's LV wall. Tests were run with the FPS used first to statically fill the balloon and record the pressure produced against the balloon by the heart's pumping. This also served to see what volume of water had to be pushed into the balloon to produce a significant change in MR. Once this was complete, the system was set to pump on trigger. Figure 13 shows the on-heart elements sutured to the sheep's LV.

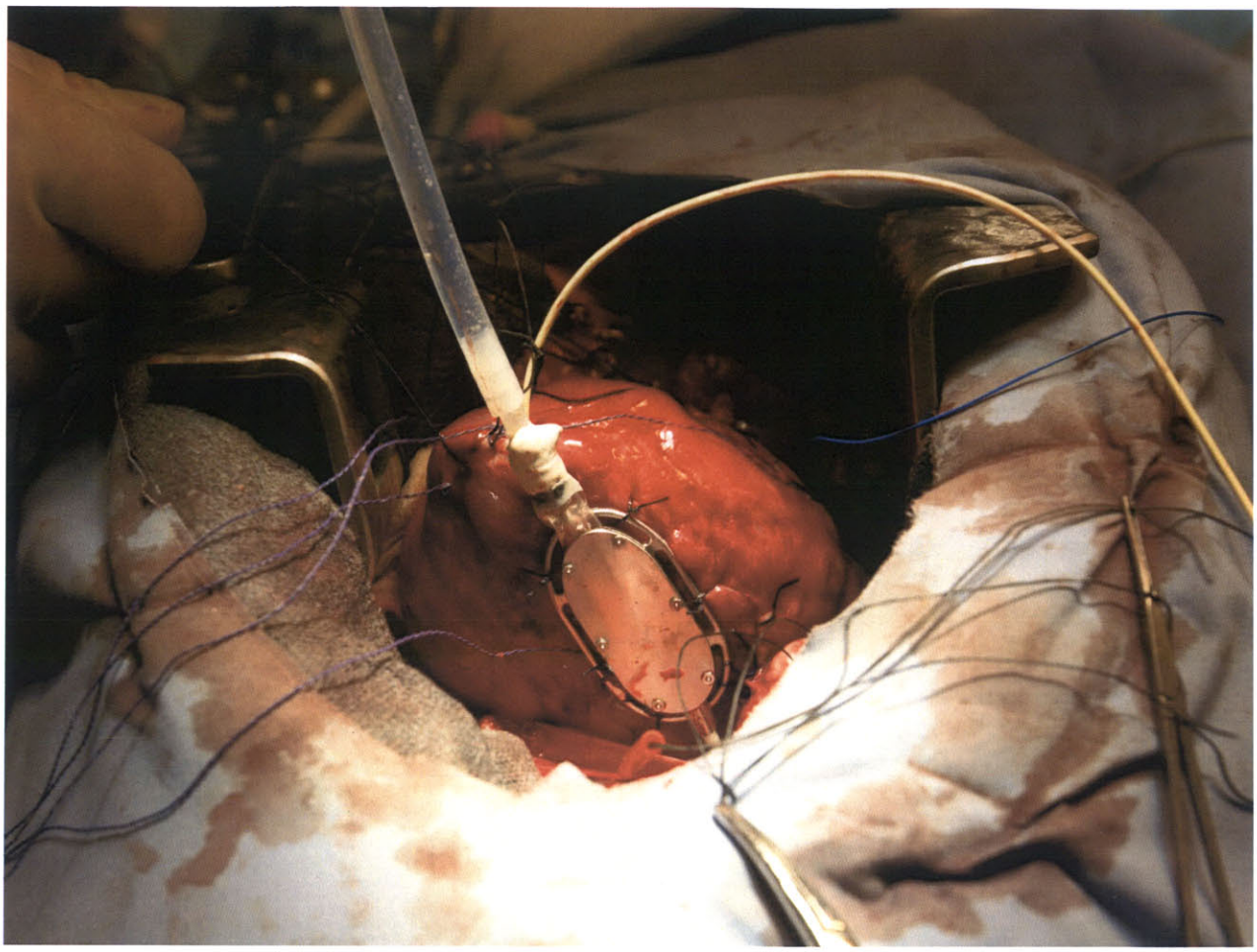

Figure 13: On-heart elements sutured to LV epicardium during first in-vivo procedure.

After approximately 4 hours of testing, during which the sheep fell into cardiac arrest and required defibrillation to re-stabilize, the sheep's heart function had become too weak for any further experimentation data to be reliable and the procedure was halted.

2.3.3 Issues Encountered

It was discovered immediately after opening the sheep's thoracic cage that its heart had not developed the extent of ischemic MR required for the experiment. Two more coronary arteries were ligated to cause further ischemia in the LV. This led to the formation of some MR

but it was sporadic and the sheep's heart function became quite weak due to the added trauma of a second ligation procedure. This made all observation of MR during the procedure problematic and generally cast doubt on the validity of the results obtained.

Another minor issue was the source of the EGS triggering signal. Shortly before the procedure it was decided to take the triggering signal from the heart's sinoatrial (SA) node by attaching a lead directly to it. This should have produced a trigger signal that was approximately 30 ms before LV systole[12], giving a certain buffer of time before the FPS needed to be activated. Once in the OR, however, receiving a clear signal from the SA node or from the LV was difficult therefore the EGS was connected directly to an EKG monitor through a BNC cable.

Finally, the balloon's base ring was not the ideal shape for such a procedure. The pocket where the balloon was sitting was too deep, which restricted the balloon's maximum protruding distance into the LV. In order to achieve some level of MR relief it was necessary to place a 5 mm thick backing made from electrical tape to further extend the balloon. Figure 14 shows this addition to the base ring.

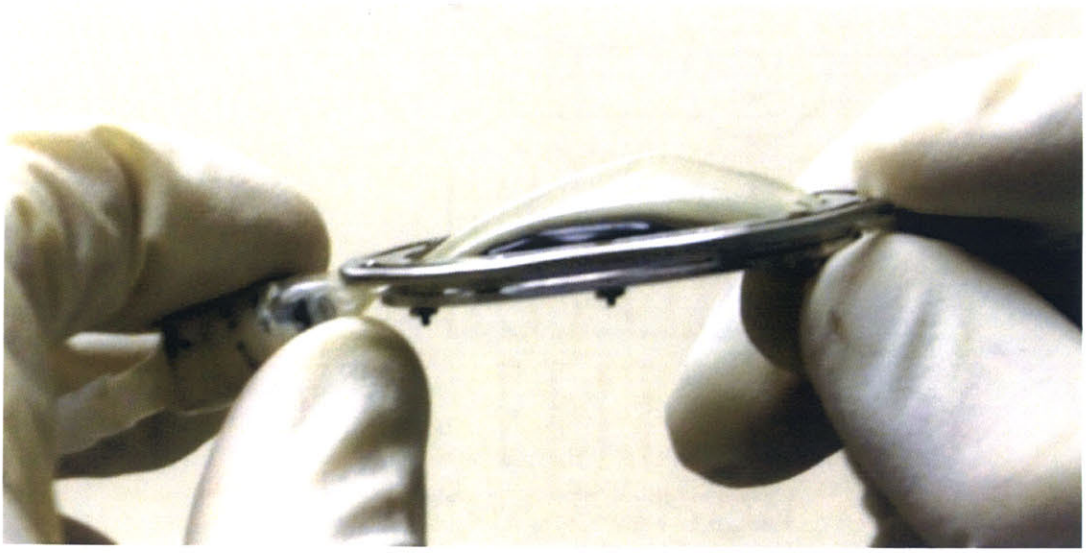

Figure 14: Addition made to Base Ring during in-vivo procedure 1.

2.3.4 Data Acquired

Many different volumes and frequencies were tested by adjusting the output waveform's characteristics. Pressure and flow data were recorded for each waveform used. Because of the poor condition of the test animal, none of the echocardiograph recordings were of particular benefit. Since persistent MR could not be established, it was impossible to discern whether the apparatus was performing according to theoretical predictions. The most relevant data extracted from this procedure were related to the simulation apparatus itself. Recordings of the linear actuator's actual position versus its demanded position ($\lambda/2$ output waveform) were taken while the on-heart elements were sutured to the LV epicardium and the FPS was pumping on trigger. The actual position did lag significantly when the output waveform was set to a period of 250 ms or shorter, but this speed of actuation did retract the balloon before the end of systole. Once this was observed, the waveform was rejected. A waveform with a period of 400 ms was found to work best.[19] Figure 15a shows the actuator's lag with the 200 ms period waveform. Figure 15b shows that the actuator still lags slightly behind the demand waveform. This confirms that there is a certain variation introduced by the actuator in the timing of the balloon's inflation within the operating range used during the procedure.

[19] A longer-period waveform would have inflated the balloon too slowly.

a) b)

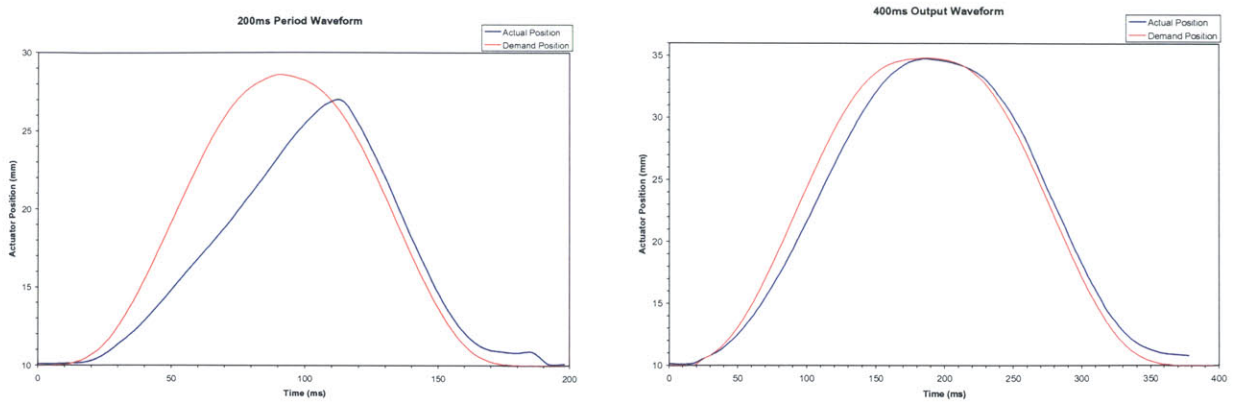

Figure 15: Comparison of λ/2 output waveform versus actual actuator position: a) 200 ms period waveform; b) 400 ms period waveform.

Pressure and flow data were also recorded both before the on-heart elements were sutured to the LV and while they were being tested. The flow data obtained showed that the sensor lagged significantly behind the FPS' actuation. This was due to the inability of the flow sensor's turbine mechanism to keep up with the rapid changes in flow rates and directions being produced. The pressure data were not reliable because of the aforementioned issues encountered during the procedure. They were therefore discounted from further analysis.

2.3.5 Discussion of Results

As previously discussed, the state of the sheep's heart was such that most if not all of the MR-affecting data are suspect since persistent MR could not be established. It was impossible to tell if the MR was actually being relieved by the balloon device's inflation or if improvements were due to temporarily-improved heart function. As such, no conclusion about the balloon's effect on the sheep's MR can be established.

Despite its limitations, several significant pieces of information were extracted from this procedure. First, the linear shape of the base ring unnaturally distorted the LV's shape while the LV was at rest. All of the surgical staff agreed that a base ring better fitted to the heart's curvature would improve both device and heart function.

Another valuable observation was that the output waveform executed by the FPS needed to be optimized to better match the LV's motion. The $\lambda/2$ sine wave used failed to account for the delay due to inertia that occurred during the transition between systole and diastole. This resulted in a premature retraction of the balloon prior to the completion of the LV's contraction and allowed some MR to occur before diastole. Overall, the $\lambda/2$ sine wave was not ideal for this application since its adjustability was limited. An increase in the period would lengthen the balloon's total inflated time but would also increase the delay before the balloon was at full inflation. A waveform with a rapid rise followed by a plateau at the balloon's full inflation level and a rapid drop would have better followed the heart's actual movements.

Another element that caused some data discrepancies was the use of an EKG signal as the triggering signal for the EGS. The EKG waveform was erratic which caused the EGS to sometimes trigger the FPS too late or not at all. A better source for the triggering signal would have to be found for the ensuing in-vivo study.

In light of these shortcomings, the pressure values obtained during this in-vivo experiment are unreliable. By changing the output waveform, base ring configuration and timing of the FPS' activation, this value could vary significantly. Another experiment addressing the above issues was performed to obtain more credible data.

2.4 *In-Vivo Experiment 2 (Performed August 11th, 2003)*

2.4.1 Improvements to Instrumentation

For the second in-vivo experiment, all of the lessons learned in the previous in-vivo procedure were used to improve the simulation apparatus. The most important change to the device was the creation of a new base-ring design. This new base ring held the balloon much as the original ring had but its suturing loops were extended away from the balloon in its long direction to reduce the amount of stress placed on the sutures when the balloon was inflated. The ring was also curved to approximate the LV's exterior contour. This design was built on a Stereolithography machine (SLA) and had only two parts. The first was an oval frame with four arms extending from the oval's ends. These arms ended with small oval loops where the sutures could be attached. The second part was a backing that fit on top of the oval frame to hold the balloon in place. Figure 16 shows the CAD assembly of the new base-ring design.

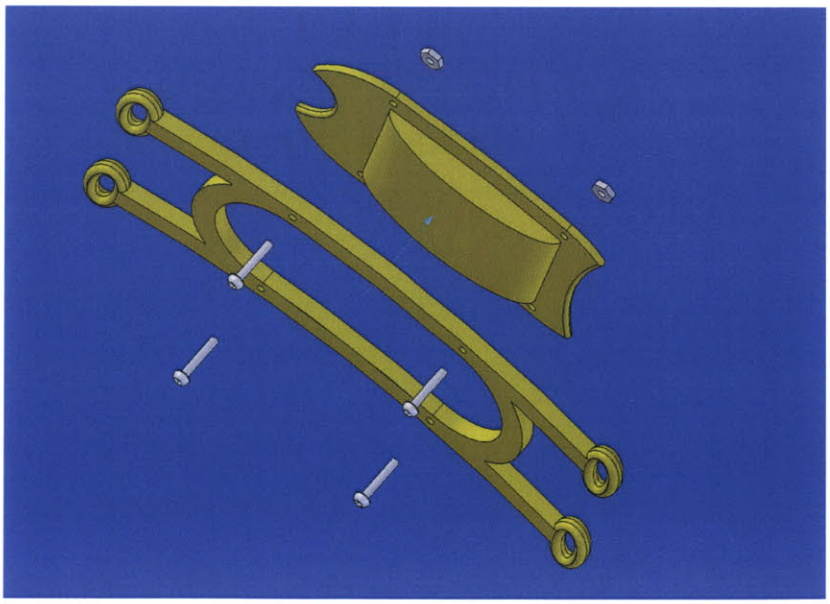

Figure 16: CAD assembly of Base Ring 3 used for second in vivo procedure.

Based on the first in-vivo study's experiences and on the general unpredictability of biological systems, an entire series of frames and backings with different characteristics were prepared so that the best-fitting frame and backing could be fitted to the new test animal's heart. Various frames were built with suture loops extended outwards to different distances and with extending arms arrayed in asymmetrical configurations. Curved protrusions were added to a series of backings in order to increase the maximum depth of indentation that the balloon could effect. Backings with protrusions ranging from 2 to 5 mm were prepared. Finally, two sets of all frame and backing designs were built, each with a different curvature. Figure 17 shows the entire series of devices prepared for the procedure. Dimensional schematics can be seen in Appendix A, Figure 53 and Figure 54.

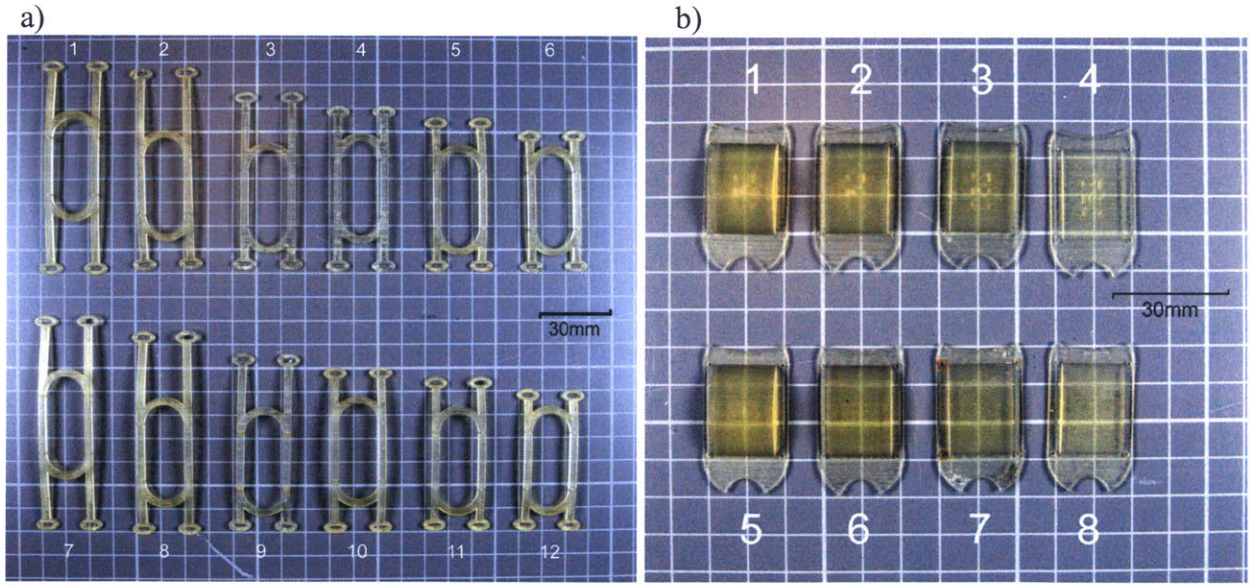

Figure 17: Series of devices prepared for second in vivo procedure: a) Base frames; b) Backings.

Improvements were also done to the FPS' output waveform. A new waveform configuration was created to replace the $\lambda/2$ waveform from in the first experiment. This new waveform used a $\lambda/4$ section of sine wave to provide the rise and fall in amplitude (position) of

the waveform. A plateau was inserted into at the waveform's maximum amplitude to extend the balloon inflation period. This waveform was custom configured for this particular application. Due to the time required to make adjustments to this waveform, a series of preconfigured waveforms were prepared prior to the in-vivo experiment. These waveforms varied in inflation and deflation time (30 ms to 50 ms) and also in the length of their plateau (50 to 200 ms). Figure 18 shows an example of one of the output waveforms.

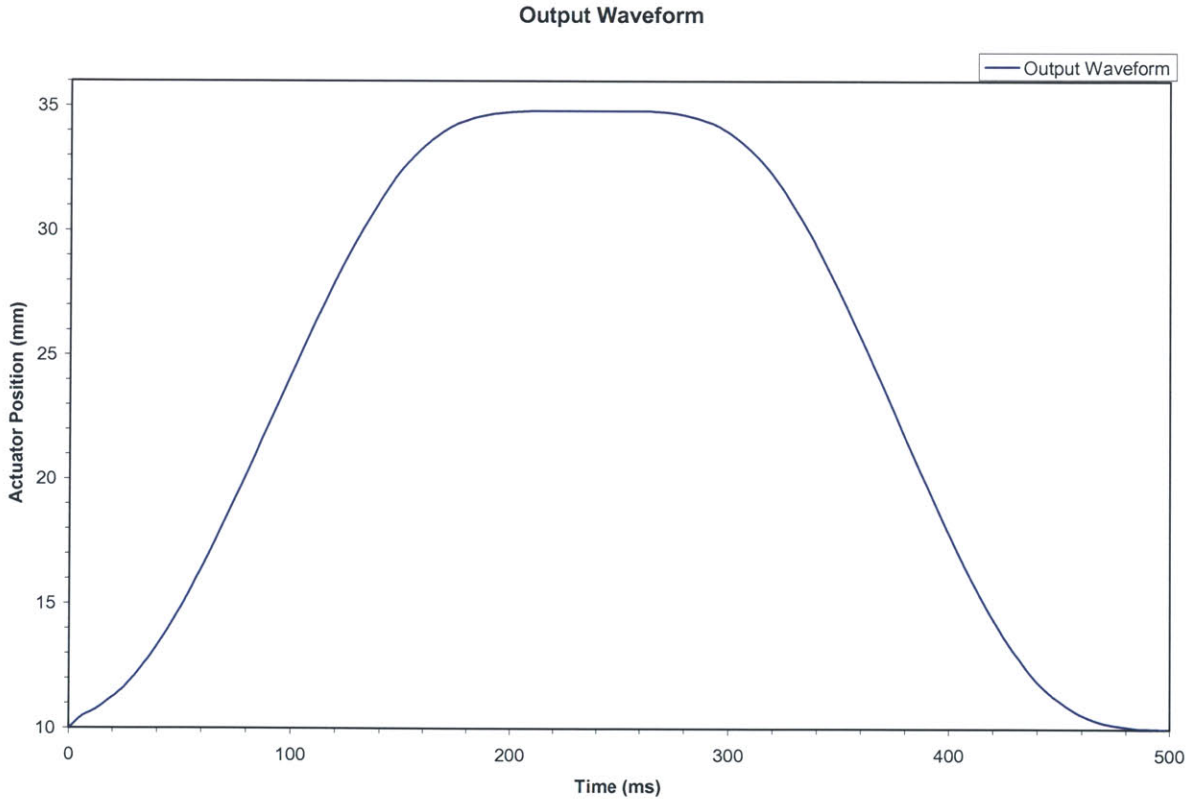

Figure 18: Output waveform prepared for second in-vivo study.

2.4.2 Summary of Procedure

Logistically, the second in-vivo study proceeded in the same way as the first. The simulation apparatus was moved to MGH and set up outside of the OR. During this time, the

sheep was brought into the OR and prepared. The sheep's heart was examined by echocardiography before beginning any testing. It was observed that the sheep had developed a much more significant amount of chronic MR than the previous test animal. The base ring frames and backings were arrayed before the surgeon, who chose the best fitting pair for the test animal's heart (Figure 17, frame number 3 and backing number 3). The on-heart assembly was then sutured onto the LV and connected to the FPS. The EGS input was connected to an LV pressure monitor that received its data from a Millar catheter[20] [18] inside of the LV. This provided a signal directly related to the motion of the LV. Although the use of this signal meant that the FPS would activate when the LV was already beginning systole, the clarity of the signal from the Millar catheter outweighed the slightly delayed triggering of the FPS. Furthermore, the ability of the linear actuator to accelerate extremely rapidly[21] was used to compensate for the late triggering. Figure 19 shows the EGS' trigger output and the Millar catheter input.

[20] A Millar catheter is a pressure measuring device that consists of a pressure transducer placed at the distal end of the catheter. This allows the transducer to be inserted directly into the LV to obtain precise LV pressure measurements.

[21] The Linmot PS01-37x240's maximum acceleration is 268 m/s^2.

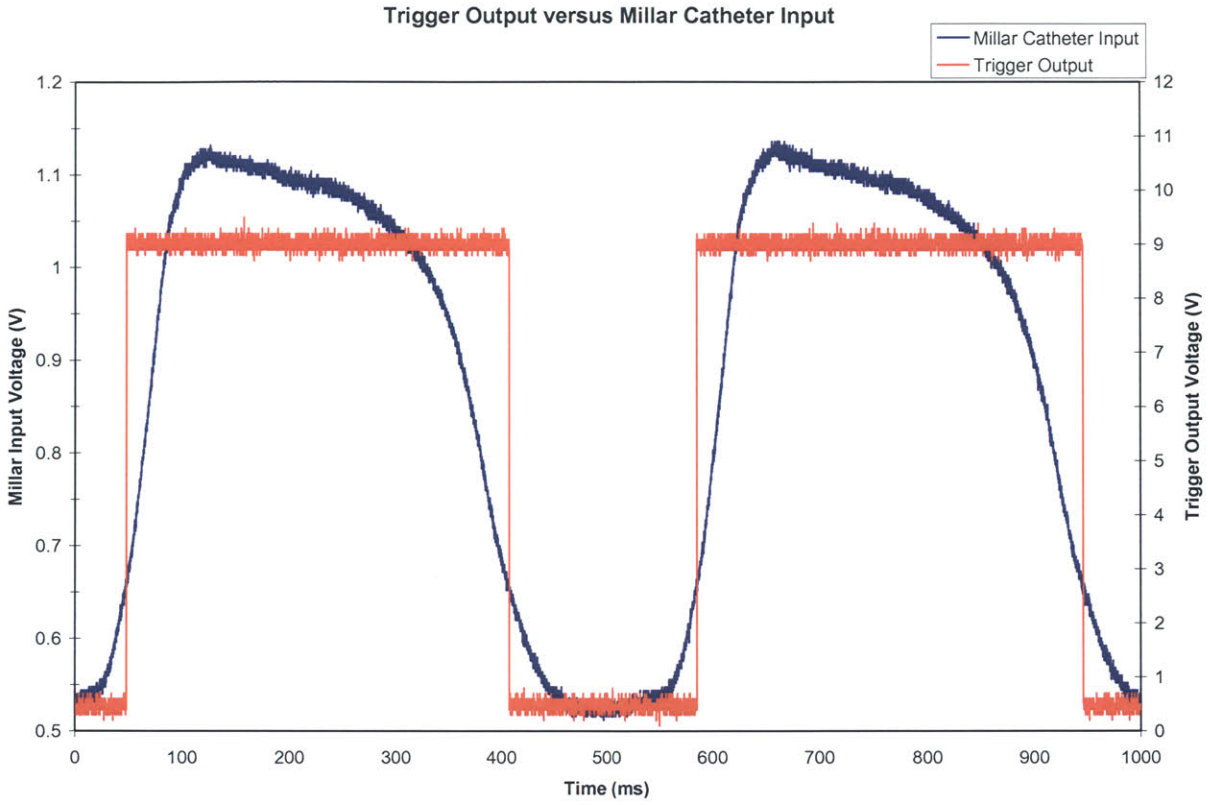

Figure 19: EGS trigger output from Millar catheter input.

Initial tests were performed to determine the balloon inflation volume required to affect the sheep's MR. Once this was determined, testing began with the EGS controlling the FPS. Figure 20 shows the on-heart elements sutured to the sheep's LV while the balloon is at full inflation.

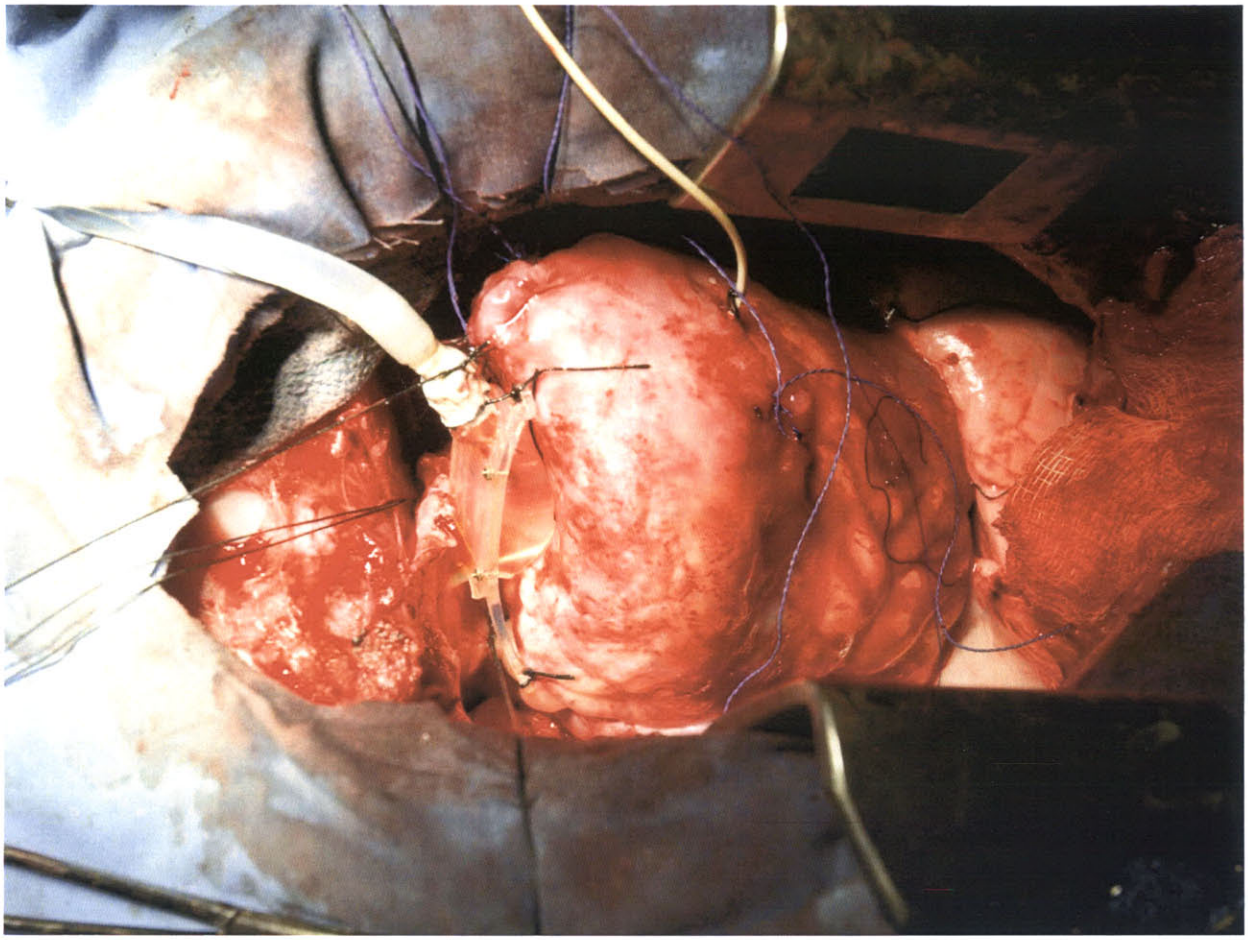

Figure 20: On-heart elements sutured onto LV epicardium during second in-vivo procedure.

2.4.3 Data Acquired

The same tests were performed during the second in-vivo study as in the first procedure. The output waveform and actual position were plotted while the FPS was pumping on trigger to verify that the actuator did not lag behind its demand position. Figure 21 shows that the actuator did not lag significantly behind its demand position.

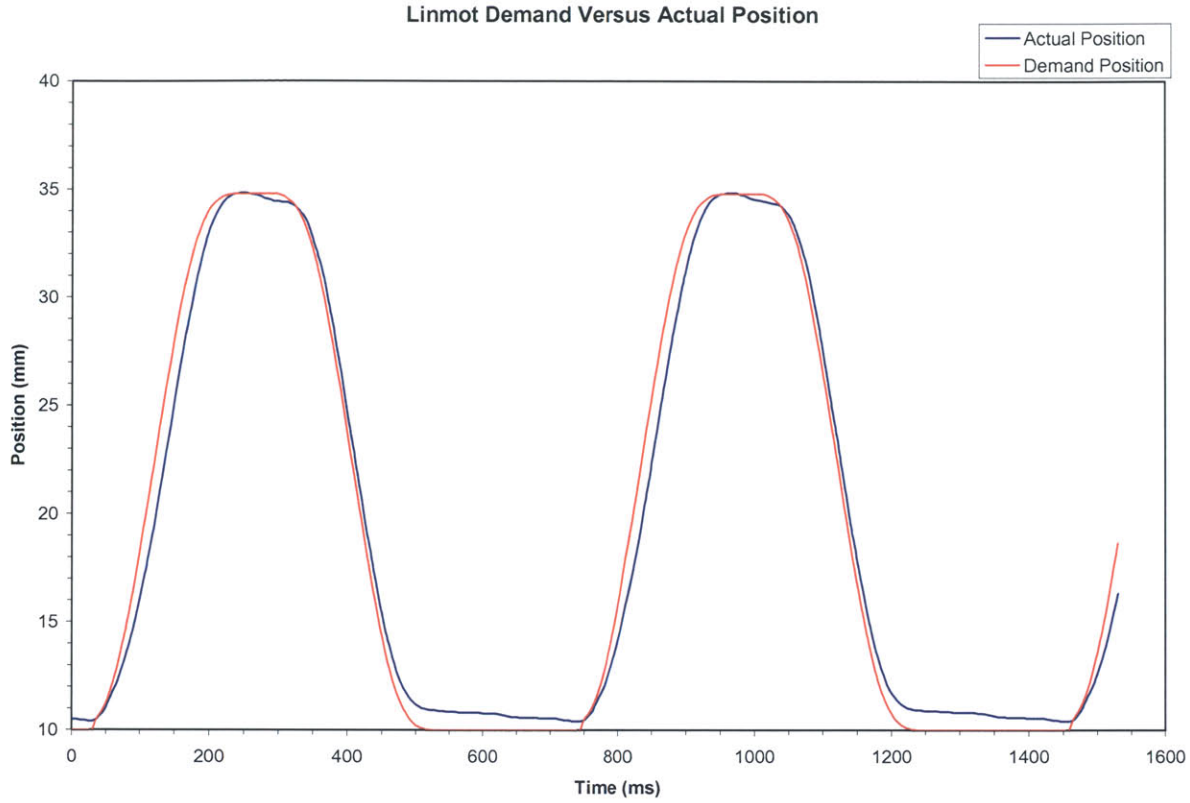

Figure 21: Comparison of output waveform demand position versus actual actuator position for second in-vivo study.

Pressure and flow data were again recorded to measure the balloon countering pressure (BC pressure (P_{BC})) of the LV with the new simulation apparatus configuration. Figure 22 shows the pressure measurements taken while the FPS was pumping on trigger before suturing the on-heart elements to the sheep's LV. They provide baseline data for the FPS's function independent of any contribution from the LV wall against the balloon's surface. Figure 23 shows the pressure measured after the on-heart elements were sutured onto the LV epicardium. Flow data were also taken for the first few series of measurements but a malfunction in the flow sensor prevented further data recording. Fortunately these data were not critical to the performance analysis.

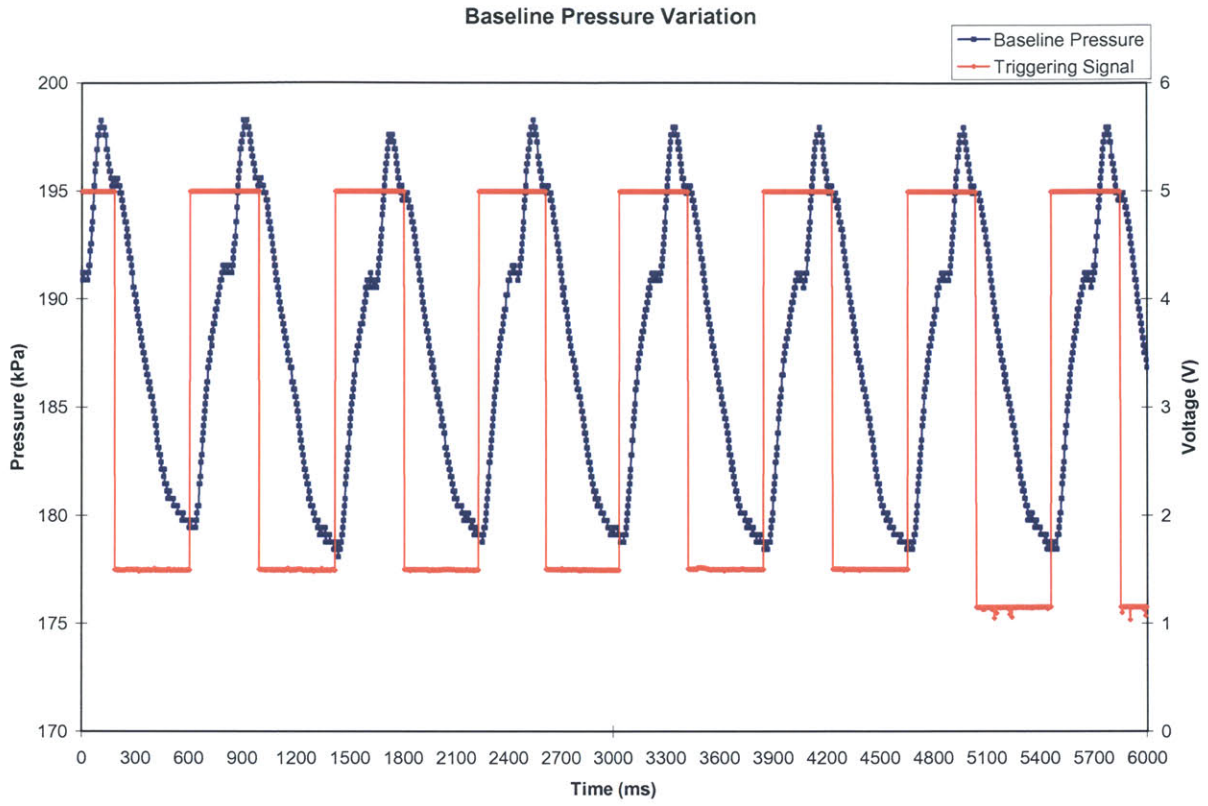

Figure 22: Pressure (blue) and Trigger Signal (red) with FPS pumping on trigger prior to the on-heart elements' installation (baseline measurement).

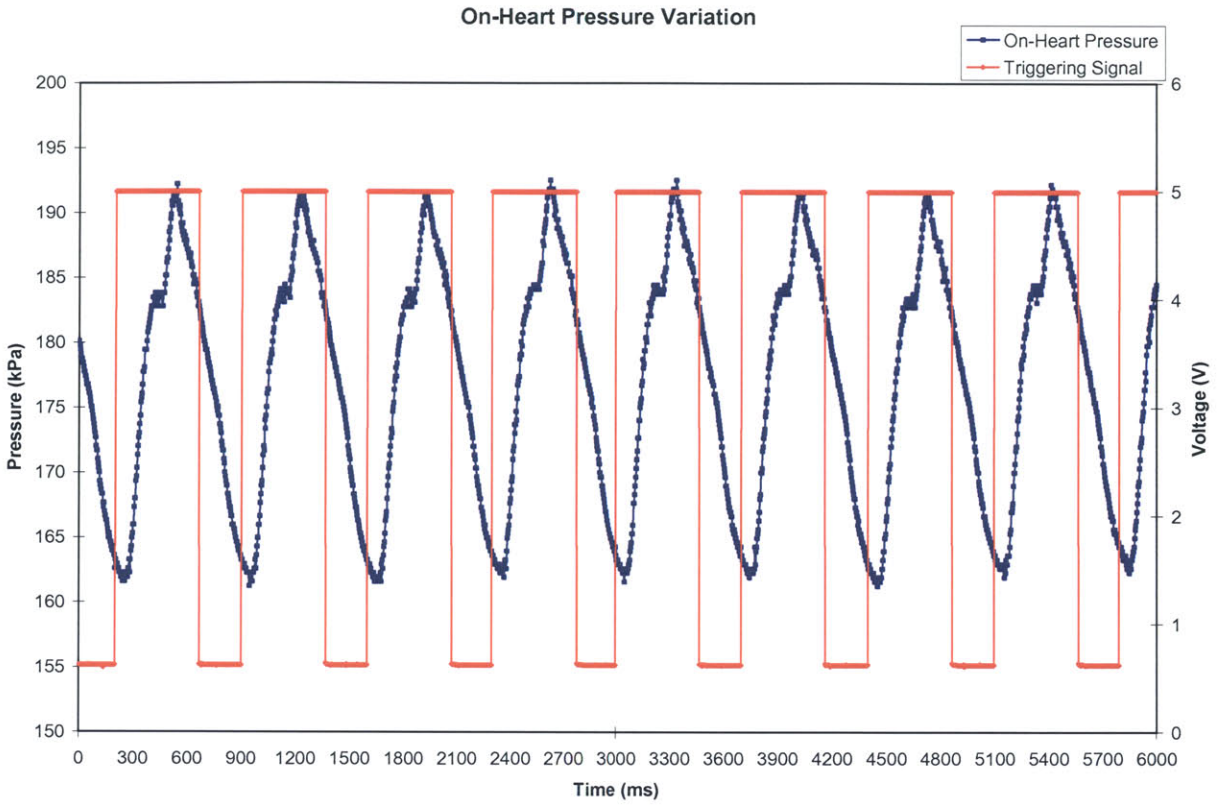

Figure 23: Pressure (blue) and Trigger Signal (red) with FPS pumping on trigger and the on-heart elements' sutured on the LV.

Equation (2) was used to calculate the BC pressure (P_{BC}) from the data in Figure 22 and Figure 23. Variations in pressure (ΔP) were calculated by subtracting the height of a valley minimum from the height of the following peak's maximum. The values from a data set were averaged and compared to the averaged value from the baseline data set to obtain the BC pressure. The baseline pressure curve was compared in this manner against four measurements taken during the course of the procedure with output waveforms of different periods. A ΔP was calculated for each one and the baseline ΔP was subtracted from them, yielding a series of BC pressure values. All ΔP and P_{BC} values are shown in Table 2. On average the LV exerted 10.31 kPa of pressure against the balloon while the FPS was pumping on trigger.

(2)
$$P_{BC} := \frac{\sum_{n=0}^{n} \left(P_{PA}(n+1) - P_{VA}(n)\right)}{n} - \frac{\sum_{n=0}^{n} \left(P_{PB}(n+1) - P_{VB}(n)\right)}{n}$$

OUTPUT WAVEFORM PERIOD	AVERAGE ΔP (KPA)	STANDARD DEVIATION	P_{BC}
Baseline	20.20	0.61	-
500 ms -1	33.34	0.64	13.15
500 ms -2	30.17	0.40	9.97
400 ms	26.49	0.37	6.29
200 ms	32.01	0.53	11.81
		Average:	**10.31**

Table 2: Recorded ΔP values throughout second in-vivo procedure.

The most intriguing observation from the second in-vivo study was that the active patch device simulator was successful at relieving the sheep's MR. While the system was pumping on trigger it could be seen on an echocardiograph that the sheep's MR would consistently decrease. If the system was halted, the MR would return almost immediately. Figure 24 shows an image recorded on an echocardiograph of the sheep's LV and LA during systole with the simulation device inactive. The blue plume representing blood returning through the open mitral valve is quite prominent.[22]

[22] An echocardiograph set in color vector mode such as this one displays all flows moving towards the scanning probe in red and all flows moving away from the probe in blue.

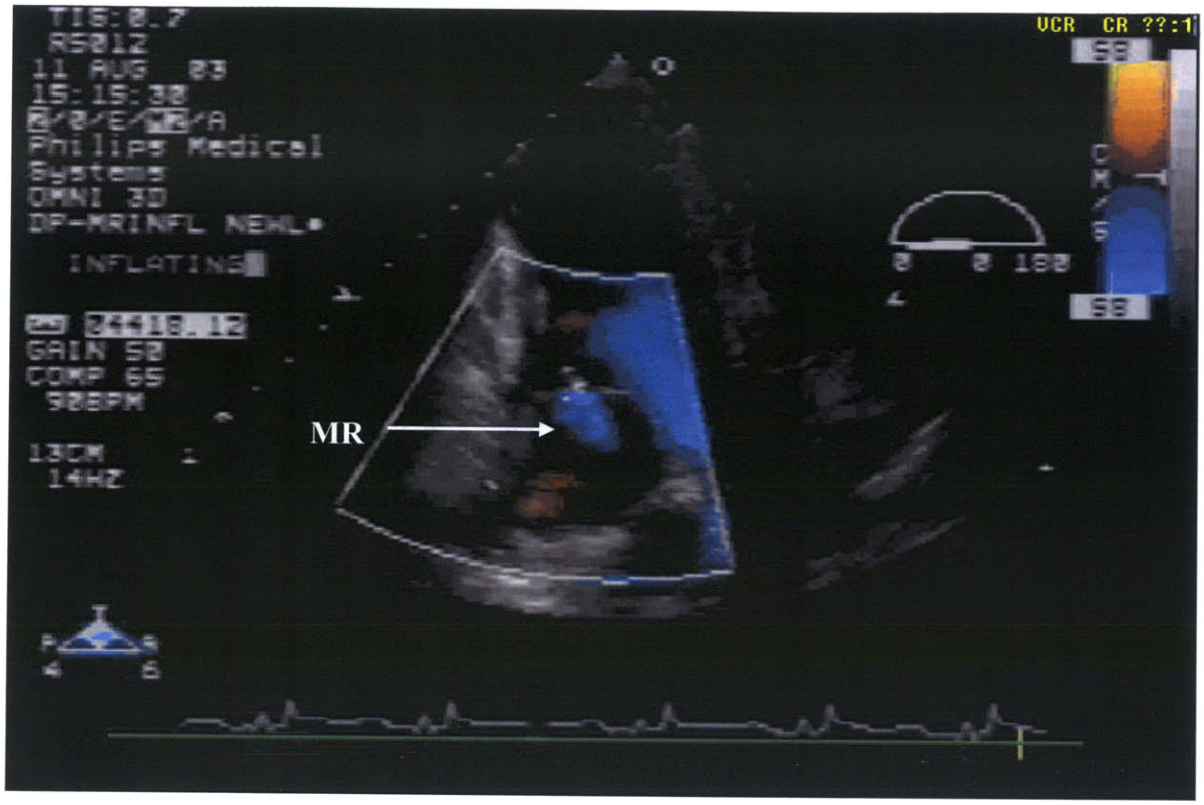

Figure 24: Echocardiograph image recorded during the second in vivo study showing prominent MR with the active patch simulation device inactive.

Figure 25 shows an image taken as the balloon was inflating on trigger with the heart.

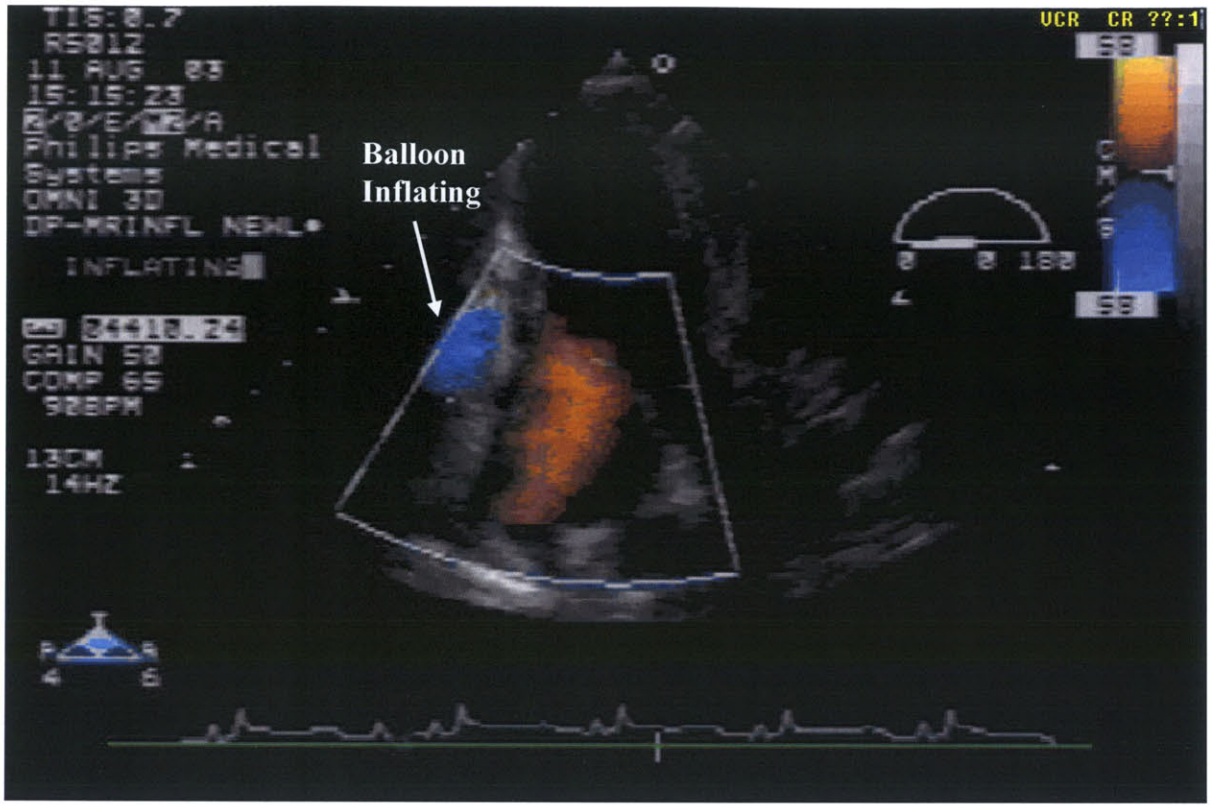

Figure 25: Echocardiograph image recorded during the second in-vivo study showing the AMP simulation device's balloon inflating on trigger with ventricular systole.

In comparison to Figure 24, Figure 26 shows an echo image of the sheep's LV and LA during systole. The MR plume is not present as it was in Figure 24. The MR was consistently reduced or eliminated each time the simulation device was activated.

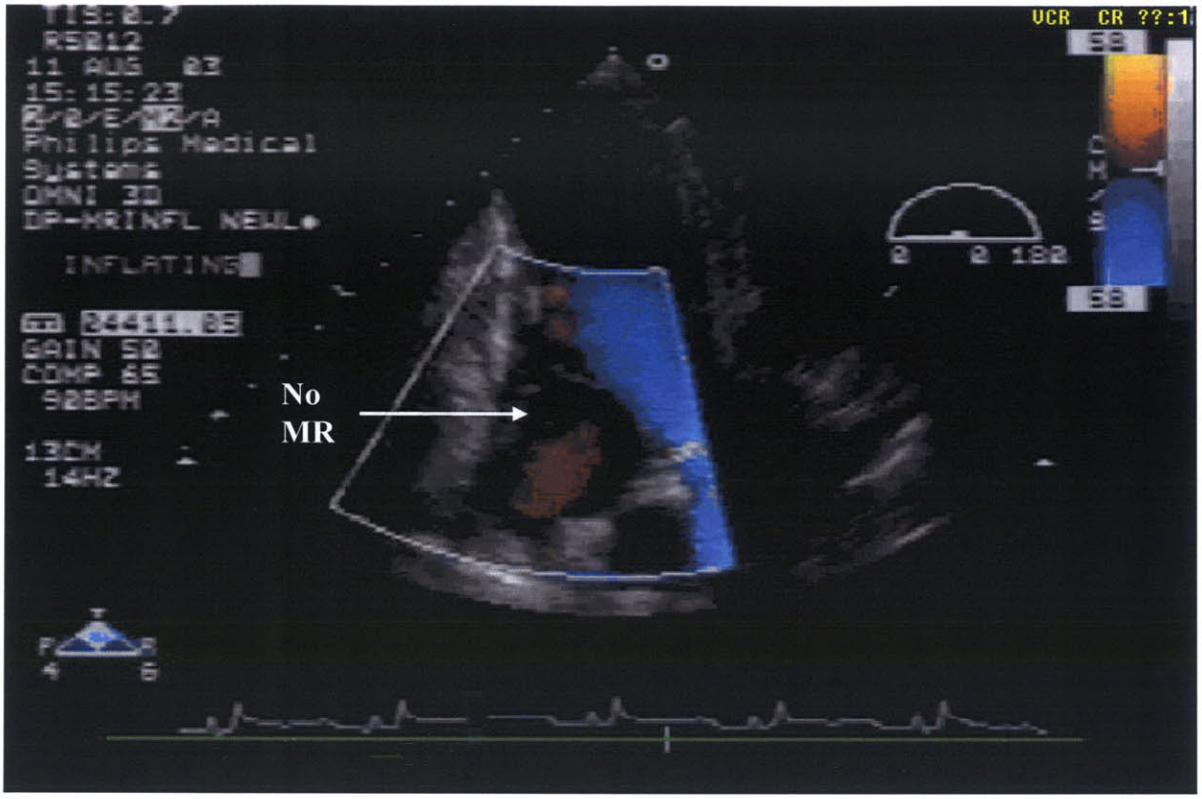

Figure 26: Echocardiograph image recorded during the second in-vivo study showing relief of MR by the active patch simulation device.

This relief of MR was obtained by filling the balloon with 8 mL of fluid. Post-operatively, this volume was injected back into the balloon in order to measure the depth of protrusion that the balloon was creating. Figure 27 shows an image taken with the balloon filled with 8 mL of fluid. From this image, the depth of protrusion was measured to be 12 mm.

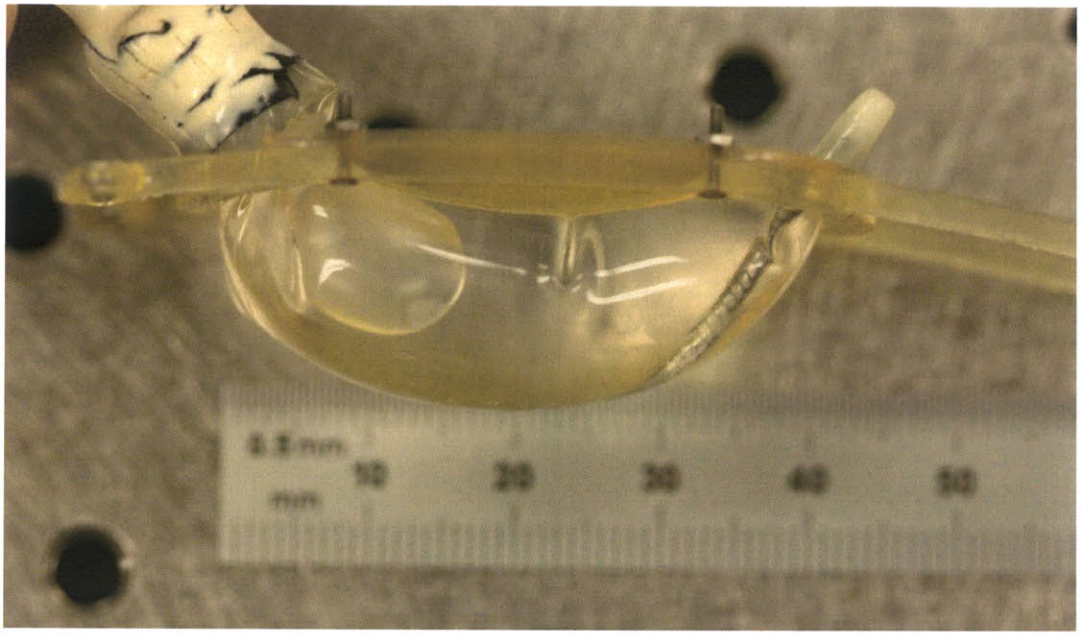

Figure 27: Balloon filled with 8 mL of fluid.

2.4.4 Discussion of Results

The healthy state of the test animal's heart greatly contributed to the overall success of this second experiment. Whenever the simulation device was inactive, the echocardiogram showed the MR consistently returning to its original level (prior to installing the base ring onto the LV). This made the effects of the simulation device on the MR quite apparent.

Although there was a significant amount of variation in the calculated BC pressures for different attempts, this experiment was very successful in establishing a lower bound for the pressure that an artificial muscle would be required to produce to affect MR in a sheep's LV.

Most importantly, the success of the active patch simulation device at relieving MR in this test animal proves the concept of active patch therapy, one of the major goals of this endeavor.

2.5 Future Research

There are a number of potential uses for the AP simulation apparatus in future research. It could be used to test various attachment configurations for an implantable device. One of the important issues to resolve for such a device is what configuration of suture points would produce the most efficient LV deformation to relieve MR. The AP simulation system could be used with a variety of base ring configurations to study this problem experimentally. Another potential avenue of research is into the timing of the FPS activation and duration, which could be further studied to enhance the output waveform and provide the most efficient MR relief. These data would provide a significant contribution to the development of a future AMP apparatus.

3 In Vitro Model Development

3.1 Background

Cardiology experiments are traditionally conducted in-vivo on sheep, pigs or dogs. It is currently the only method to test how a particular treatment or device will behave in a living system, which has many more variables than can be accounted for in a bench-top laboratory setting. In the case of novel instrument development, however, the laboratory development of an in vitro model offers several benefits. Even simple design problems can take many hours to correct and must therefore be dealt with prior to the start of an in-vivo procedure where time is critical. Furthermore, sensors of various types such as force transducers, motion sensors and even visual recording equipment can be integrated into the model to gather a baseline of experimental data that can be later compared to in-vivo results. In light of this, the development of an in-vitro simulation model for intermediary testing prior to an in-vivo procedure is advantageous for humanitarian, cost, and research reasons. Such models have been used in the past to show the particular mechanism of MR to great effectiveness[19]. With an in-vitro model to consult, almost all of the instrument's parameters can be resolved to a greater degree of certainty without the risk of a failed in-vivo procedure.

3.2 Design and Manufacture

In order to design properly an effective in vitro sheep heart model, it was necessary to base the dimensional criteria on an accurate representation. This was provided by Professor Peter Hunter of the Bioengineering Institute at the University of Auckland in New Zealand. Professor

Hunter's group developed a finite element model of the ventricles of a pig's heart (essentially the same as a sheep's heart) for organ function simulation and analysis with the Bioengineering Institute's in-house developed CMISS mathematical modeling software[20]. One of the boons of the CMISS software is that it is able to export its models in various formats such as the STL format[23] used by Stereolithography (SLA) machines. After receiving the file, the model was prepared and manufactured in high resolution mode[24] over an 18-hour period. The resulting model is shown in Figure 28.

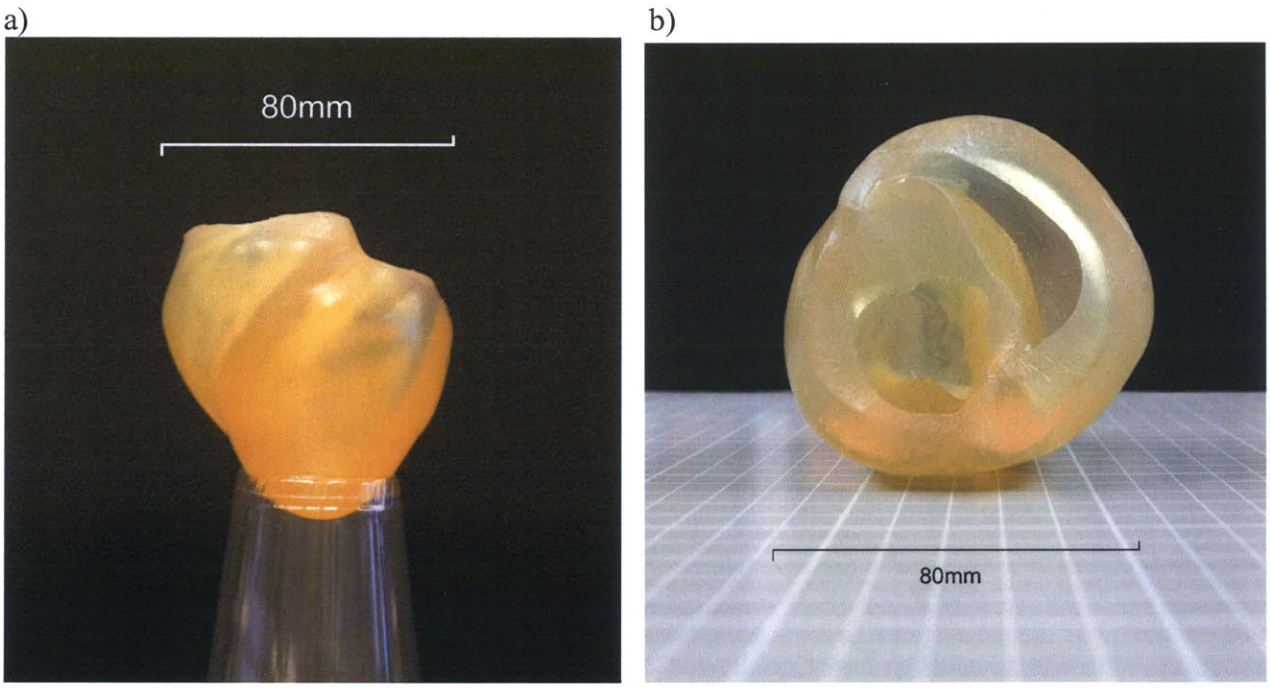

Figure 28: SLA manufactured model of a pig heart's ventricles: a) Side view; b) Top view.

This SLA-printed heart could not be used directly as an in-vitro model because of the inflexibility of its walls; however, it was an excellent starting point and, with some

[23] A file in STL format is essentially a cloud of points mapping the surfaces of the model. From these points, the surface of the heart is extrapolated.

[24] High resolution mode for a Viper Si2 SLA has 50 μm thick layers and a laser beam diameter of 75 μm. Low resolution mode uses a 100 μm layer thickness with a 200 μm beam diameter.

modifications, could serve as the foundation for the final instrument. The most important change required was to use a molded flexible polymer compound to replace the LV section of the model. For immediate purposes, the SLA heart model was used to size the various devices being developed for in-vivo testing and as a basis for sizing the following iteration of the in-vitro instrument.

3.3 Version 1.0

The development of a comprehensive in-vitro instrument would have required a substantial amount of time. It was decided that developing a simpler version that could be used sooner was best, and that the task of designing and building a more complex version could be addressed at a later time. The simplified design would be a half-ellipse of similar dimensions as the SLA model's LV and would be made from a polymer molding compound that would best match the properties of a sheep's LV wall.[25]

3.3.1 Design

The first step in developing this iteration of the in-vitro instrument was to design a negative mold in the shape of the desired LV ellipse[26] that was appropriate for the chosen molding compound. A flange was also added to the ellipse's edge so that it could easily be clamped into a holding frame. The mold was created in CAD, then manufactured using an SLA. Figure 29a shows the CAD assembly of the first version of the LV ellipse mold. Figure 29b

[25] See data and calculations from Section 2.4.3.

[26] The actual shape of the model is not perfectly elliptical. The peak of the ellipse was offset to one side to better approximate the geometry of a real sheep's heart. The result, as can be seen in Figure 29, is more of a half egg configuration but for simplicity's sake, it will still be referred to as the LV ellipse.

shows the resulting SLA part. All dimensions and schematics can be viewed in Appendix A, Figure 55. The mold was designed to have interchangeable male sections. The female section set the exterior dimensions of the mold while the male section could be modified to vary wall thickness (thus adjusting the flexibility of the ellipse's wall) and also to accommodate the different molding compounds and techniques to be used (casting and press-molding). It was designed to be used as a press mold for a high viscosity Silicone putty compound. As such, it was designed with much thicker walls than would be necessary for a regular casting mold in order for it to withstand the forces needed to press the silicone-epoxy paste into the mold shape.

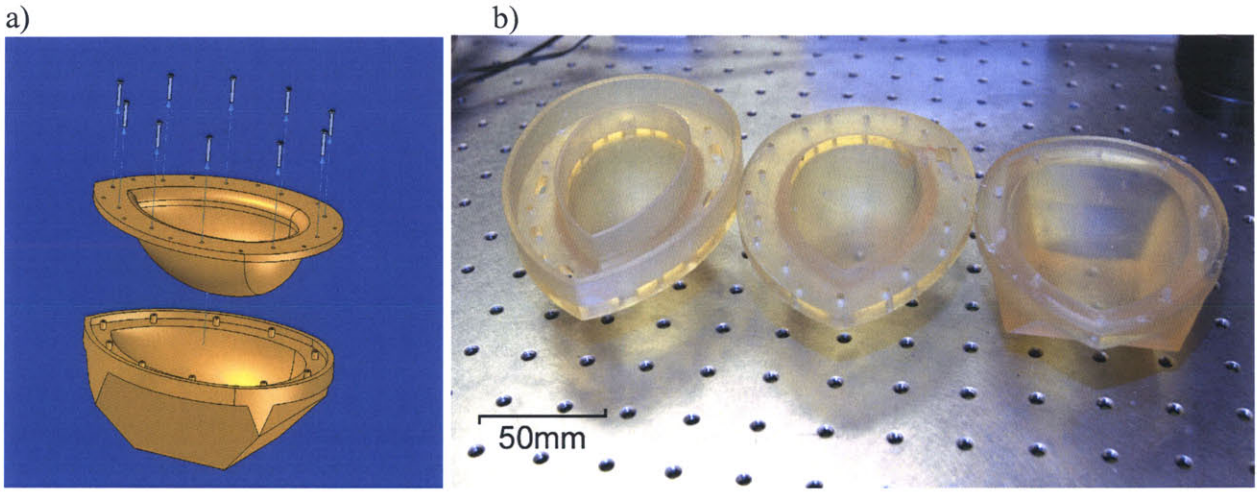

Figure 29: a) CAD assembly of the half ellipse mold Version 1. b) Photo of the SLA manufactured mold pieces.

3.3.2 Manufacture

Two types of molding compounds were tested in this mold. The first was President Putty/Putty Soft from Coltène[21]. It is a high-viscosity, fast-curing A-silicone-based putty designed to be used in a press mold for dental applications. The second was a low-viscosity, 24-

hour addition-curing silicone rubber made by Silicones, Inc.[22] designated P-4. The properties of the two compounds are listed in Table 3.

	P-4	COLTÈNE PUTTY
Mixing Time	-	45 s
Working Time	2 to 3 hours	130 s
Setting Time	16 to 24 hours	255 s
Strain in Compression	-	2.0% to 3.0%
Shore Hardness	41	-
Tensile Stregth	4.82 Mpa	-
Elongation	150%	-
Recovery after deformation	-	≥99.0%

Table 3: Properties of compounds used to mold the LV ellipse.[27]

The advantage of using the Silicone putty was that its curing time was approximately 5 minutes. As such, any mistakes resulting in an inadequate molding could be addressed without a significant time penalty. The disadvantages were that it cured so quickly that its working time was quite short (approximately 90 seconds), resulting in the first few iterations being unsatisfactory. In addition, the physical properties of the putty compound were not ideal, meaning that it would tend to yield stiffer ellipses than were desired. On the other hand, the P-4 silicone rubber required much more time, as it had to be vacuumed both prior to and after pouring into the mold to remove all air bubbles from the mixture. It also required 24 hours of curing time.

The different compounds required two slightly different types of molds. The Silicone putty needed to be pressed into the ventricle shape. This required the mold to be very sturdy. In light of this, the female section was designed with thick sidewalls and the male portion was designed with a flat top so that they could both easily be pressed together. The P-4 compound did

[27] Properties taken from the manufacturer's data sheet provided with each compound. Note that because of the provenance of the Coltène putty from dentistry, it was difficult to obtain standard mechanical specifications.

not demand any significant physical properties from the mold but did require that the top have many venting holes and a receptacle section around the venting holes to capture the excess mixture that seeped out while pressing the mold together and also while in the vacuum phase of the process. This enclosure also ensured that enough material was present to fill any voids that might form while moving the mold. Wall thickness for both moldings was 4 mm. All components for the mold were built using SLA.

3.3.3 Silicone Putty Molding

The Silicone putty LV ellipse was molded by mixing equal parts of the putty's two components together and kneading them by hand for approximately 60 seconds. The combined paste was then placed in the valley of the female mold and roughly distributed around the ellipse wall to help the mixture spread more easily during the actual molding process. (Mold release was generously applied to both parts of the mold before mixing the paste.) The male section of the mold was inserted into the female section and the mold parts were turned upside-down and pressed together by placing an 85 kg weight on top of them for 60 seconds.[28]

The first two attempts at molding the LV ellipse with the Silicone putty yielded poor results due to the mold either being too full and/or not being pressed enough during the working time, or not being filled enough and the compound not spreading to the flange's edges. After these two failed attempts, a successful iteration was created. The resulting molding is shown in Figure 30. This type of compound does not hold air bubbles within the mixture, however certain thin regions and voids existed where the mold could not be pressed together sufficiently enough before the compound set.

[28] The experimenter stood on top of the mold.

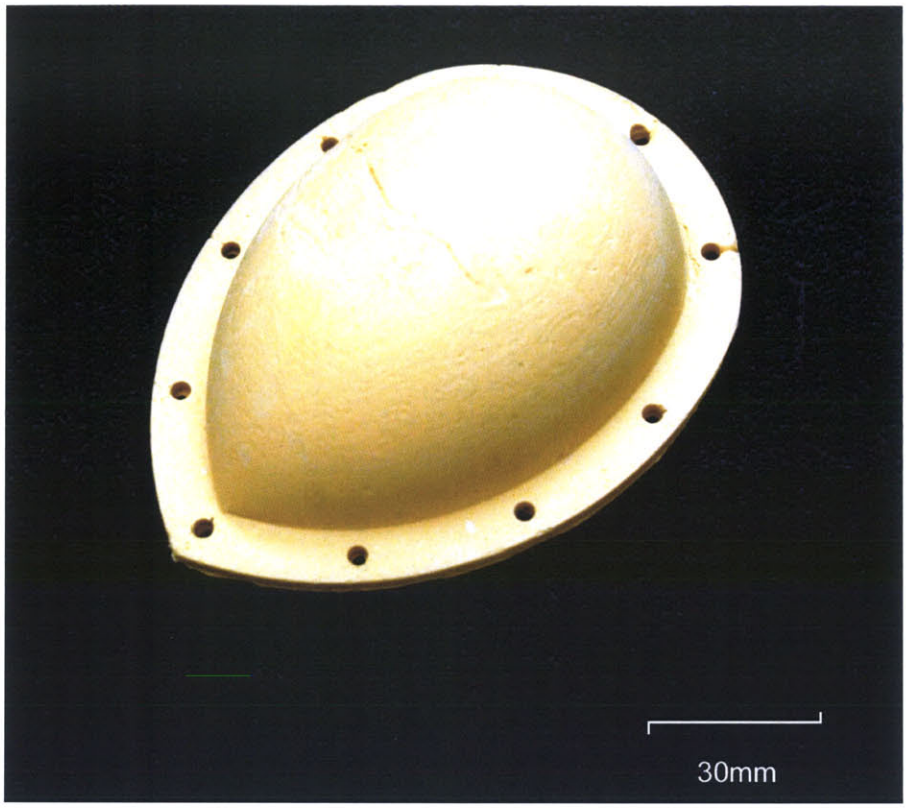

Figure 30: Isometric view of Silicone putty LV ellipse molding.

3.3.4 P-4 Silicone Rubber

Molding a ventricle using the P-4 silicone rubber was far less time critical than with the Silicone putty. The silicone rubber and hardener were mixed together in a 10:1 ratio (by weight), stirred thoroughly for 5 minutes then placed in a vacuum chamber for 15 minutes to remove the air bubbles from the mixture. A generous coating of mold release was applied to both parts of the mold during this time. When bubbles no longer rose to the surface of the mixture the silicone rubber was poured into the female half of the mold and the male half was pressed into it and screwed in place to align it properly. The mold was then placed back into the vacuum chamber for 45 minutes to remove all of the air bubbles contained within the mold. The mold was then

left to cure for 24 hours. The P-4 compound yielded a very good LV ellipse on the first attempt. Figure 31 shows the resulting molding.

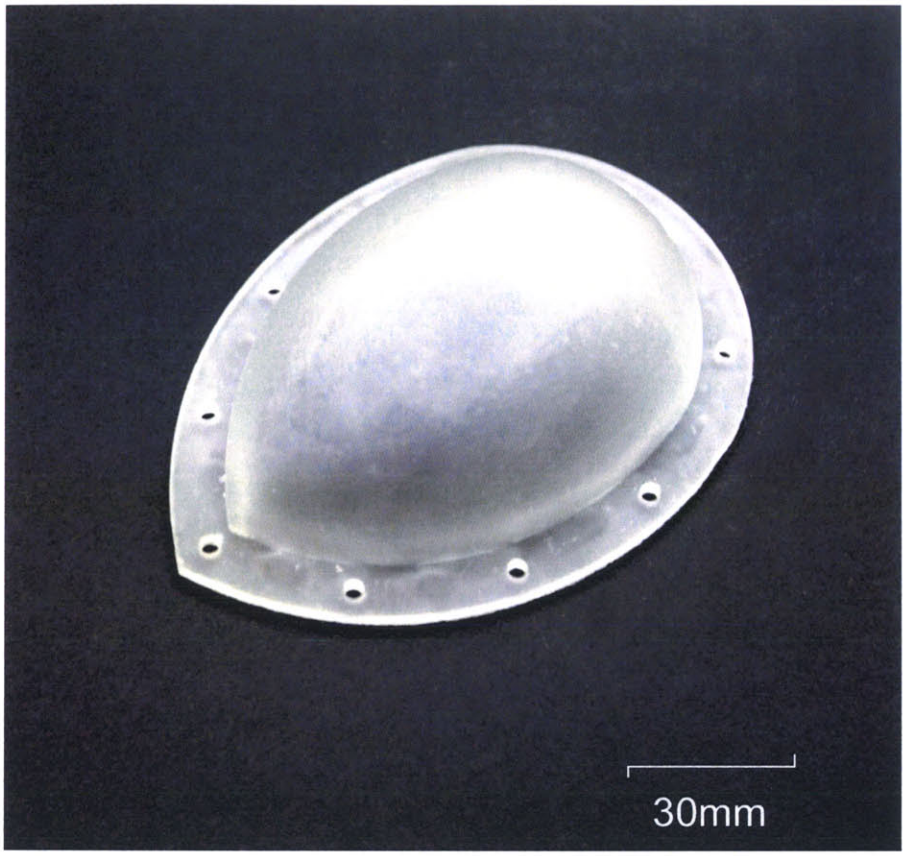

Figure 31: P-4 Silicone-Rubber molding of the in-vitro LV ellipse.

3.3.5 Ventricle Frame

Once the LV ellipse moldings were complete, the holding frame that would immobilize the LV ellipse and provide a steady base for experimentation was designed and manufactured. The frame was built to clamp the flange of the LV ellipse. A substantial protrusion was also added to one side of the frame to provide a location to fit the frame into a vise. The frame was manufactured on an SLA. Figure 32a shows the CAD assembly of the frame and LV ellipse. Figure 32b shows the constructed assembly. Dimensional schematics can be seen in Appendix A, Figure 56.

a) b)

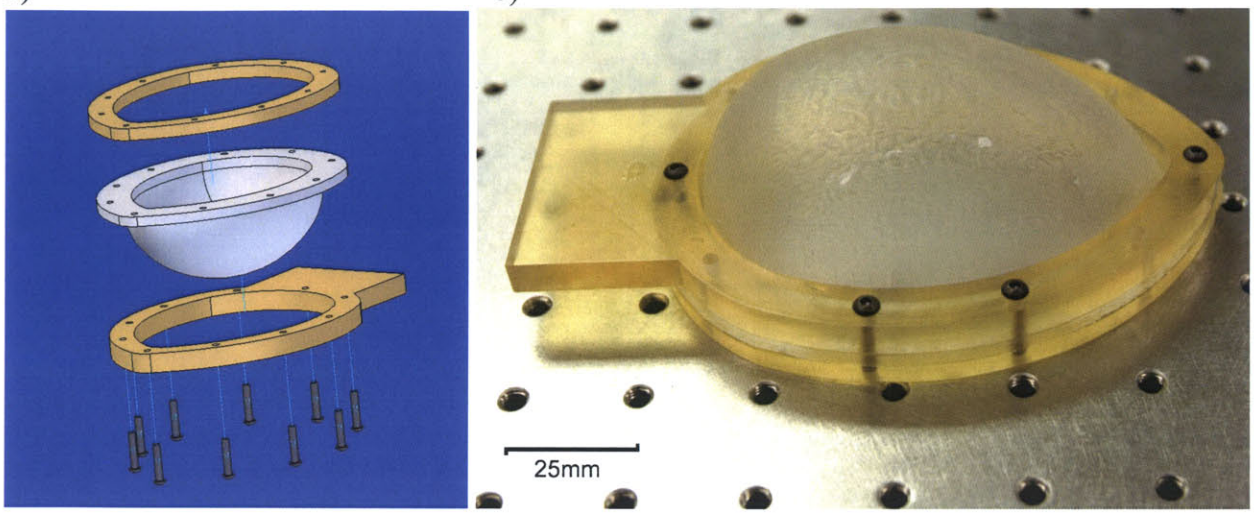

Figure 32: a) CAD assembly of the half ellipse in vitro model b) Photo of the SLA-manufactured frame and silicone rubber molded half-ellipse assembled for use.

3.3.6 Force Measurements and Redesign

Force measurements were taken at the peak of the ellipse by pressing a force transducer against the immobilized LV ellipse. The measurement was taken once the ellipse had been displaced inwards by 12 mm.[29] Figure 33 shows the experimental measuring setup. The results obtained from these measurements on both of the LV ellipses can be viewed in Table 4.

[29] Displacement figure was taken from the experimental value obtained from in-vivo experiment 2 (Section 2.4.3).

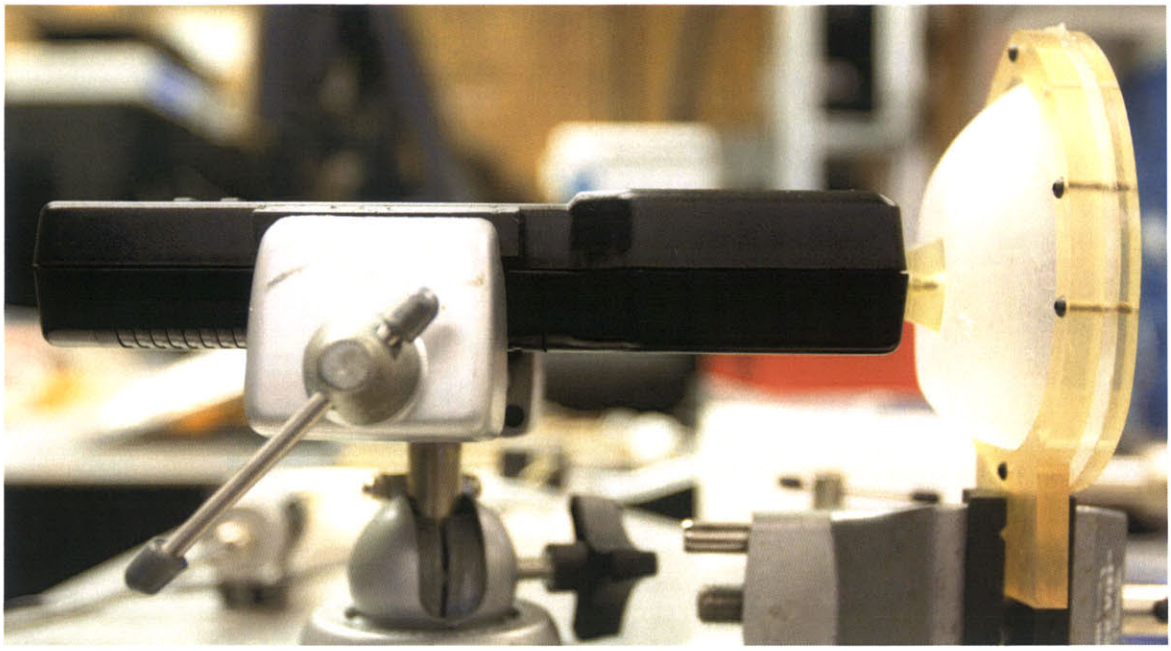

Figure 33: Experimental setup for force measurements of the P-4 Silicone-Rubber LV ellipse.

COMPOUND	FORCE (N)	AREA (M^2)	PRESSURE (KPA)
Silicone Putty	52.57	3.81E-04	138.05
P-4 Silicone Rubber	12.83	3.81E-04	33.69

Table 4: Results from force measurements of LV ellipse.

The results show that the Silicone putty ellipse is decidedly not flexible enough to serve as a good LV simulation. The P-4 ellipse was also not quite flexible enough but was overall a much easier compound to work with for this particular application. It was decided to create a new molding using the P-4 compound but to reduce the wall thickness of the ellipse in order to increase its flexibility and improve its performance relative to a real LV. A new male half was created with an SLA to give the molding a 2.75 mm wall thickness. A new ellipse was molded and the force measurements were redone on this version. This version only required 3.06 N (8.04 kPa equivalent) of force to displace its wall by the proscribed 12 mm, making it a much better instrument for its intended purpose.

3.4 Future Work

Future work to develop an in-vitro model of an LV could be very far-reaching. An ideal model would have a soft tissue-like reproduction of an entire heart along with pumps to actuate its cavities. For the active patch application, multiple position sensors could be embedded into the LV wall to allow a real-time observation of LV deformation with and without a patch device present. The pumps could also have alterable rates and strokes in order to modify the pumping rate, size and internal pressure of the simulated LV. This would provide excellent testing for a device that needs to function under various conditions (such as while a patient is exercising). Such a device could also be easily modified for use in research on other cardiac conditions currently under study, such as an enlarged heart.

4 Shape Memory Alloy AMP Prototype Development

The final goal of this research project was the design, development, and testing of an active muscle patch based on shape memory alloy technology. This chapter introduces that technology, reviews the designs considered, and discusses the results of the two AMP iterations developed. The section ends with future plans for research in this area.

4.1 Background on Shape Memory Alloy

Shape memory alloy (SMA) is an alloy that undergoes a phase transformation in its crystal structure that changes the material's shape and properties when it is heated above a particular temperature[23]. When the SMA is brought above this transition temperature it changes from the Martensitic state to the Austenitic state. This is characterized by a change from an acicular crystal structure of Martensite to the face-centered cubic structure of Austenite[24,25,26]. Martensite is weaker than Austenite but it is a very elastic form of the NiTi alloy. Its deformation stress ranges from 70 MPa to 140 MPa[30] but it can absorb up to 8% recoverable strain. In comparison, Austenite is not elastic but its yield strength ranges between 240 MPa and 690 MPa[23]. The transition temperature of the alloy varies depending on its proportions of nickel and titanium. The SMA wires used in this series of experiments were Flexinol™ wires purchased from Dynalloy Inc.[27]. This variety of SMA is a Nickel and Titanium alloy that has a transition temperature of 70°C[31].

[30] The exact value depends on specific alloy content.

[31] All future references to Shape Memory Alloy (SMA) wires are to the Flexinol™ Ni-Ti alloy.

4.2 Potential Designs

Many designs for the use of SMA wires in a semi-implantable AMP device were conceived. The greatest design challenge for an SMA device was to amplify the SMA's displacement (4% of its length) in order to produce a 12 mm protrusion[32] into the LV. Furthermore, an implantable device had to meet certain size constraints in order to properly fit into the sheep's chest cavity and not obstruct normal heart function. A summary of the established criteria is shown in Table 5.

CRITERIA	VALUE
Size (approx.)	60 mm length by 30 mm width by 10 mm height
Operating Frequency	2 Hz[33]
LV Protrusion Depth	12 mm
Minimum Protrusion Pressure Output	13.15 kPa[34]

Table 5: Summary of design criteria for SMA prototype.

Most designs were eliminated due to impracticality. Two designs were taken to early development. The first used a lever to achieve its displacement magnification while the second used a sliding mechanism to bend a thin piece of stainless steel shim.

4.2.1 Lever Prototype

4.2.1.1 Design

The first design to be prototyped was based around a lever in order to achieve the 12 mm protrusion required to affect MR in the LV. The lever ratio to obtain 12 mm of protrusion was calculated and a lever was designed that would fit within the size constraints of an implantable

[32] Calculated from the experimental data in Chapter 2.

[33] A 2 Hz (120 bpm) heart rate is the upper norm for a stabilized sheep under anesthesia.

[34] 13.15 kPa was the highest value obtained from the second in vivo procedure (Section 2.4.3). The highest value was used in order to set a conservative lower bound for the design criteria.

device. A curved surface or paddle at the lever's contact point was also added to the lever in order for it to depress more evenly a larger region of an LV. An analysis was performed to determine the optimal lever arm angle and the force required from an SMA wire. This helped determine the proper diameter SMA wire. According to the calculations shown in Appendix C, a wire producing a force of approximately 6N was required. This corresponded to an SMA wire of 200 μm in diameter.[35] A frame to hold the lever and the SMA wires was then designed. Two counteracting SMA wires were incorporated into the design. The first wire would extend the protruding lever while the second would retract it and reset the device. The resetting wire would need to be wound around a pulley for it to attach onto the lever from the opposite side. Figure 34 shows the CAD assembly of the Lever prototype. Dimensional schematics can be seen in Appendix A, Figure 57.

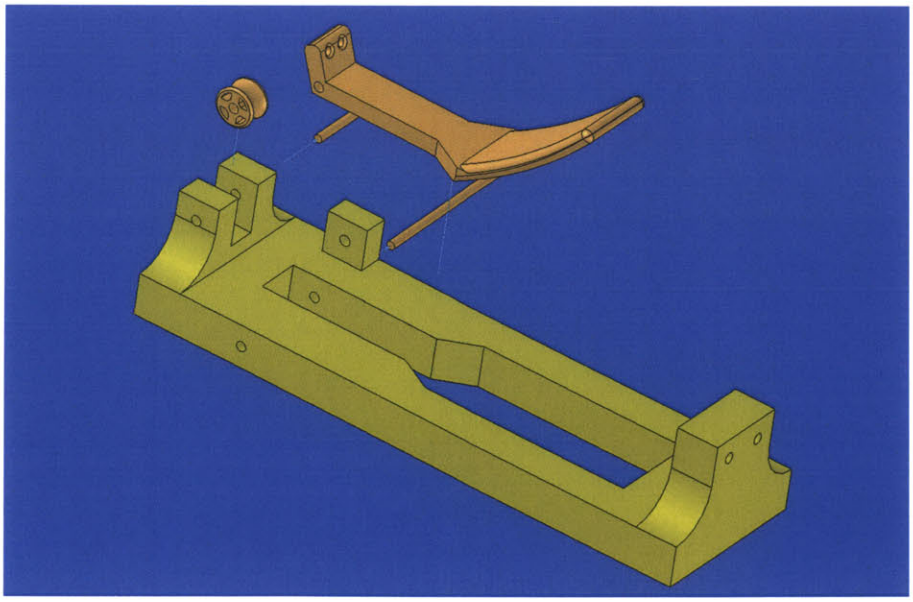

Figure 34: CAD assembly of lever prototype.

[35] Calculation made from manufacturer's published specifications.

4.2.1.2 *Manufacturing and Assembly*

The lever prototype's components were manufactured on an SLA. All parts were assembled and the SMA wires were tied through two holes to the lever's arm and run to two 1.6 mm screws on the frame's end. These also served as the electrodes where power supplies could be connected. Figure 35a and Figure 35b show the final assembly while Figure 35c shows the device with its lever deployed.

a)

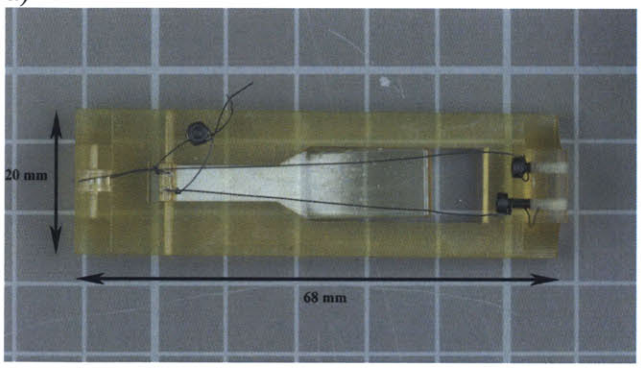

b)

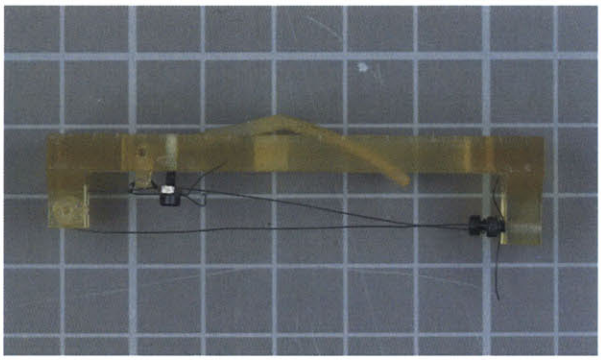

c)

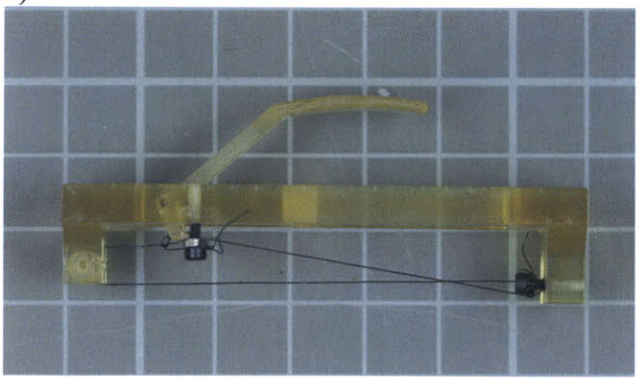

Figure 35: a) Top view of manufactured assembly; b) Side view of manufactured assembly; c) Lever prototype with lever deployed.

4.2.1.3 Testing

Testing of the lever design was done by connecting two power supplies to the device, one to each of the 1.6 mm screws. The two wires were of different length and therefore required different voltages to achieve a 1 A activation current. The protrusion wire's electrical resistance was calculated at 2.36 Ω[36] while the resetting wire's resistance was 1.57 Ω.[37] The protrusion wire therefore required 2.36 V while the resetting wire required 1.57 V to reach 1 A according to Ohm's law (Equation (3)).[38]

(3) $V = R \times I$

During testing, the device achieved approximately 12 mm of protrusion depth, but the activation of the SMA wires was very slow relative to the desired operating frequency of an implantable device. The slow activation also meant that the wires would convey more heat to the SLA resin and would melt it wherever the two came into contact (such as the pulley and the attachment points of the lever).

4.2.1.4 Status

At present there are no plans to further the development of this prototype, although its principles are sound. The design could be improved and problems addressed at a later date.

---

[36] Note that the electrical resistance of an SMA wire changes as it transitions from Martensite to Austenite. This value can only be used as a baseline for the voltage requirement.

[37] Based on manufacturer's published specifications[27].

[38] 1 A maximum sustained operating current obtained from the manufacturer's published specifications for 250 μm wire[27].

4.2.2 Bowing Shim Prototype

4.2.2.1 Design

The second prototype to be developed used a mechanism that would slide upon SMA wire activation, causing a thin piece of stainless steel shim to bow outwards. The advantages of this design were that the bowing shim would by nature provide a fairly large, curved, protruding surface, and more importantly, the bending of the shim through lateral compression would inherently provide a self-resetting element for the SMA wires. The disadvantage of this design was that there was no significant mechanical amplification of the SMA wires' displacement. Longer wires would need to be incorporated into the design in a shoelace configuration, wound around a rod on each end of the frame. This configuration enabled the wire to be crossed five lengths of the frame giving each wire a length of 300 mm. A Macor[39] rod was used on each end of the frame instead of SLA manufactured pulleys in order to avoid the melting issues encountered with the lever prototype. The shim would be held by two end caps. One would be fixed to the inside of the frame by a rod running through it, allowing the cap to swivel as the shim bows outwards. The other cap would be free to slide in a track on the inside of the frame. The free cap would have two screws in it where the SMA wires would attach. Figure 36 shows the CAD assembly of the bowing shim prototype. Dimensional schematics can be found in Appendix A, Figure 58.

[39] Macor is an ultra-high temperature glass-mica ceramic characterized by its good machinability.

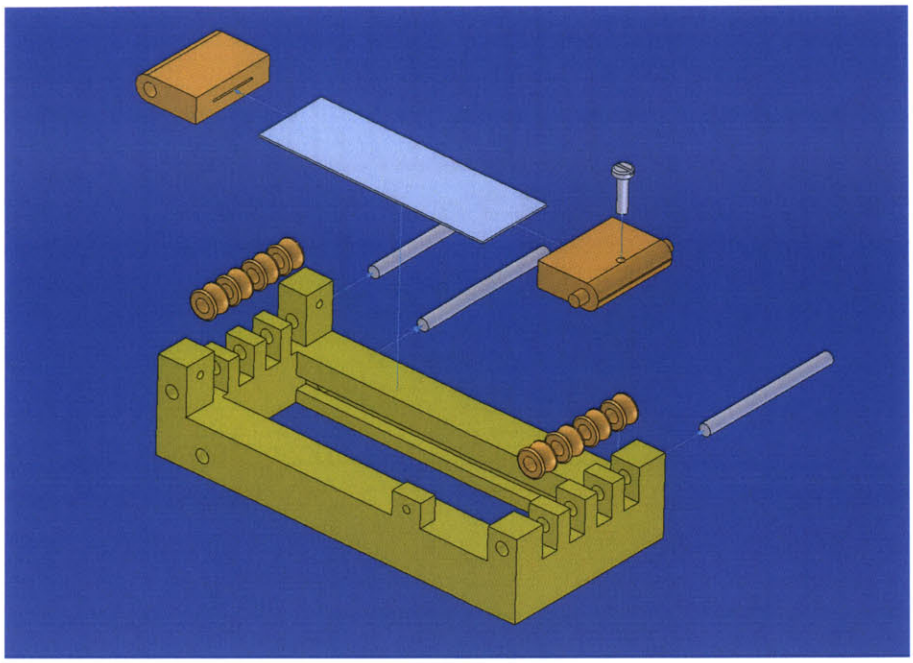

Figure 36: CAD assembly of bowing shim prototype.

Two wires would be used in this design. They would be activated alternately to allow one wire to cool down while the other wire contracted. This would allow the device to cycle more quickly.

4.2.2.2 Manufacturing and Assembly

The bowing shim prototype's frame and shim caps were manufactured on an SLA. The Macor rods were purchased in the right diameter (1.6 mm) and were cut to the width of the frame. They were then inserted into holes running through posts on each end of the frame. Two 200 μm diameter by 300 mm length SMA wires were held to the sliding end cap by pinching their ends against the cap with the screws. The free ends of the wire were run off to the side of the frame where a screw was placed to act as the grounding electrode. The wires were looped back and forth five times and pinched against the frame with two 1.6 mm by 10 mm screws that

also served as each wire's electrode. Figure 37a and Figure 37b show a top and isometric view of the assembled bowing shim prototype.

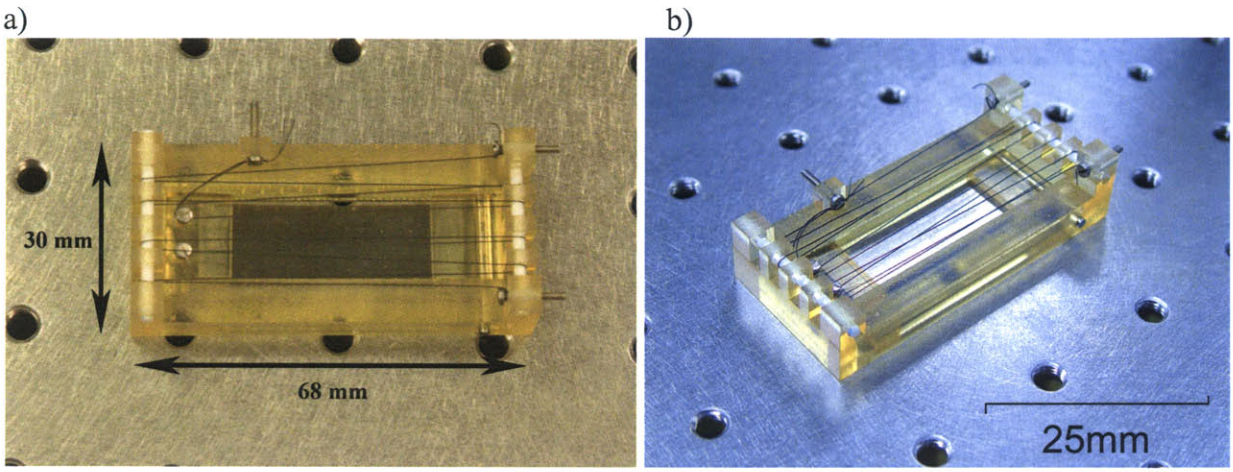

Figure 37: a) Top view of bowing shim prototype; b) Isometric view of bowing shim prototype.

4.2.2.3 Testing

The prototype was set up in a small vise for stability and a power supply was attached to each of the SMA wires. The two 200 μm diameter by 300 mm length wires had a calculated electrical resistance of 9.5 Ω each. This required the power supplies to be set to 5.8 V to provide the wires with a 610 mA operating current.[40] The power supplies were triggered manually in sequence once the shim pushed the SMA wires back to their at-rest position. The shim did successfully bow outwards by approximately 12 mm, as shown in Figure 38, but it quickly became apparent that the bowed shim could not produce enough force to reset the SMA wire quickly enough. This essentially negated the advantage of having two alternately actuating wires. Furthermore, the power source used to activate the SMA wires was not ideal. A 610 mA constant

[40] 610 mA sustained operating current obtained from the manufacturer's published specifications for 200 μm wire[27].

operating current was recommended in the manufacturer's specifications but this actuated the wires very slowly. A higher current could be used for shorts periods of time.

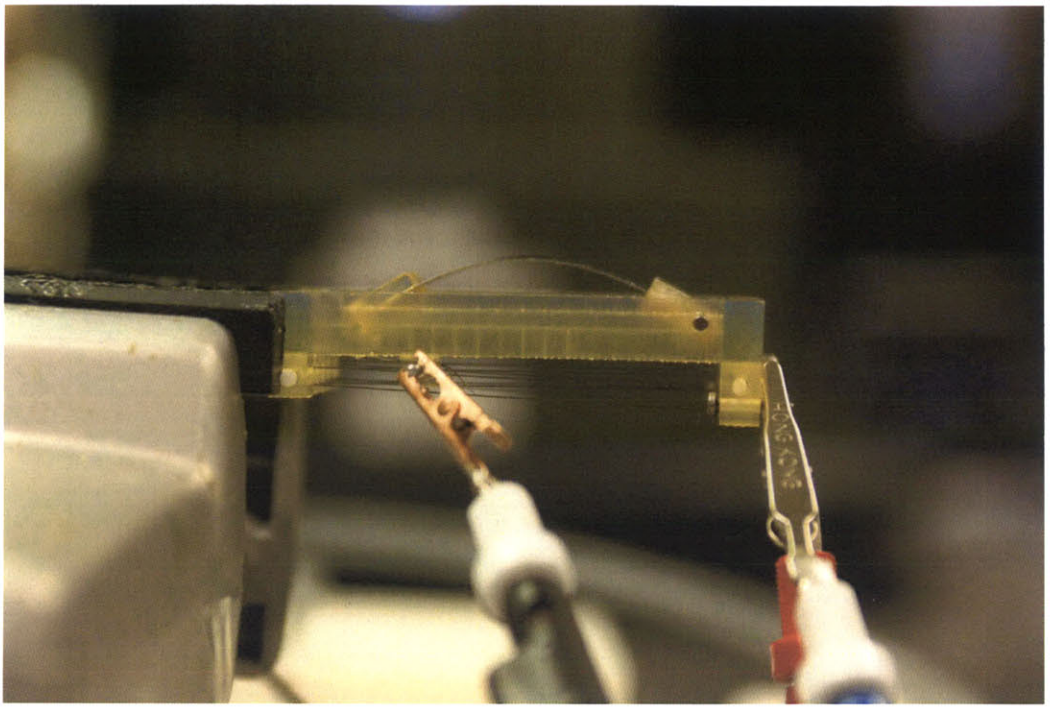

Figure 38: Bowing shim prototype actuating during testing.

4.2.2.4 Status

Although this first iteration of the bowing shim prototype had shortcomings, its development continued with modifications, leading to version 1 of the SMA AMP device discussed in the following section.

4.3 SMA AMP Device Version 1

4.3.1 Design

The first full version of the SMA device used a mechanism that was essentially the same as for the bowing shim prototype. Modifications to the original mechanical and electrical designs resulted in improved performance and brought it closer to an implantable prototype.

4.3.1.1 Mechanical System Modifications

The most significant modification to the bowing shim design was to incorporate four wires into the device. The published specifications for SMA wires recommended a 5.5-second cool-down time for a 250 μm diameter wire[27]. If only two opposing wires were used, each would be under electrical tension for approximately 100 ms and would rest for approximately 400 ms.[41] In order to increase the length of the rest period for each wire, two additional wires were added. These could be actuated in sequence to give each wire a 100 ms uptime with a 900 ms downtime. This 900 ms rest period was still not equal to the manufacturer's recommendations but it was estimated that it would be long enough to allow the device to function for brief periods of time. The addition of two more wires also doubled the number of wire lengths crossing the top of the device. This meant that the pulley slots at each end of the frame had to be doubled in number and each had to be narrowed in order to maintain a reasonably compact form factor for the frame. Ceramic pulley wheels each 2 mm wide with a 1.6 mm rod running through them were designed to fit into each slot. Two new screw-electrodes also had to be added to the frame's end. Finally, the frame itself was given a curved base to better fit

[41] Time estimates based on a 2 Hz (120 bpm) pulse, the upper norm for a stable test animal.

onto the epicardium of the LV. Figure 39 shows the CAD assembly design of the modified frame. Dimensional schematics can be seen in Appendix A, Figure 59.

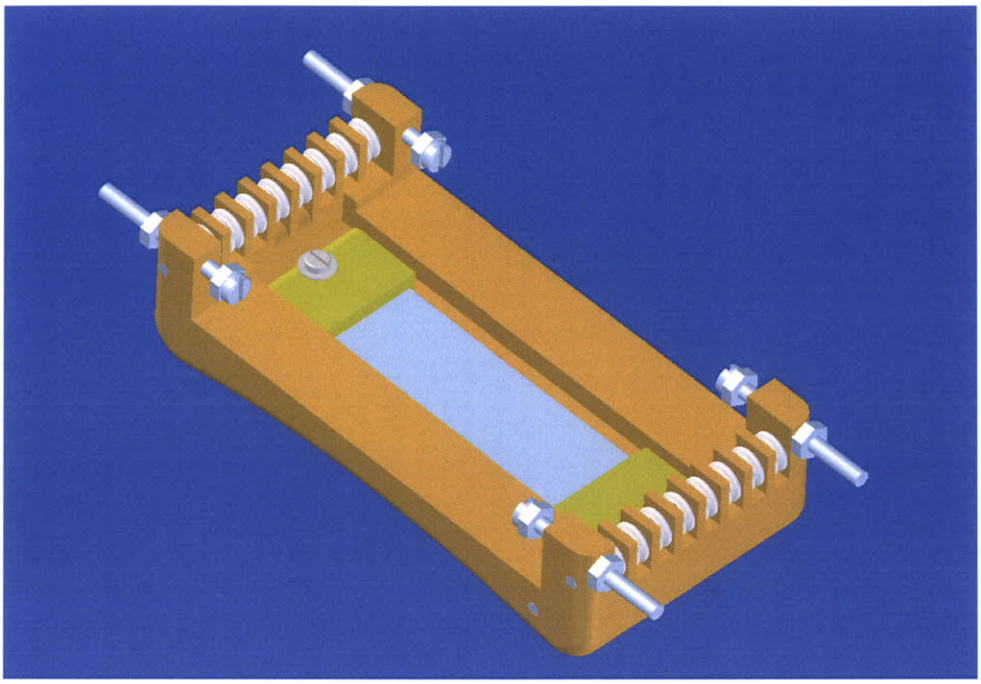

Figure 39: CAD assembly of SMA AMP device Version 1.

4.3.1.2 Electrical System Modifications

As noted during the testing phase of the bowing shim prototype, the contraction of the SMA wires when using a DC power source was too slow to actuate the wires at the desired rate. The updated design employed large electrolytic capacitors instead of DC power supplies. The capacitors used were Mallory 33 mF, 75 V electrolytic capacitors. The charge capacity of these capacitors was calculated based on the Joule heating required to bring a 350 mm long, 250 μm diameter SMA wire to its transition temperature of 70°C. Equation (4) was used to calculate the mechanical work performed by the SMA wire. Since SMA has an electrical to mechanical

energy transfer efficiency of 3%, the number yielded by Equation (4) was divided by 0.03 to find the electrical energy required to heat the wire[28].

(4) $$W := F_{SMA} \cdot \Delta L$$

It was calculated that 4.7 J would be needed to heat the wire to above its transition temperature. Four 33 mF electrolytic capacitors were available from lab stores. Equation (5) was used to calculate the voltage required to store the 4.7 J of energy in 33 mF capacitors.

(5) $$E := \frac{1}{2} \cdot C \cdot V^2$$

It was calculated that the capacitors would need to be charged to 16.9 V in order for them to store the required amount of energy (shown in Appendix D). This number was rounded up to 20 V to compensate for the fact that a capacitors discharge follows a negative exponential curve, and the end of the discharge would be too slow to be effective. The discharge time would be regulated manually.

4.3.2 Manufacturing and Assembly

The frame and shim end caps were manufactured on an SLA, then assembled with an 45 mm long by 12.7 mm wide by 150 μm thick piece of shim. Ceramic pulleys were machined[42] and inserted into each slot (16 in total) and a 1.6 mm stainless steel rod was inserted through each set of 8 pulleys at each end of the frame. A 1.6 mm rod was inserted into the frame through

[42] This process is discussed further in the next subsection.

the static shim end cap. Four 350 mm long by 250 μm diameter wires were cut and screwed down, two facing in each direction along the frame's length, into the sliding shim end cap with a 1.6 mm screw and washer. The wires were threaded five times across the length of the frame and pinched between the screw head and a nut of an M1.6 by 20 mm long screw. Each screw was entered through a 1.6 mm hole in the screw-electrode mounts on each corner of the frame. A nut was placed on the opposite side of the mount to allow the tension on the wire to be adjusted. Two 120 V, 0.25 A power supplies were each connected to two 33 mF capacitors. High-current rated toggle switches were placed after each capacitor and the toggles' outputs were each connected to one of the SMA wires' electrodes. This allowed each wire to be toggled on and off manually. Figure 40 shows a photo of the device assembly.

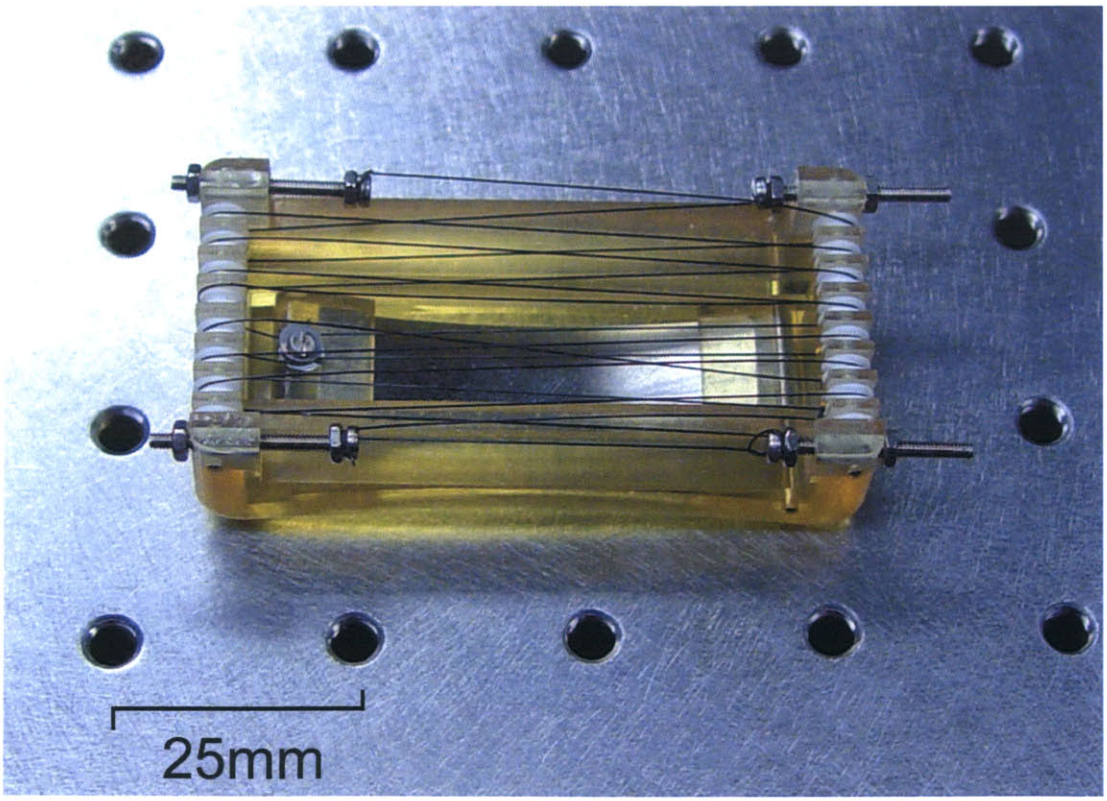

Figure 40: Final assembly of SMA AMP device Version 1.

4.3.2.1 Ceramic Pulley Machining

Machining small components from ceramic is inherently difficult even when dealing with machinable ceramics such as Macor since it easily chips or breaks. Proper execution of the SMA AMP device required 5 mm diameter pulley wheels machined from ceramic that would allow SMA wires looped around the ends of the base frame to roll smoothly and not hinder the device's actuation while at the same time electrically isolating the wires from one another. The CAD design of these pulley wheels is shown in Figure 41 while the dimensional schematics can be seen in Appendix A, Figure 60.

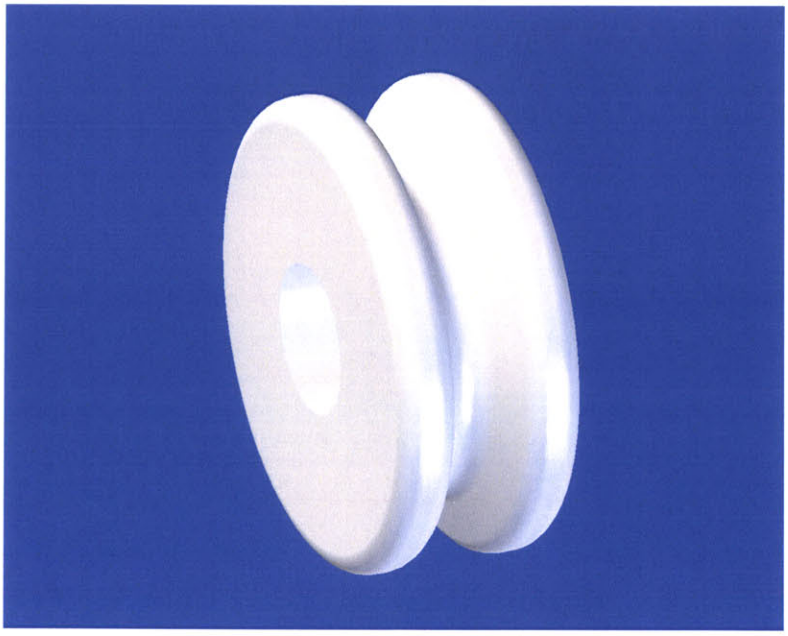

Figure 41: CAD of Macor pulley wheel.

The pulley design is quite simple but the wheels' scale made their production using only a CNC lathe problematic. The stock used for the wheels was a 6.35 mm rod of glass-mica machinable Macor. The profile of the wheel could be turned fairly easily using a very low material removal rate but the wheels could not be cut off without breaking the rod where the

collet of the lathe held the stock. A two-part process was developed where the profile was turned on a Mazak CNC lathe and the wheel was separated from the stock on a HAAS 3-axis CNC mill using a custom-built cutoff jig. A buffing grinder was then used to finish the sides of the wheels. The cutoff jig needed for the 3-axis mill enabled the mill to perform a precise cut at a reasonably high throughput rate. The jig was machined from a 50 mm by 50 mm by 20 mm thick block of aluminum. A 2 mm high step was machined out of one of its sides and two holes were drilled near the edge of the step where a carbide grit saw blade was bolted. Figure 42 shows the assembled cutoff jig.

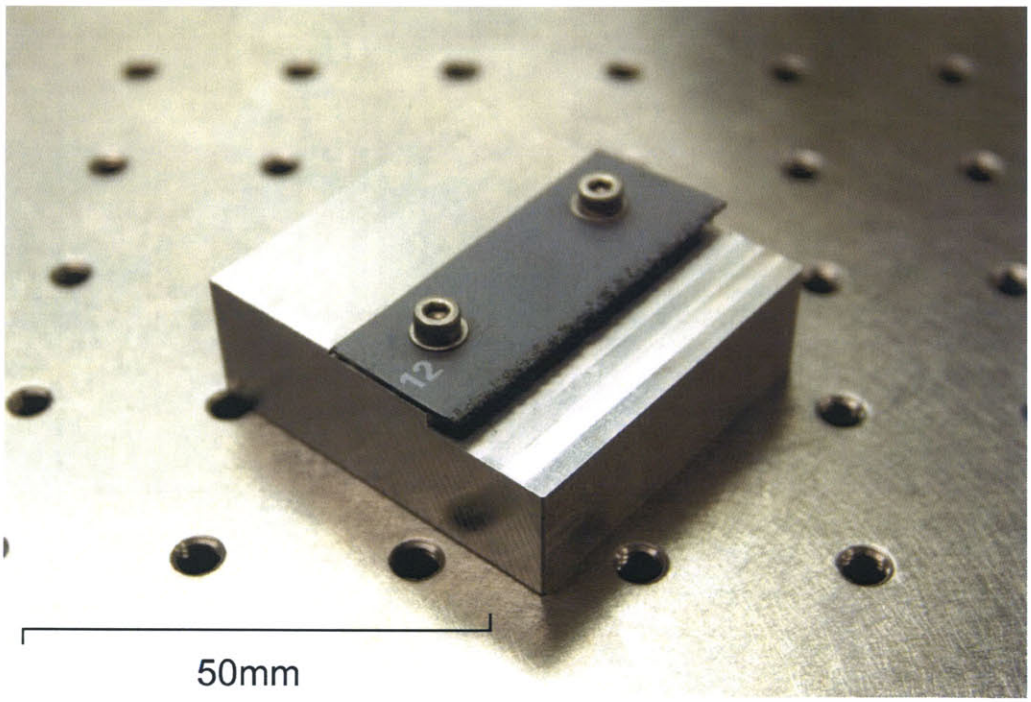

Figure 42: Ceramic pulley wheel machining cutoff jig.

Once assembled, the jig was secured in a vise and the Macor rod with the turned wheel profile was inserted into a drill chuck in the mill's spindle. The wheel was touched down against the step's bottom, then the rod was slowly fed against the carbide grit blade. Only a small

amount of finishing work was required to deburr the wheel's inner edge and to adjust the thickness of the wheel down to 2 mm.[43] Figure 43a and b Figure 43show a finished wheel.

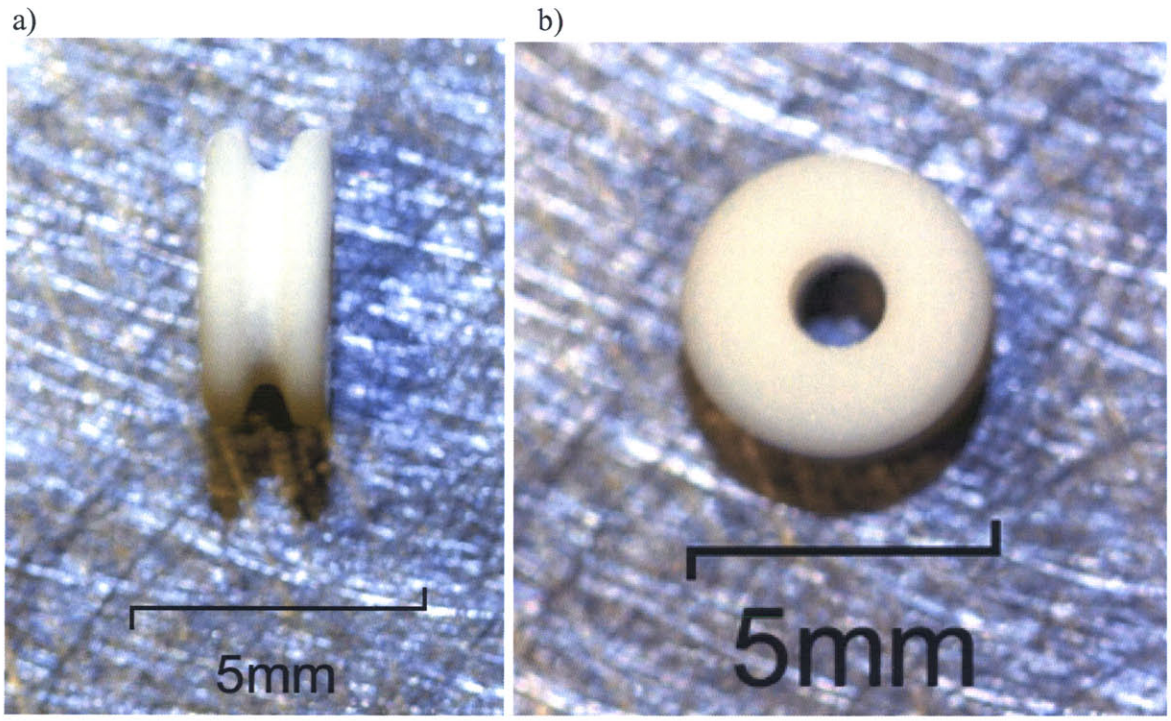

Figure 43: Ceramic pulley wheel, finished product: a) Frontal view; b) Side view.

4.3.3 Testing and Analysis

Tests were performed on this shim bowing device to see if the mechanism functioned as effectively as desired. First, a test of the device's outward displacement of the shim was measured. A power supply was connected to a 33 mF electrolytic capacitor that was in turn connected to a toggle switch. The toggle switch's output was connected to one of the device's protrusion wires.[44] The power supply was set to 20 V and the capacitor allowed to charge for at

[43] Since the carbide grit blade was not perfectly straight, there were some variations in wheel thicknesses after the cutoff step.

[44] For ease of reference, the wires that bow the shim are referred to as protrusion wires while the wires that return the shim to its original flat position are referred to as resetting wires.

least 10 seconds. Once the capacitor reached its set voltage the toggle switch was triggered and the wire bowed the shim to a bulge that extended 13 mm out from the frame.[45] The force output of the device was also measured. With the same electrical connections in place, the device was placed in a clamp with the shim in the vertical plane when at rest. An Extech Instruments 475040 force transducer was placed beside the device with the transducer's probe 5 mm away from the frame's edge. The toggle was triggered for approximately 1 second and the force on the transducer's gauge was recorded. This procedure was repeated three times then the transducer was moved 3 mm away from the frame's edge. This did not have a significant effect on the result. Table 6 shows the results obtained from the series of tests.

ATTEMPT	FORCE (N)	AREA (M^2)	PRESSURE (KPA)
1	13.42	2.65E-04	50.66
2	14.14	2.65E-04	53.38
3*	15.14	2.65E-04	57.15

*Measurement taken at 3 mm from base.

Table 6: Force measurement results from tests to SMA AMP device Version 1.

The area in Table 6 was calculated from the dimensions of the probe used at the tip of the force transducer. A probe approximating the profile of the simulation apparatus' balloon was manufactured on an SLA. This was done to better compare the pressure output of the SMA device with the data obtained from the simulation experiments. As can be seen, the pressure output of the device surpasses by far the 11 kPa minimum determined from the experiments.

Once these tests were performed, all of the wires were connected to their power sources. The wires were manually actuated in sequence every second. This form of actuation is decidedly

[45] Measured by placing a ruler on the frame beside the shim bulge.

imprecise but accomplished the main goal, which was to see if this method of actuation was feasible or if the opposing wires would place too much stress on the wire connections.

4.3.4 Status

The mechanism was tested and performed well enough to warrant further development. Certain shortcomings such as the wire connections would have to be improved before a successor to this design could be taken to an in-vivo test. It should also be tested on the in-vitro model described earlier but the frame first had to be redesigned to include loops that can be used to suture the device to the LV ellipse's surface and ultimately to an in-vivo animal's epicardium.

4.4 SMA AMP Device Version 2

4.4.1 Design

SMA AMP Version 1 served to test the function and feasibility of the shim bowing mechanism for potential use in an implantable device. Version 2 of this AMP device functioned in the same fashion as Version 1 but its packaging and electronics were built according to the specifications required for in-vivo testing.

4.4.1.1 Mechanical System Modifications

In the second iteration of this device, the shim bowing mechanism remained identical to the one in Version 1. Changes were made to compact the device's frame as much as possible to enable it to properly fit inside of a sheep's pericardial space. Version 1's frame was relatively quite thick. This was purposely done after discovering in an early version of the original bowing

shim prototype that the entire frame would flex under the strain of the SMA wires. In order to avoid this problem in Version 2, a 1.6 mm diameter cylinder was removed from the length of the frame and replaced with a stainless steel rod to increase the frame's stiffness. The frame's width was reduced by thinning the separators between each Macor pulley and also thinning the electrode posts at each corner of the device. Overall, the frame's dimensions were reduced from 70 mm long by 35 mm wide by 19 mm thick for Version 1 to 65 mm long by 27.3 mm wide by 14 mm thick for Version 2. Suturing loops also had to be added to the frame's exterior to allow the device to be fixed to the in-vitro testing apparatus and eventually to a sheep's heart. A cutout was also made at one end of the frame where a five pin plastic male plug-in could be inserted. Finally, a removable top had to be built to insulate the SMA wires from potentially touching any tissue during an in-vivo study. Snap-in grooves were designed into the frame's sides and the male equivalent was built into the top's inner sides. Figure 44 shows the CAD assembly design of the modified frame. Dimensional schematics can be seen in Appendix A, Figure 61.

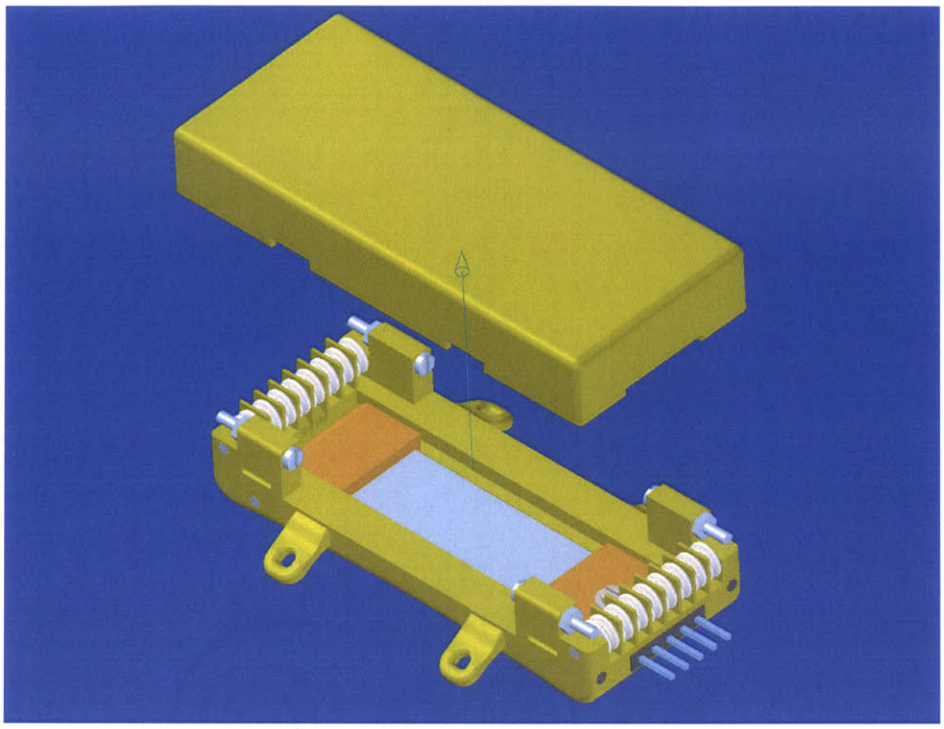

Figure 44: CAD assembly of the SMA AMP device Version 2.

4.4.1.2 Electrical System Modifications

The power source used for Version 2 was essentially the same as that of Version 1 save one new element. Two DC power supplies were again used to charge four 33 mF electrolytic capacitors. The new element was a power-triggering circuit based around four Insulated Gate Bipolar Transistors (IGBT). IGBTs are a particular variety of bipolar transistors that are capable of switching very high voltages and currents with a relatively small gate (input) voltage (15V). One IGBT was used for each SMA wire. Each IGBT collector was connected to one of the 33 mF electrolytic capacitors while their emitters would be connected to the SMA AMP Version 2 device. A non-inverting amp of Gain 3 was placed between the outputs and the gates of each IGBT so that the gate input would only need to be a standard 5 V digital signal. In this configuration, a square wave generator could be connected to two IGBTs leading to the device's

protrusion wires with its complementary output connected to the other IGBTs leading to the device's resetting wires. This provided a frequency adjustable triggering signal that would be the first step towards a gating system. A circuit diagram of the power-triggering circuit is shown in Figure 45.

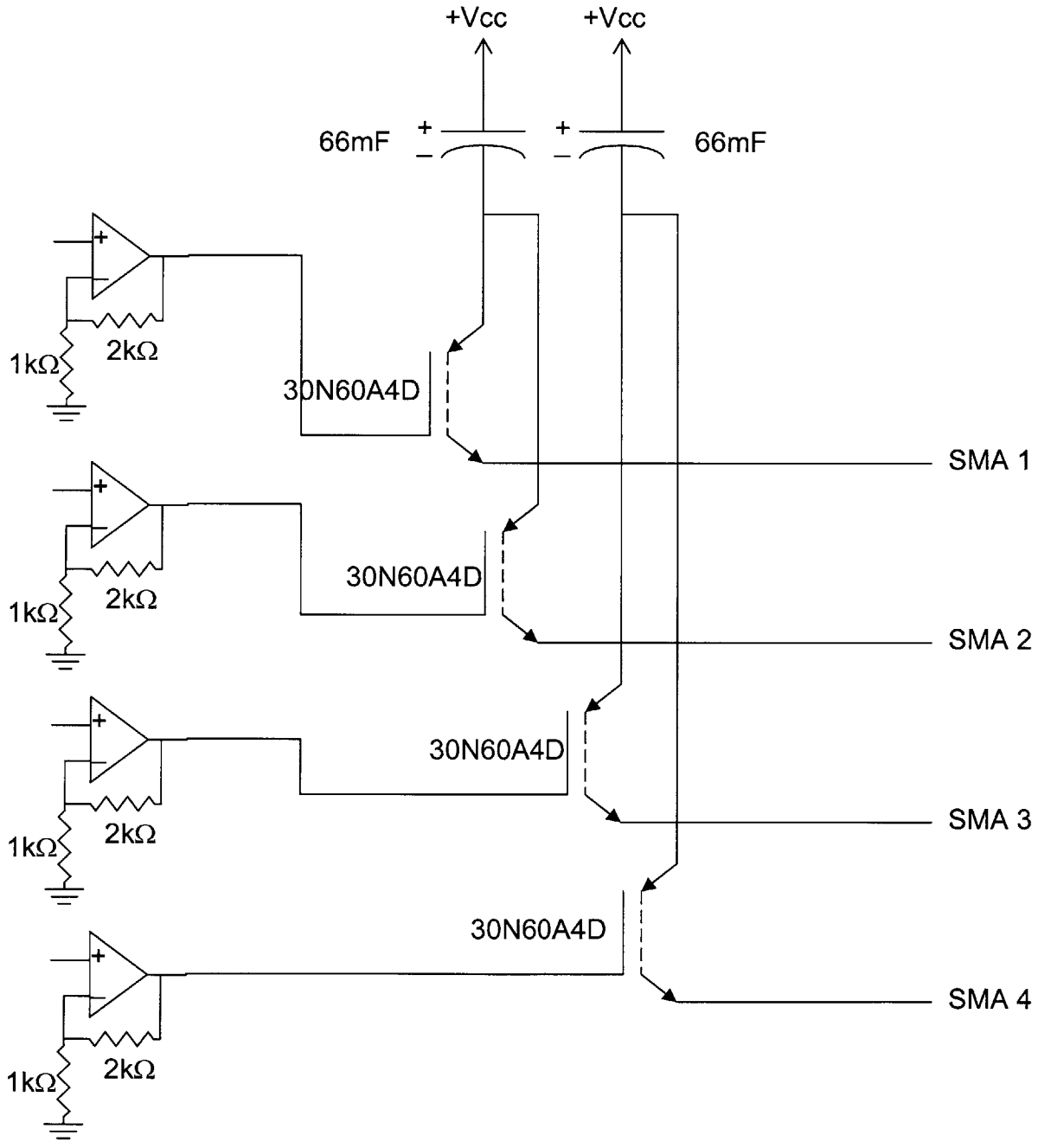

Figure 45: Circuit diagram of the SMA AMP Version 2 power triggering circuit.

4.4.2 Manufacturing and Assembly

The frame and removable top were both manufactured on an SLA. Once completed, the 40 mm long by 12.7 mm wide by 150 μm thick piece of shim, the Macor pulleys, stainless steel rods and screw electrodes were set into place. Electrical connections needed to be run from the screw electrodes to the 5-pin connector. The two electrodes on the opposite side of the connector were attached to the stainless steel rod running the length of the frame. The other end of the rod was then connected to the appropriate pins on the 5-pin connector. Four 325 mm long by 250 μm diameter SMA wires were threaded from the static shim end cap, through the pulleys, then attached to their respective electrodes. Figure 46 shows the final assembly of the device.

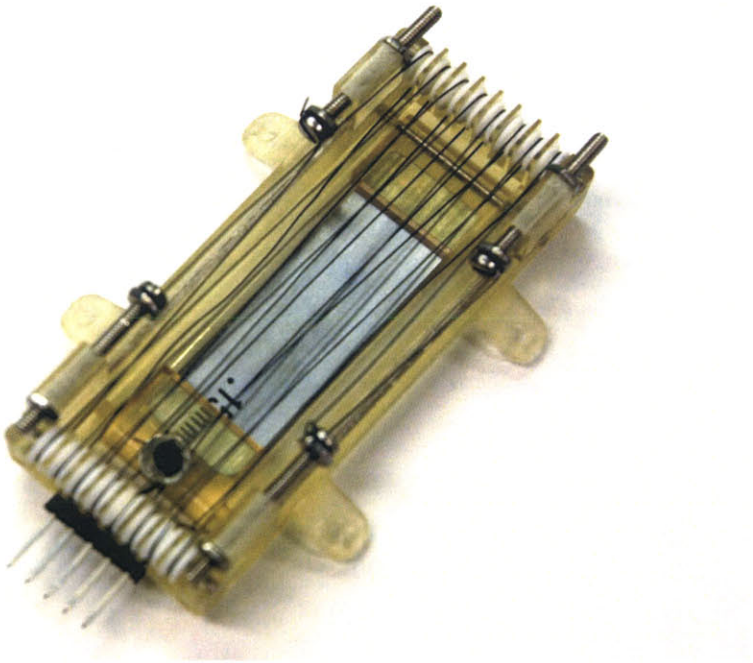

Figure 46: Final assembly of SMA AMP device Version 2.

The power-triggering circuit was designed in the Allegro software program and built out of a double-sided copper prototyping board. It was then populated with the IGBTs, op-amps and other components and female banana plugs were installed at the circuit's inputs and outputs.

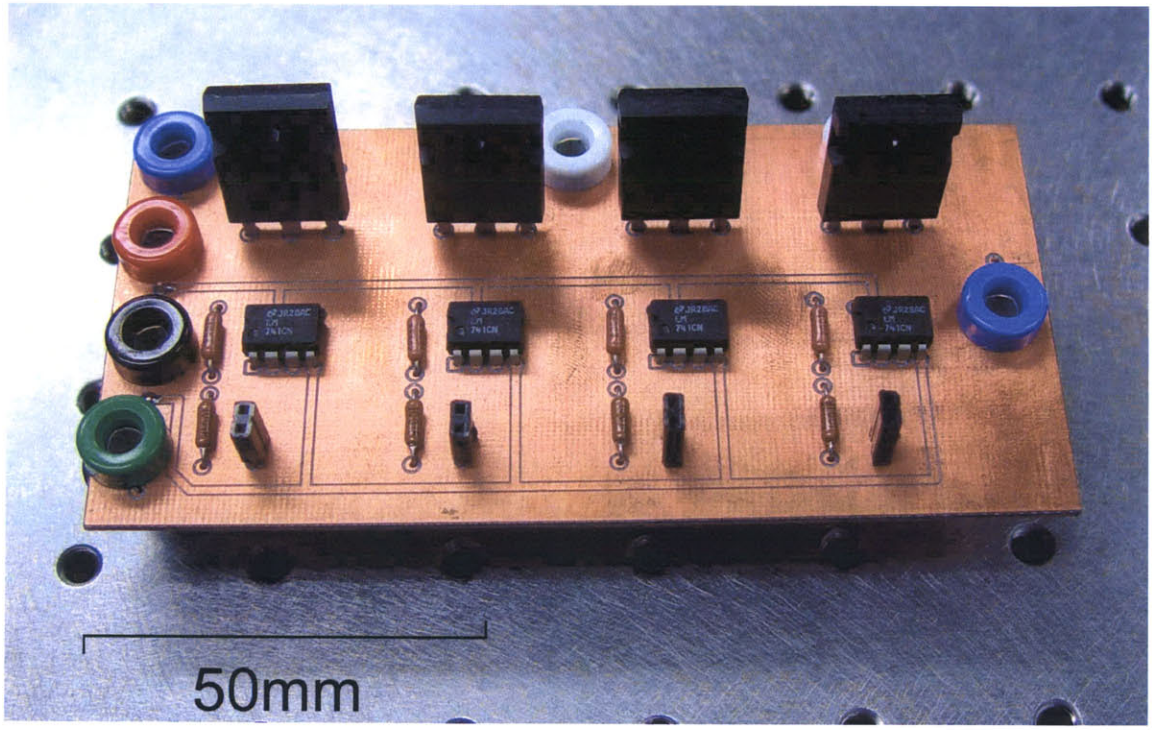

Figure 47: Power triggering circuit.

4.4.3 Testing and Analysis

Testing of the SMA AMP Version 2 device was performed on the in-vitro instrument. Since the mechanism design was the same as for SMA AMP Version 1, force measurements were not repeated. Instead the in-vitro instrument was used to test the device's depth of protrusion when placed against a load. The device was sutured onto the LV ellipse using sewing buttons as a backing support. The device was then connected to the capacitor-toggle box setup used earlier for SMA AMP Version 1 tests. The capacitors were charged to 20 V, the toggle was

tripped and the protrusion's depth was measured with a ruler held beside the frame. The device's protrusion depth was approximately 10 mm. This slightly shallower protrusion was most likely due to the extra resistance caused by the close proximity of the suture points. This device also used slightly shorter wires than the SMA AMP Version 1 (325 mm versus 350 mm) giving it a slightly shorter contraction length. Sequential contraction was then attempted using the toggle box's switches, however the screw that attaches the wires to the shim's sliding end cap remains problematic. After only a few contractions, two of the wires separated from the screw, rendering the device inoperative.

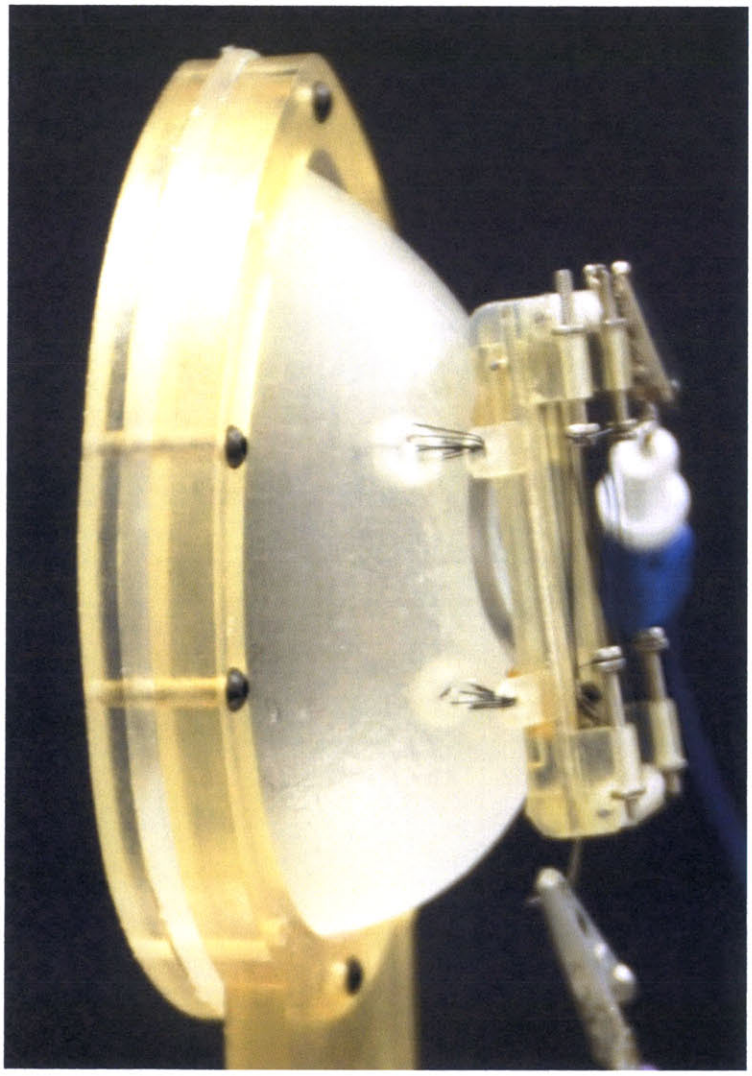

Figure 48: SMA AMP Version 2 device sutured to in vitro ellipse.

4.5 Future Research

Future development of this SMA device will continue. The current iteration of SMA AMP device has proven effective at creating the displacements required to treat MR through LV remodeling but will require certain improvements before it is reliable enough to use during an in-vivo procedure. Further research also needs to be directed towards making this device truly gated to the heart's cycle. A VB interface should be created to do this. A future iteration of the SMA AMP will be tested in-vivo as soon as an effective solution to the gating problem has been found and the device performs reliably enough to warrant an in vivo experiment.

5 Conclusions and Future Research

The previous chapters present advances in the design and development of a new approach to the treatment of ischemic mitral regurgitation. The concept of using an artificial muscle patch to treat MR has been proofed. The AMP simulation device showed in vivo that an active patch device can relieve MR by displacing the papillary muscles of the left ventricle by approximately 12 mm.

Device performance data also provided useful specifications for ongoing development of this approach. Calculations indicated that the simulation device needed to exert at least 11 kPa of pressure against the LV wall in order to displace it. Information on the timing of the AMP simulator's activation was then used to develop design criteria for a shape memory alloy AMP device as described in Chapter 4.

Two SMA AMP devices were built and tested. The first was a non-implantable version used to test the design's force output. A maximum force output of 15.14 N was achieved, yielding an equivalent of 57.15 kPa for the test probe used. The second iteration was designed as an implantable version with all suturing loops, electrical connections and device coverings required for use in an in-vivo study. This second device was tested with the in-vitro instrument (the development of which is described in Chapter 3).

A number of design and manufacturing challenges were overcome in this research which provide lessons for further work on artificial muscle technologies. Many different mechanisms for displacement magnification needed to be tested in order to achieve the 12 mm displacement required to affect MR. This was made more difficult by the need to keep the device small enough to fit within a sheep's pericardial space without affecting its normal heart function. Development

of an SMA device that could be implanted into a living animal also proved to be challenging. Special attention needed to be paid to the device's electrical connections and to the SMA wires to ensure that they could not touch any tissue within the chest cavity.

From a manufacturing perspective, many machining challenges were overcome. The most prominent of these was the machining of small Macor parts. A novel strategy was developed to enable the production of a large number of Macor pulleys with the existing equipment (CNC lathe, 3-axis CNC mill). Since small detailed Macor parts are invaluable in creating SMA assemblies and devices, this style of manufacturing will undoubtedly find future uses.

Future work will be directed to the further development of the SMA AMP device. Once an advanced prototype has been completed, in-vivo testing will be undertaken. Looking beyond SMA technology, conducting polymer actuators will be the next step for active patch development. Conducting polymer actuators have the advantage of being a very low-power consumption technology. This would enable the creation of a much more compact implantable device that can eventually be considered for clinical use. More development will also be done on the in-vitro testing instrument. A more comprehensive instrument incorporating a variety of sensors will be built to test future AMP prototypes.

References

1 Hung J, Guerrero JL, Handschumacher M D, Supple G, Sullivan S, Levine R A. **Reverse Ventricular Remodeling Reduces Ischemic Mitral Regurgitation Echo-Guided Device Application in the Beating Heart**, *Circulation*, 2002; 2594-2600.

2 Lamas GA, Mitchell GF, Flaker GC, Smith SC, Gersh BJ, Basta L, Moye L, Braunwald E, Pfeffer MA. **Clinical Significance of Mitral Regurgitation After Acute Myocardial Infarction**, *Circulation*, 1997; 96:827-833.

3 Barzilai B, Gessler C, Perez JE, Schaab C, Jaffe AS. **Significance of Doppler-Detected Mitral Regurgitation in Acute Myocardial Infarction**, *Am J Cardiol*ogy, 1988; 61:220-223.

4 Grigioni F, Enriquez-Sarano M, Zehr KJ, Bailey KR, Tajik AJ. **Ischemic Mitral Regurgitation: Long-Term Out-Come and Prognostic Implications with Quantitative Doppler Assessment**, *Circulation,* 2001; 103(13):1759-64.

5 Otto CM. **Evaluation and Management of Chronic Mitral Regurgitation**, *N Engl J Med,* 2001; 345(10):740-746.

6 http://www.brighamandwomens.org/patient/cardiac_valve.asp

7 Liel-Cohen N, Otsuji Y, Vlahakes GJ, Akins CW, Levine RA. **Functional Ischemic Mitral Regurgitation can Persist Despite Ring Annuloplasty: Mechanistic Insights**, *Circulation,* 1997; 96(Suppl 1):1-540.

8 Hung J, Handschumacher MD, Rudski L, Chow C-M, Guerrero JL, Levine RA. **Persistence of Ischemic Mitral Regurgitation Despite Annular Ring Reduction: Mechanistic Insights from 3D Echocardiography [Abstract],** *Circulation,* 1999; 100(Suppl 1):73.

9 Calafiore AM, Gallina S, DiMauro M, Gaeta F, Iaco AL, Allesandro S, Mazzei V, DiGiammarco G. **Mitral Valve Procedure in Dilated Cardiomyopathy: Repair or Replacement?** *Ann Thorac Surg,* 2001; 71:1146-53.

10 Tahta SA, Oury JH, Maxwell JM, Hiro SP, Duran CM. **Outcome after Mitral Valve Repair for Functional Ischemic Mitral Regurgitation**, *J Heart Valve Dis,* 2002; 11:11-18.

11 http://www.sts.org/doc/4101

12 http://www.oucom.ohiou.edu/CVPhysiology/cardiac%20cycle%20fig.htm

13 http://www.daedalpositioning.com/

14 http://www.aerotech.com/

15 www.linmot.com

16 http://www.popperandsons.com/

17 http://msdn.microsoft.com/vstudio/

18 www.millarinstruments.com

19 He S, Fontaine A, Ellis JT, Schwammenthal E, Yoganathan AP, Levine RA. **An Integrated Mechanism for Functional Mitral Regurgitation–Leaflet Restriction versus Coapting Force: In Vitro Studies**, *Circulation*, 1997; 96:1826-34.

20 http://www.bioeng.auckland.ac.nz/cmiss/cmiss.php

21 http://www.coltenewhaledent.com

22 http://www.silicones-inc.com/

23 http://www.sma-inc.com/html/introduction.html

24 www.howcoheattreat.com/glossary/glossary.asp

25 www.jiantat.com/glossary/content.html

26 www.mametal.com/metal_working_glossary.htm

27 http://www.dynalloy.com

28 Lafontaine S. **Fast Shape Memory Alloy Actuators**, Doctoral Thesis, McGill University, Montréal Canada; 1997.

Appendix A: Dimensional Schematics

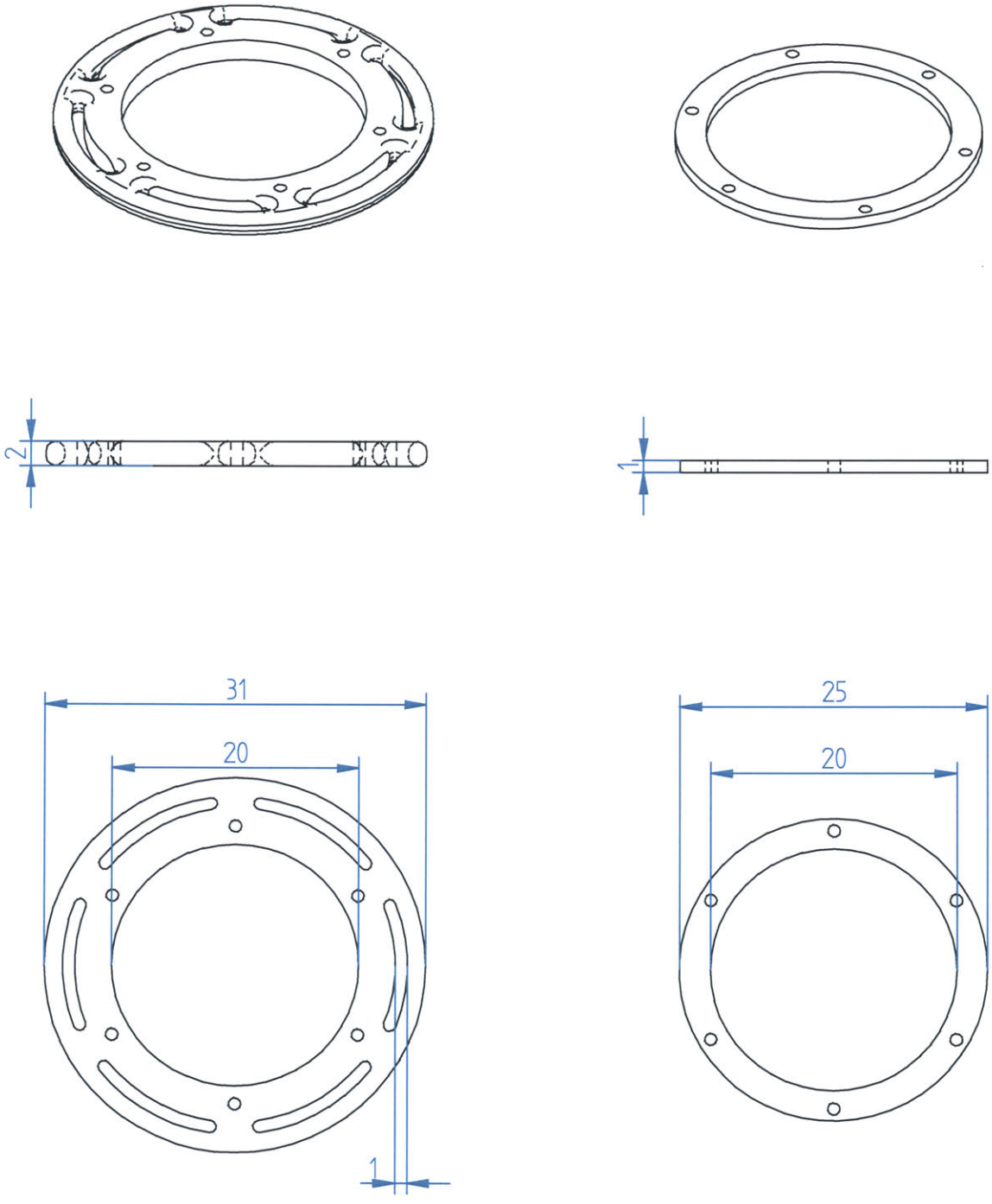

Figure 49: Schematic of Base Ring Version 1.

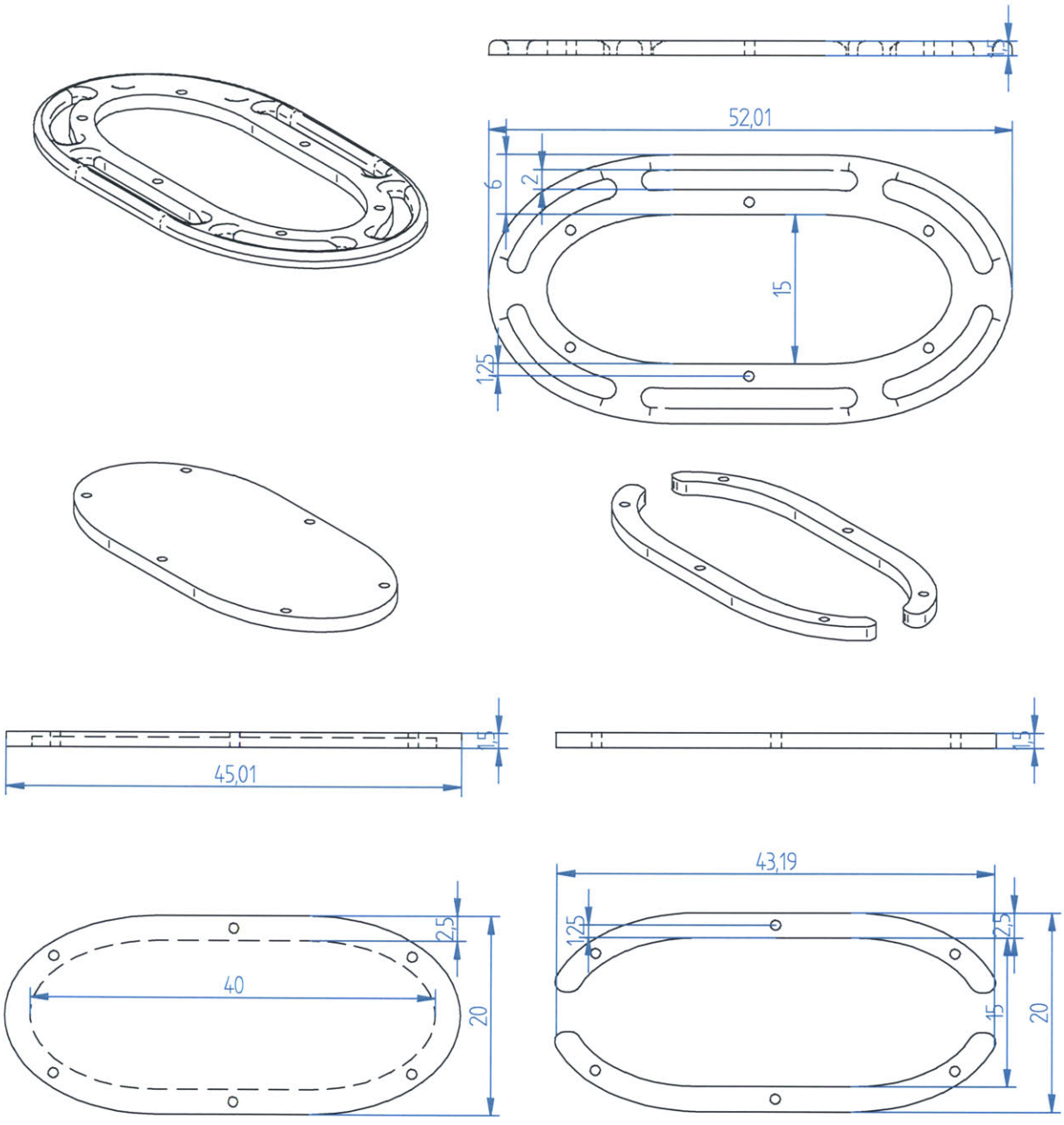

Figure 50: Schematic of Base Ring Version 2.

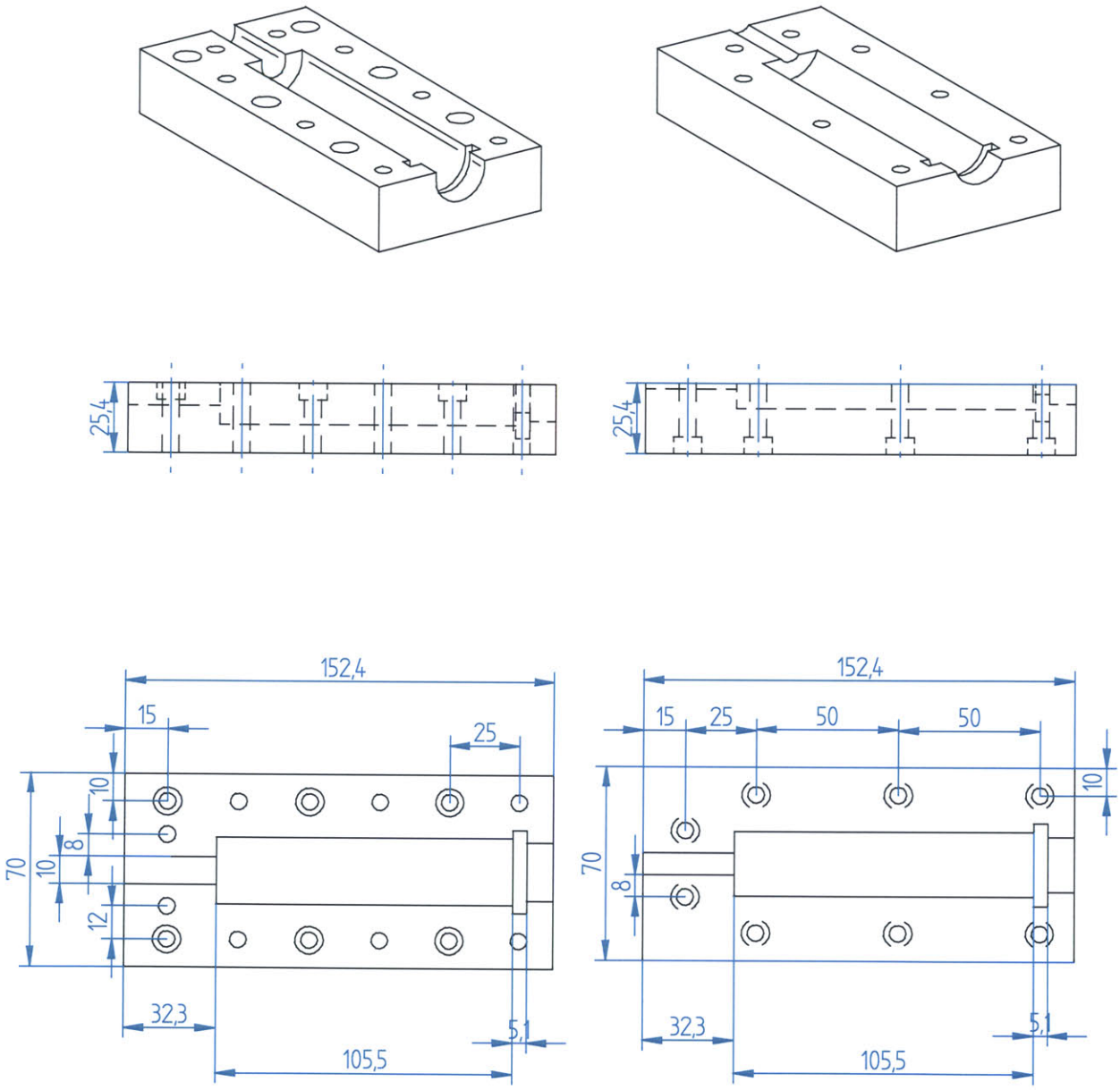

Figure 51: Schematic of Perfektum 50 mL syringe mounts.

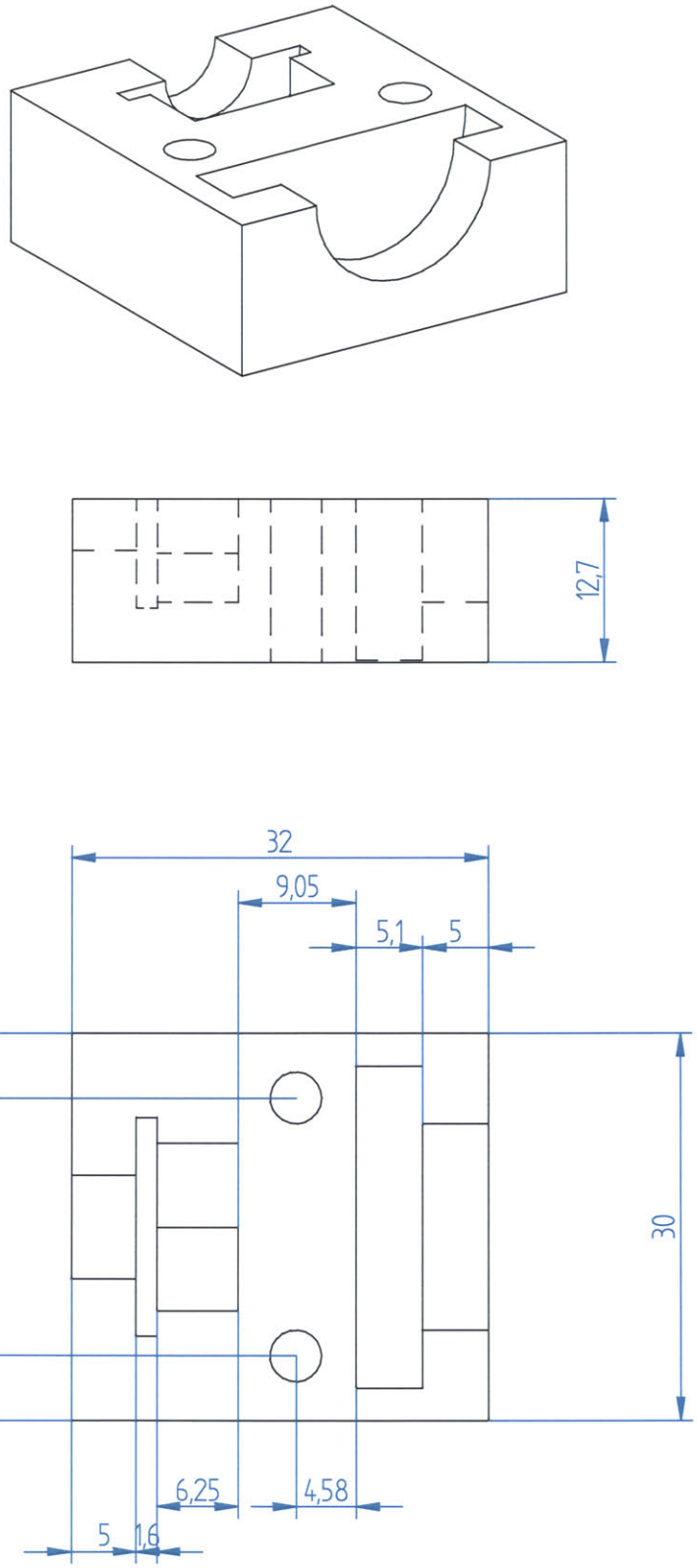

Figure 52: Schematic of syringe-actuator coupler.

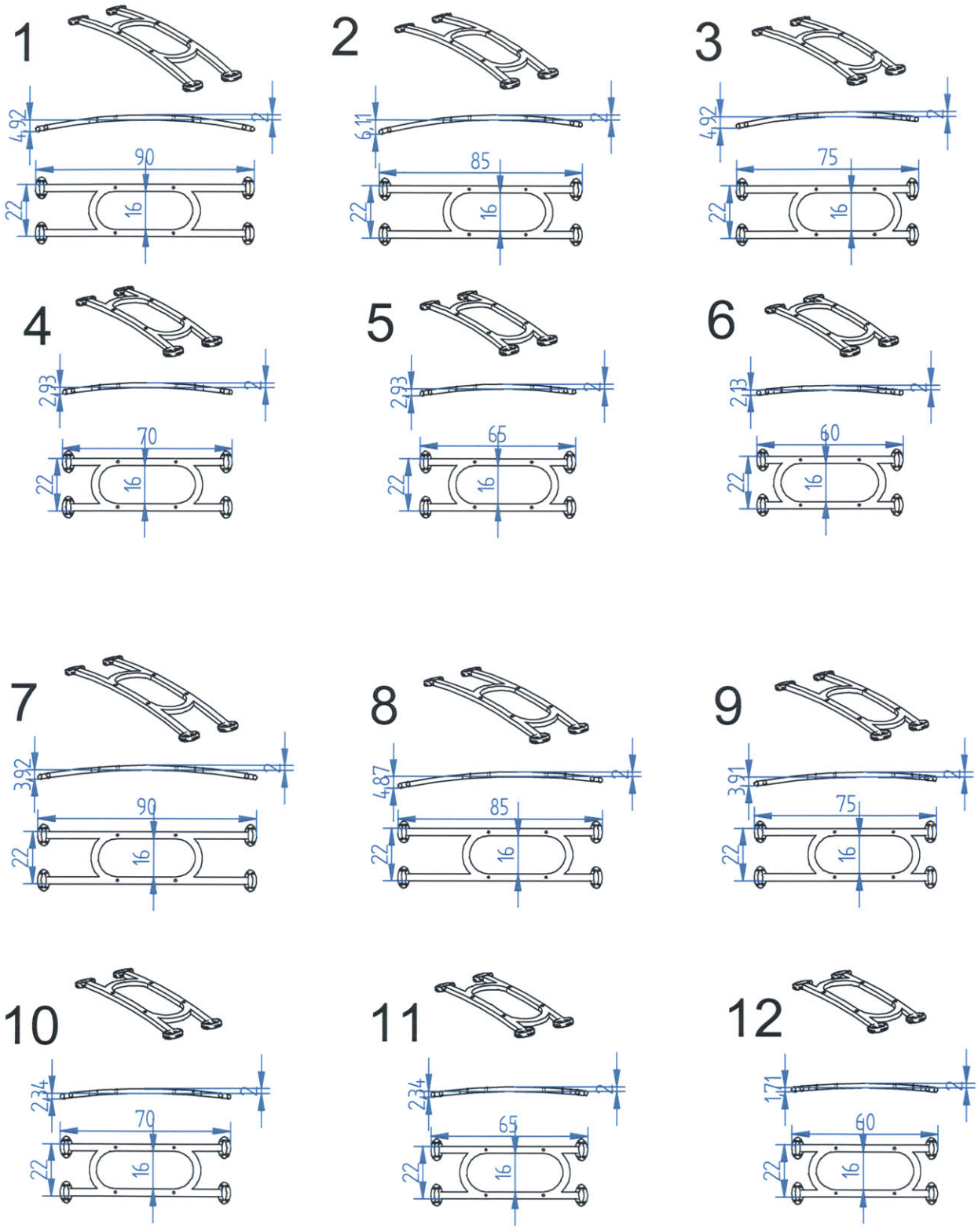

Figure 53: Schematic of Base Ring 3 frames prepared for second in vivo procedure.

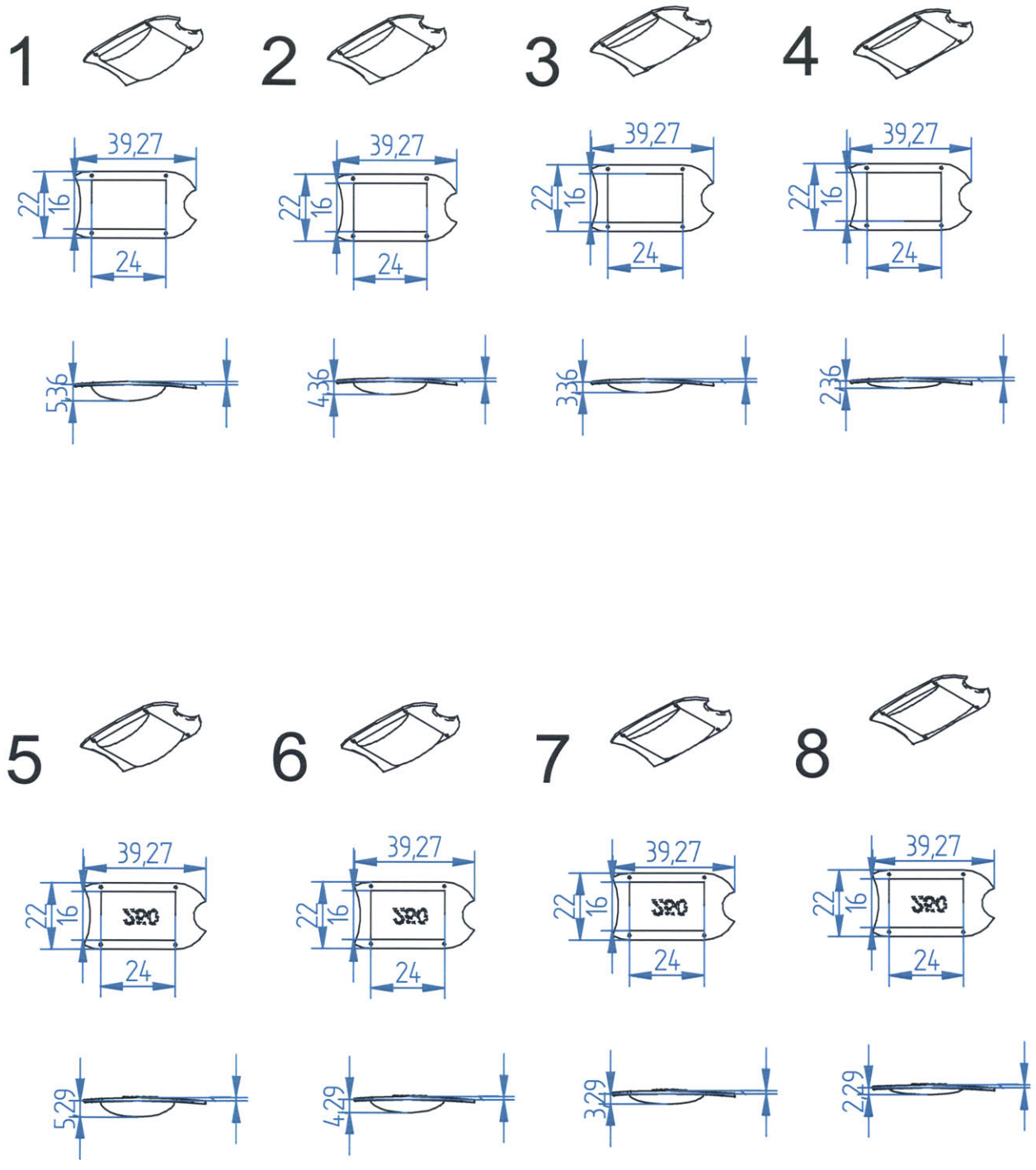

Figure 54: Schematic of Base Ring 3 backings prepared for second in vivo procedure.

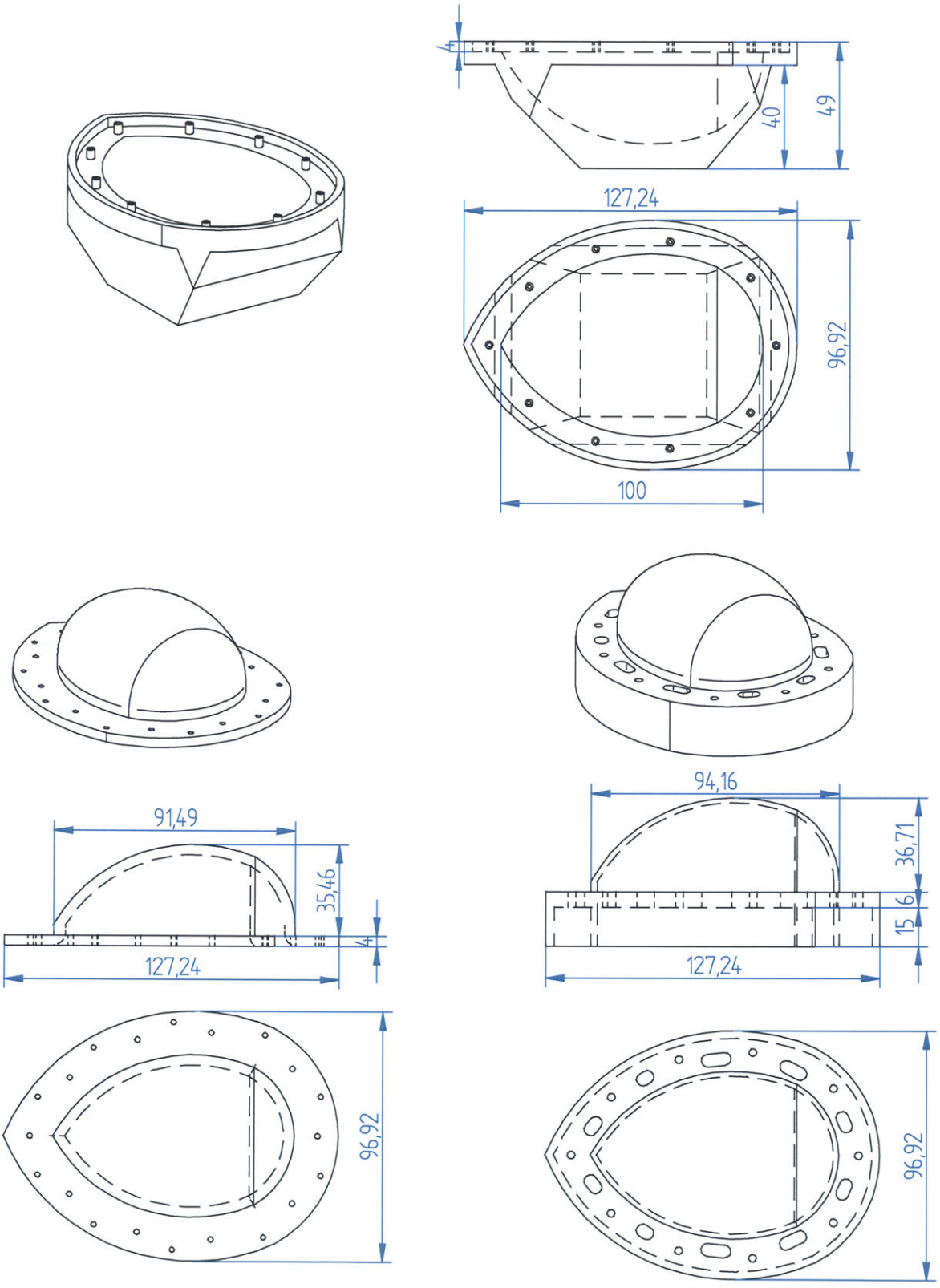

Figure 55: Schematic of in vitro half ellipse molds.

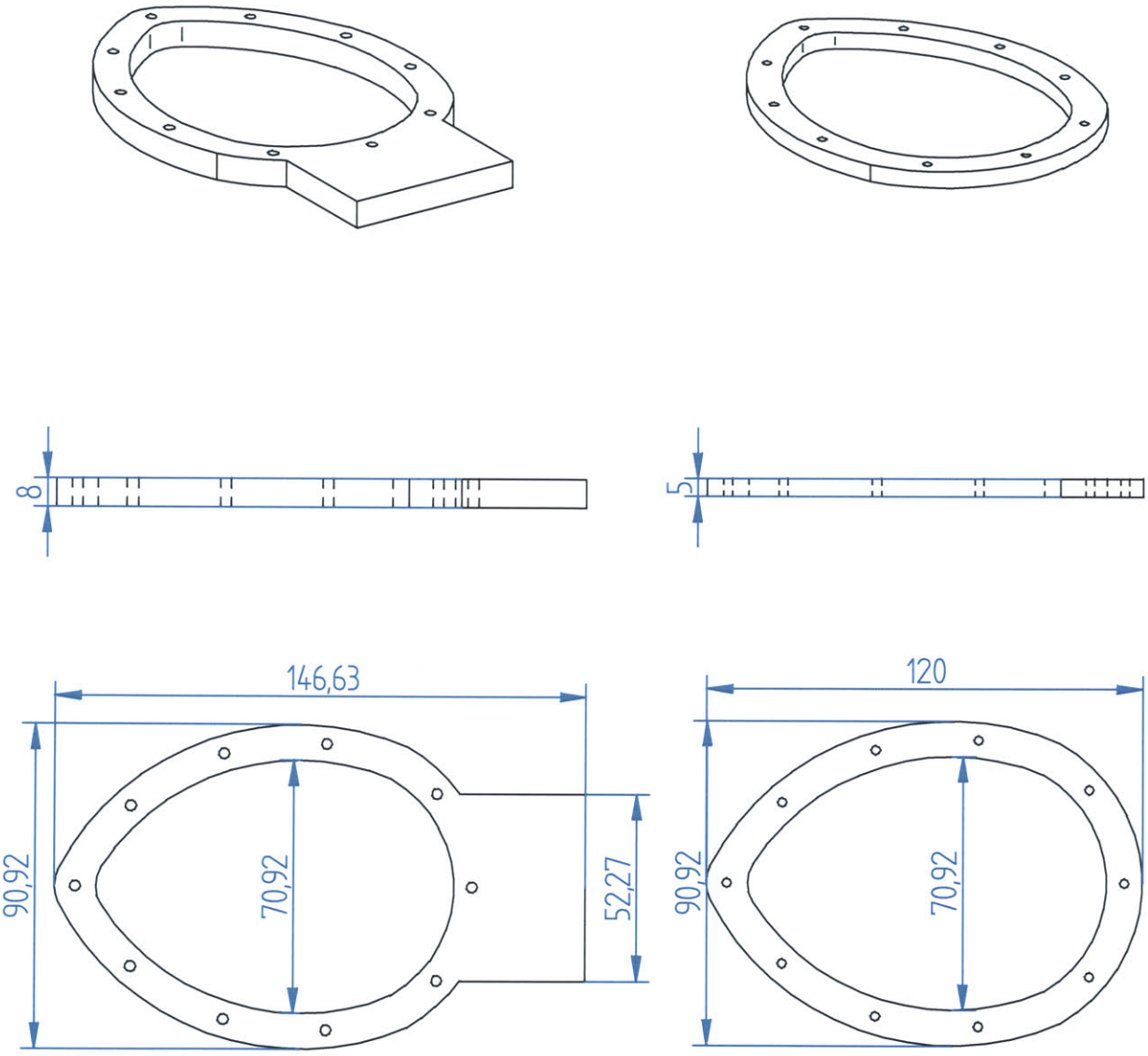

Figure 56: Schematic of in vitro assembly frame.

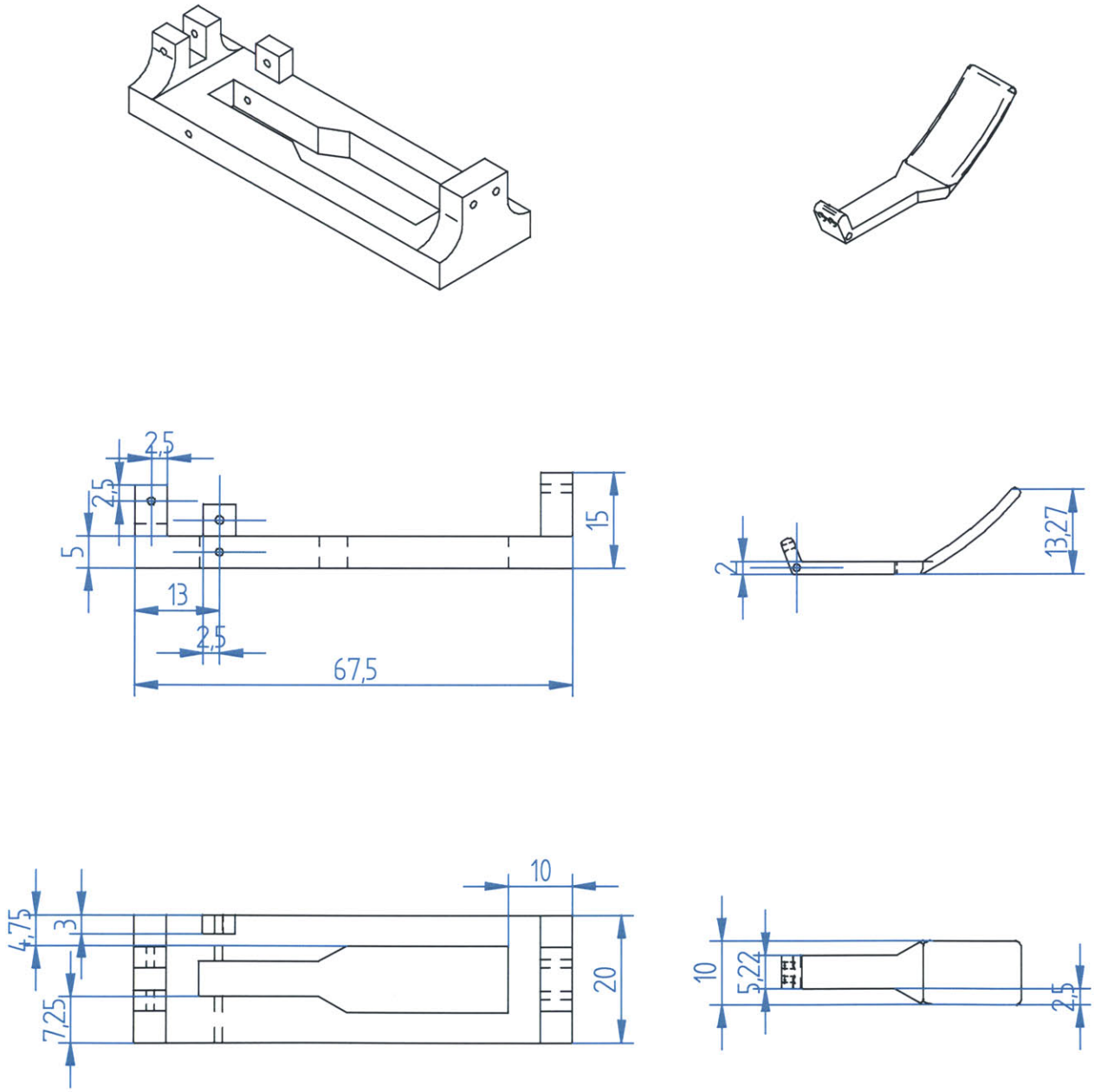

Figure 57: Schematic of lever prototype.

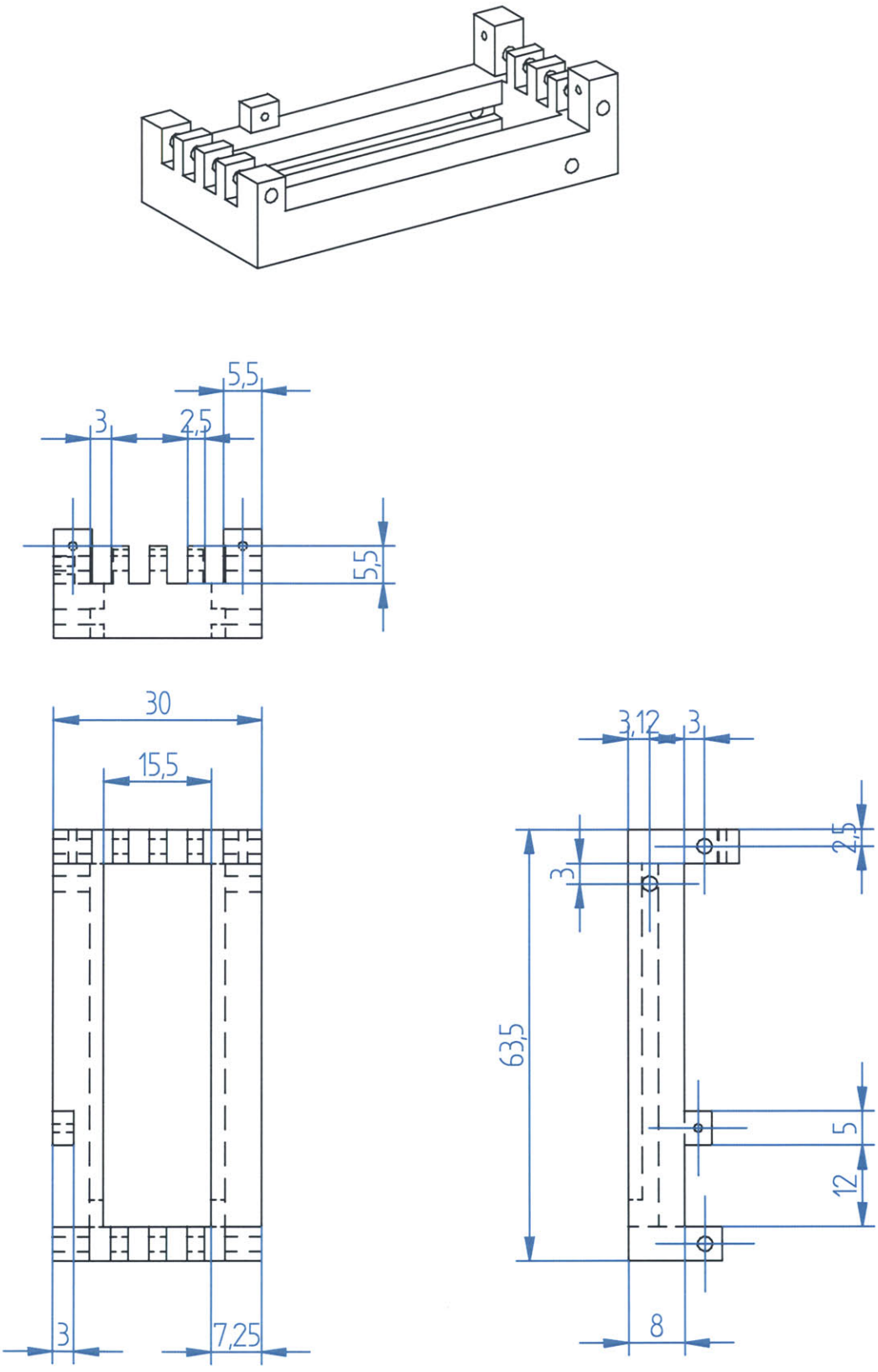

Figure 58: Schematic of bowing shim prototype.

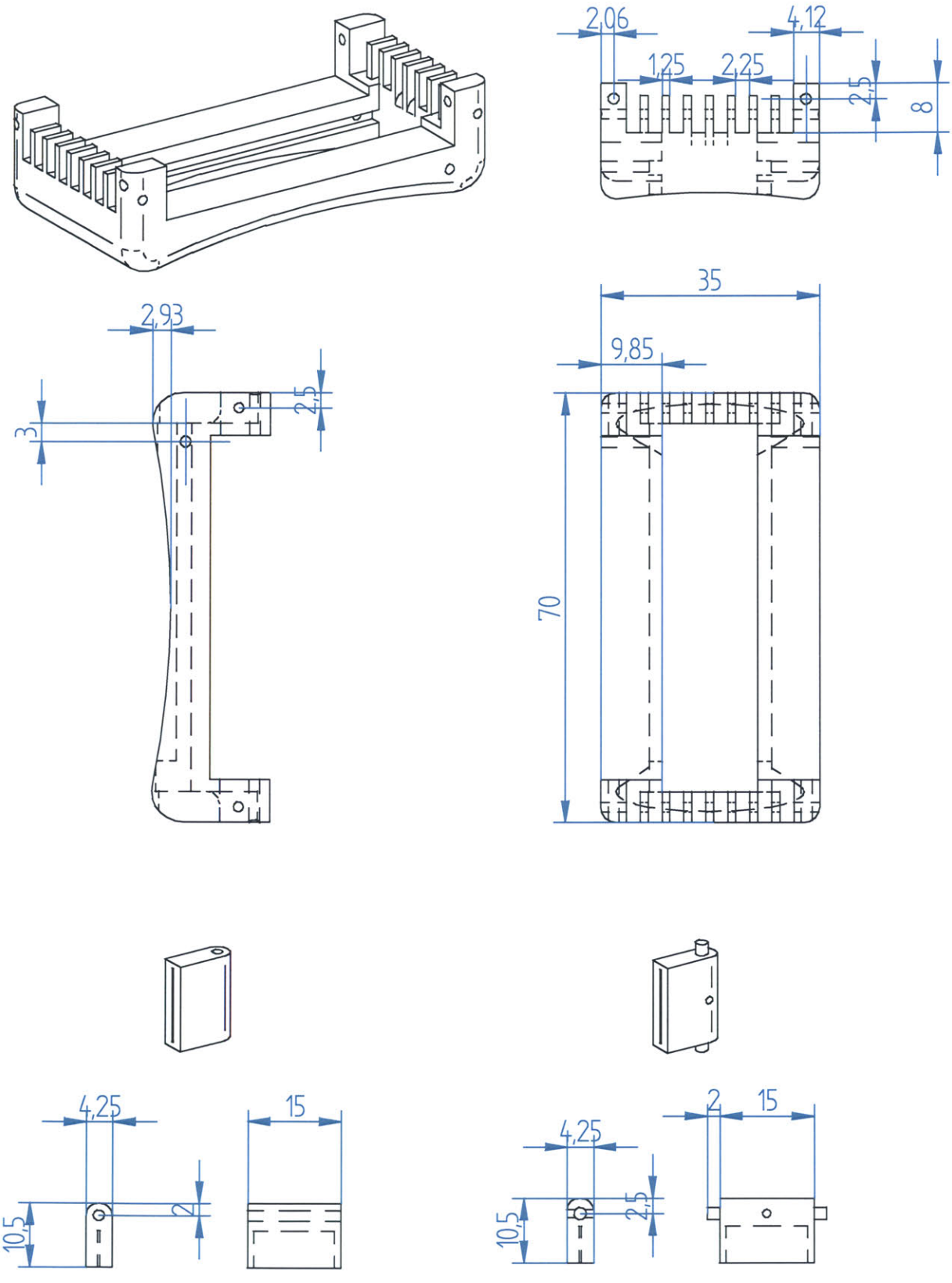

Figure 59: Schematic of SMA AMP device Version 1.

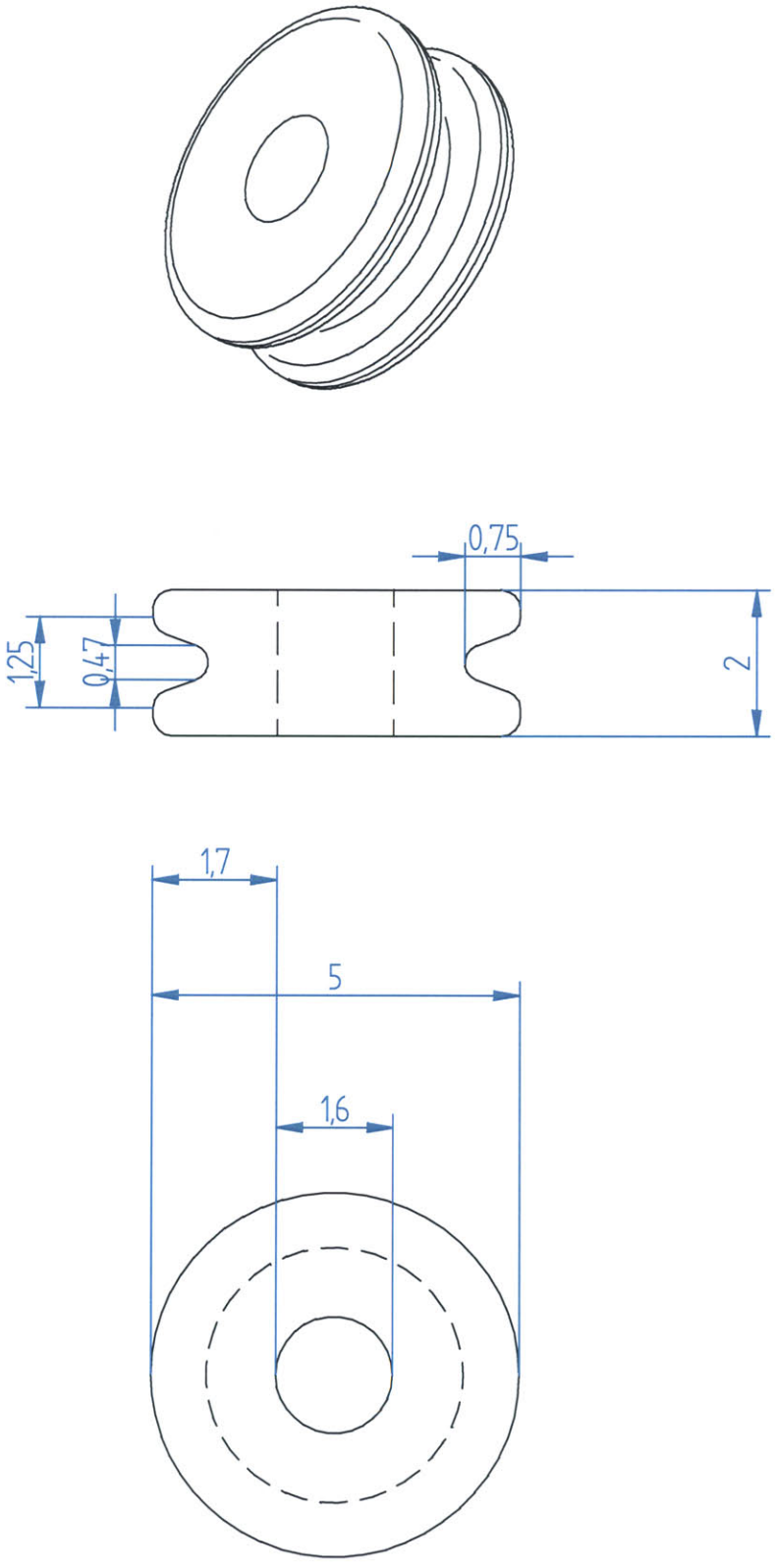

Figure 60: Schematic of Macor pulley.

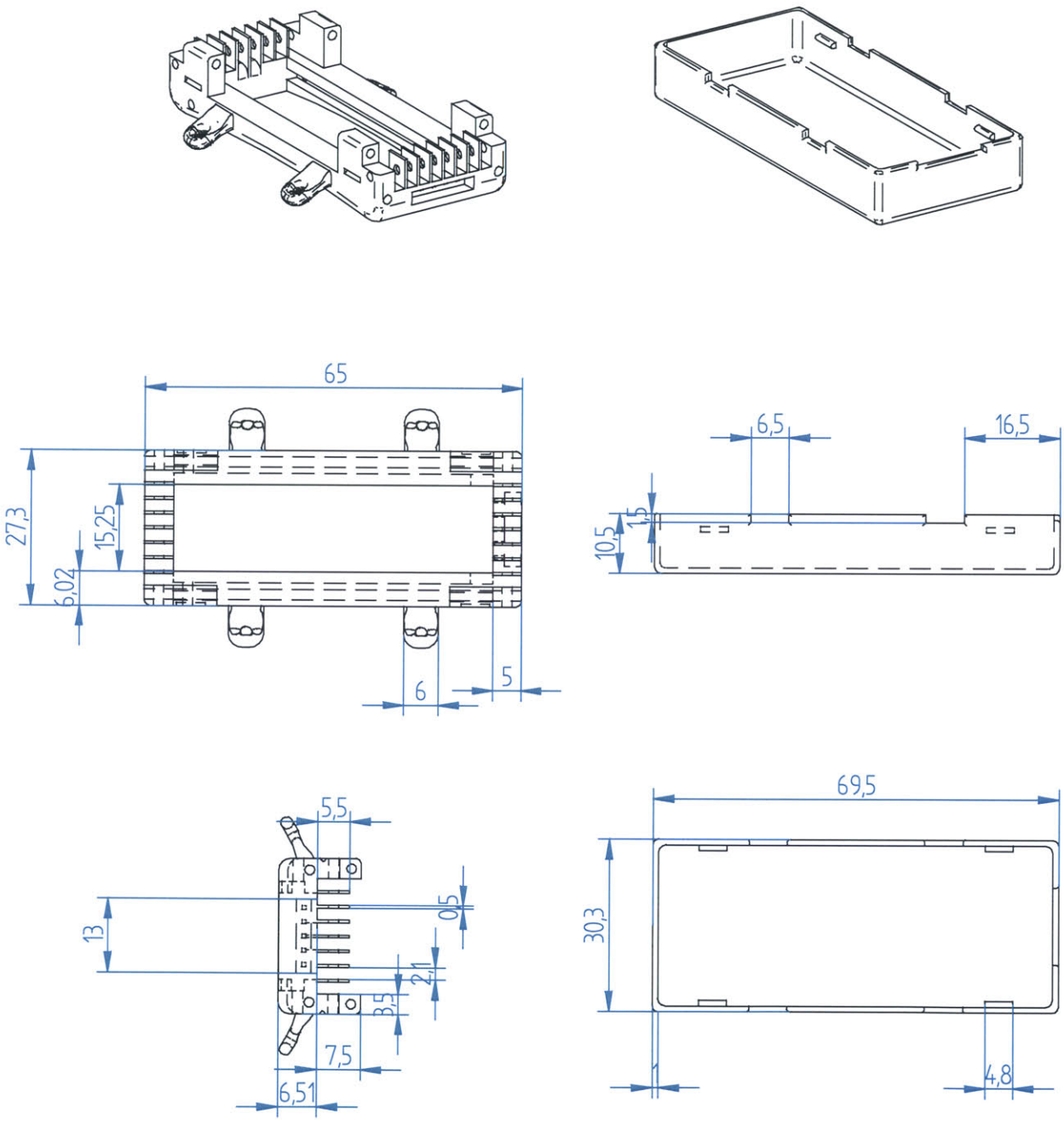

Figure 61: Schematic of SMA AMP device Version 2.

Appendix B: Calculations of Linear Actuator Requirements

Constants

$Q := 40 \cdot 10^{-6} \cdot \frac{m^3}{s}$ Average Flow Rate

$\rho := 10^3 \cdot \frac{kg}{m^3}$ Density of Fluid

$\mu := 0.00089 \cdot \frac{N \cdot s}{m^2}$ Dynamic Viscosity of Fluid

$\nu := \frac{\mu}{\rho}$ Kinematic Viscosity $\nu = 8.9 \times 10^{-7} \frac{m^2}{s}$

$g = 9.807 \frac{m}{s^2}$ Gravitational Acceleration

Pressure Drop Across Individual Sections of System

Equations derived from the Navier-Stokes equation of motion

Section 1: Syringe

$R_1 := 20 \cdot 10^{-3} \cdot m$ $L_1 := 0.1 \cdot m$

$A_1 := \pi \cdot R_1^2$ $A_1 = 1.257 \times 10^{-3} m^2$

$V_{1avg} := 0.4 \frac{m}{s}$ Mean velocity

$V_{1max} := 0.6 \cdot \frac{m}{s}$ Maximum velocity for a parabolic distribution
See lab book NS1 p.10

$t_{Vmax} := \frac{0.166s}{3}$ Time required to reach Vmax
(Based on model of 1/3t accelerating,
1/3t cst Vmax, 1/3t decelerating $t_{Vmax} = 0.055s$

$a_1 := \frac{V_{1max}}{t_{Vmax}}$ Acceleration of Fluid in Section 1
(Acceleration of Linear Actuator) $a_1 = 10.843 \frac{m}{s^2}$

$\Delta P_1 := \frac{8 \cdot \mu \cdot Q \cdot L_1}{\pi \cdot R_1^4} + a_1 \cdot \rho \cdot L_1$ $\Delta P_1 = 1.084 \times 10^3 Pa$

Section 2: Connecting Tube

$R_2 := 3.25 \cdot 10^{-3}\,m$ $\quad L_2 := 1 \cdot m$

$A_2 := \pi \cdot R_2^{\,2}$ $\quad A_2 = 3.318 \times 10^{-5}\,m^2$

$V_{2avg} := 1.2\frac{m}{s}$ Mean velocity

$V_{2max} := 1.8 \cdot \frac{m}{s}$ Maximum velocity for a parabolic distribution
See lab book NS1 p.10

$t_{Vmax} := \frac{0.166s}{3}$ Time required to reach Vmax
(Based on model of 1/3t accelerating, 1/3t cst Vmax, 1/3t decelerating $\quad t_{Vmax} = 0.055s$

$a_2 := \frac{V_{2max}}{t_{Vmax}}$ Acceleration of Fluid in Section 2 $\quad a_2 = 32.53\frac{m}{s^2}$

$\Delta P_2 := \frac{8 \cdot \mu \cdot Q \cdot L_2}{\pi \cdot R_2^{\,4}} + a_2 \cdot \rho \cdot L_2$ $\quad \Delta P_2 = 3.334 \times 10^4\,Pa$

Section 3: Patch

$W_3 := 0.03m$ $\quad H_3 := 0.06m$ $\quad L_3 := 5.56 \cdot 10^{-3}\,m$

$A_3 := W_3 \cdot H_3$ $\quad A_3 = 1.8 \times 10^{-3}\,m^2$

$V_{3avg} := 0.022\frac{m}{s}$ Mean velocity

$V_{3max} := 0.033 \cdot \frac{m}{s}$ Maximum velocity for a parabolic distribution
See lab book NS1 p.10

$t_{Vmax} := \frac{0.166s}{3}$ Time required to reach Vmax
(Based on model of 1/3t accelerating, 1/3t cst Vmax, 1/3t decelerating $\quad t_{Vmax} = 0.055s$

$a_3 := \frac{V_{3max}}{t_{Vmax}}$ Acceleration of Fluid in Section 3 $\quad a_3 = 0.596\frac{m}{s^2}$

$\Delta P_3 := \frac{12 \cdot \mu \cdot Q \cdot L_3}{W_3 \cdot H_3^{\,3}} + a_3 \cdot \rho \cdot L_3$ $\quad \Delta P_3 = 3.316Pa$

Pressure Variations Due to Head Loss

Result of viscous energy dissipation

Head loss due to friction in section 2 (Sections 1 & 3 negligible)

$f := 0.01$ Darcy Friction Factor for Plastic Pipe (From Moody diagram)

$\Delta h_f := f \cdot \left(\frac{V_{2avg}^2}{2 \cdot g} \right) \cdot \frac{L_2}{(2 \cdot R_2)}$ Head loss due to friction $\Delta h_f = 0.136m$

$\Delta P_{hf} := \Delta h_f \cdot \rho \cdot g$

$\Delta P_{hf} = 1.329 \times 10^3 Pa$ Pressure variation due to friction

Head loss due to abrupt interfaces (1 → 2 and 2 → 3)

Interface 1 → 2

$K_c := 0.4 \cdot \left(1 - \frac{A_2}{A_1} \right)$ Contraction Coefficient $K_c = 0.389$

$\Delta h_{12} := K_c \cdot \left(\frac{V_{2avg}^2}{2 \cdot g} \right)$ Head loss due to contraction $\Delta h_{12} = 0.029m$

$\Delta P_{h12} := \Delta h_{12} \cdot \rho \cdot g$ Pressure variation due to contraction $\Delta P_{h12} = 280.395Pa$

Interface 2 → 3

$K_e := \left(1 - \frac{A_2}{A_3} \right)^2$ Expansion Coefficient $K_e = 0.963$

$\Delta h_{23} := K_e \cdot \left(\frac{V_{2avg}^2}{2 \cdot g} \right)$ Head loss due to expansion $\Delta h_{23} = 0.071m$

$\Delta P_{h23} := \Delta h_{23} \cdot \rho \cdot g$ Pressure variation due to expansion $\Delta P_{h23} = 693.698Pa$

Total Pressure Drop Across System

$$\Delta P_{total} := \Delta P_1 + \Delta P_2 + \Delta P_3 + \Delta P_{hf} + \Delta P_{h12} + \Delta P_{h23}$$

$$\Delta P_{total} = 3.673 \times 10^4 \text{ Pa}$$

Required Applied Force

$P_A := 50 \cdot 10^3 \text{Pa}$

Estimated maximum pressure applied to the patch face

$$P_{2.5} := P_A + \Delta P_3 + \Delta P_{h23} + \frac{\Delta P_{hf}}{2}$$

Pressure halfway down the connecting tube (Potential site of pressure gauge)

$$P_{2.5} = 5.136 \times 10^4 \text{ Pa}$$

$P_1 := P_A + \Delta P_{total}$

Pressure at the Syringe's plunger

$$P_1 = 8.673 \times 10^4 \text{ Pa}$$

$F_{LM} := P_1 \cdot A_1$

Force required from the Linear Motor in order to produce the desired force against the myocardium

$F_{LM} = 108.993\text{N}$

Appendix C: Calculations for SMA Lever Prototype

SMA Lever Design

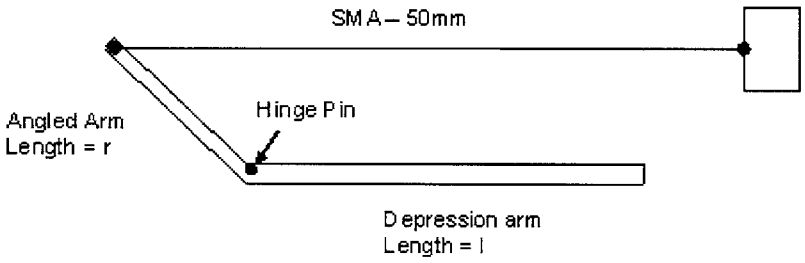

Angled Arm Length and Angle Calculation

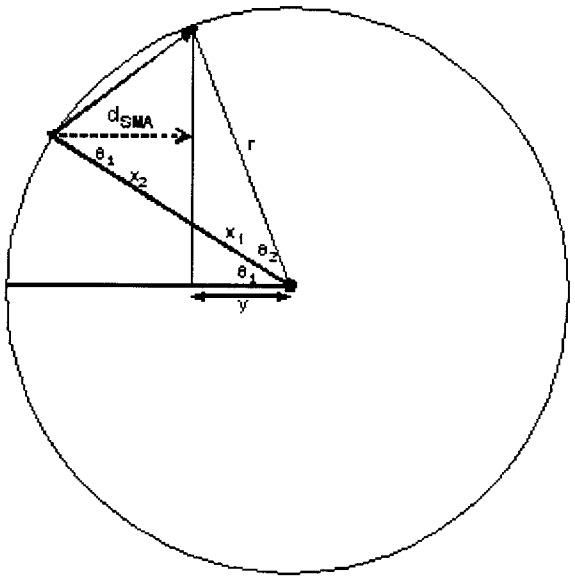

θ_1= Starting angle of arm

θ_2= Change in angle after SMA contraction

Length of SMA wire is 50mm therefore at 4% strain,

d_{SMA} = 2.0mm

$$x_2 = \frac{d_{SMA}}{\cos\theta_1}$$

$$x_1 = r - x_2$$

$$y = x_1 \cdot \cos\theta_1$$

$$\cos(\theta_1 + \theta_2) = \frac{y}{r}$$

$$\theta_2 = \operatorname{acos}\left(\frac{y}{r}\right) - \theta_1$$

Summarized equation for displacement angle

$$\theta_2 = \operatorname{acos}\left(\cos\theta_1 - \frac{d_{SMA}}{r}\right) - \theta_1$$

For fixed arm length

$r := 5mm$

$d_{SMA} := 2.0mm$

$$\theta_1 := \left(0, 0.1.. \frac{\pi}{2}\right)$$

$$\theta_2(\theta_1) := \left(\operatorname{acos}\left(\cos(\theta_1) - \frac{d_{SMA}}{r}\right) - \theta_1\right) \cdot \frac{180}{\pi}$$

$$\theta_{2r}(\theta_1) := \left(\operatorname{acos}\left(\cos(\theta_1) - \frac{d_{SMA}}{r}\right) - \theta_1\right)$$

Depression Arm Rotation as a Function of Initial Angle

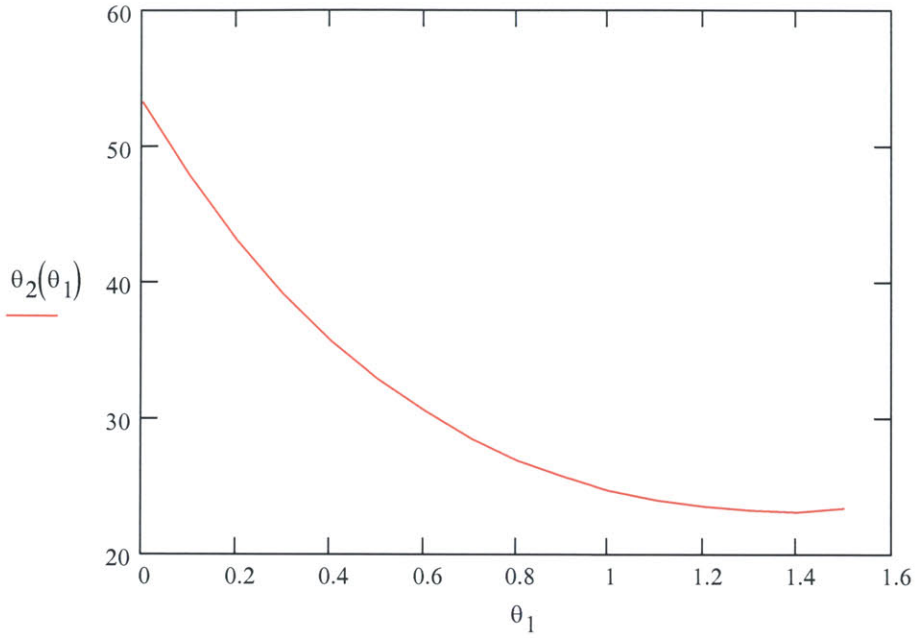

SMA Force Requirements

Pressure required

$P := 13150 \frac{N}{m^2}$

Length of depression arm

$l := 20 \cdot 10^{-3} m$

Surface area of depression arm

$A_a := 20 \cdot 10^{-3} \cdot 10 \cdot 10^{-3} \cdot m^2$ $\quad A_a = 2 \times 10^{-4} m^2$

$F_a := P \cdot A_a$ $\quad F_a = 2.63 N$

For simplicity, F_a will be taken at the equilibrium point of the depression arm (at its center)

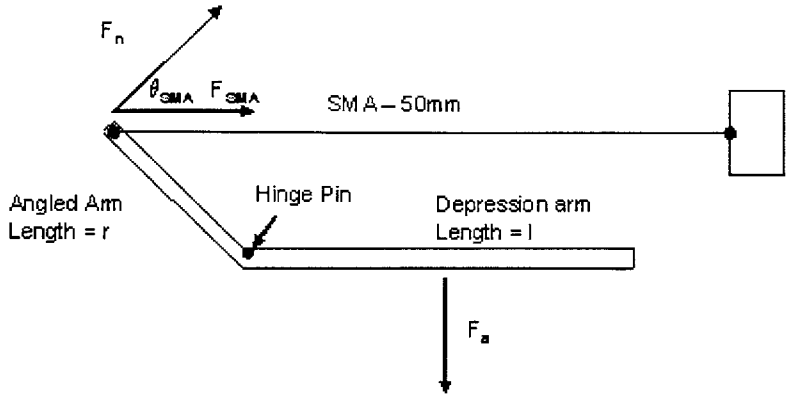

F_n is the force on the angle arm normal to its angular motion

F_{SMA} is the resulting force required by the SMA in order to achieve the desired displacement

From the Torque balance equation

$$F_a \cdot \frac{l}{2} = F_n \cdot r \qquad \text{where} \qquad F_n = F_{SMA} \cdot \cos(\theta_{SMA})$$

Therefore

$$F_{SMA} = \frac{F_a \cdot l}{2 \cdot r \cdot \cos(\theta_{SMA})}$$

From the angle calculations above, we see that θ_2 varies between 30 and 60 degrees

θ_{SMA} is taken as the angle after the SMA contraction since it is at this moment that maximum force must be applied.

For

$\theta_1 = 0$ $\qquad \theta_{SMA} = 30$

$\theta_1 = 60$ $\qquad \theta_{SMA} = 0$

$$\theta_{SMA}(\theta_1) := 90 - \theta_2(\theta_1) - \theta_1 \cdot \frac{180}{\pi}$$

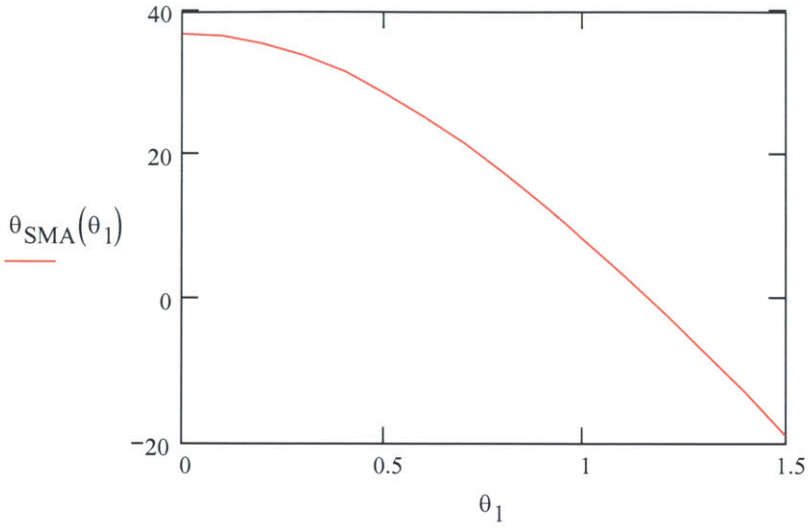

$$\theta_{SMAr}(\theta_1) := \frac{\pi}{2} - \theta_{2r}(\theta_1) - \theta_1$$

$$F_{SMA}(\theta_1) := \frac{F_a \cdot l}{2 \cdot r \cdot \cos(\theta_{SMAr}(\theta_1))}$$

Force required from SMA

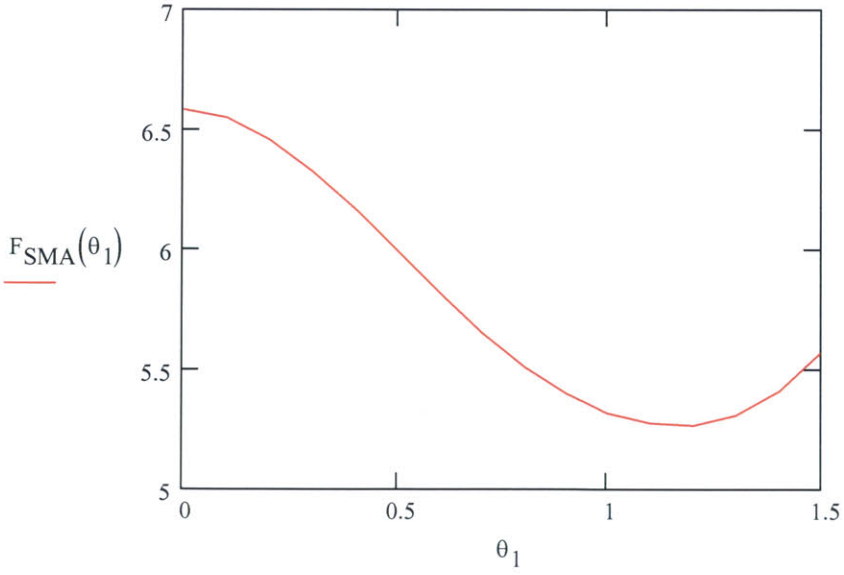

Wire Diameter Calculation

$P_{Wire} := 200 \cdot 10^6 \cdot \frac{N}{m^2}$ Maximum Force output of SMA

$$A_{Wire} = \frac{F_{SMA}}{P_{Wire}} = \frac{\pi \cdot D_{Wire}^{\ 2}}{4}$$

$$D_{Wire}(\theta_1) := \sqrt{\frac{4 \cdot F_{SMA}(\theta_1)}{P_{Wire} \cdot \pi}}$$

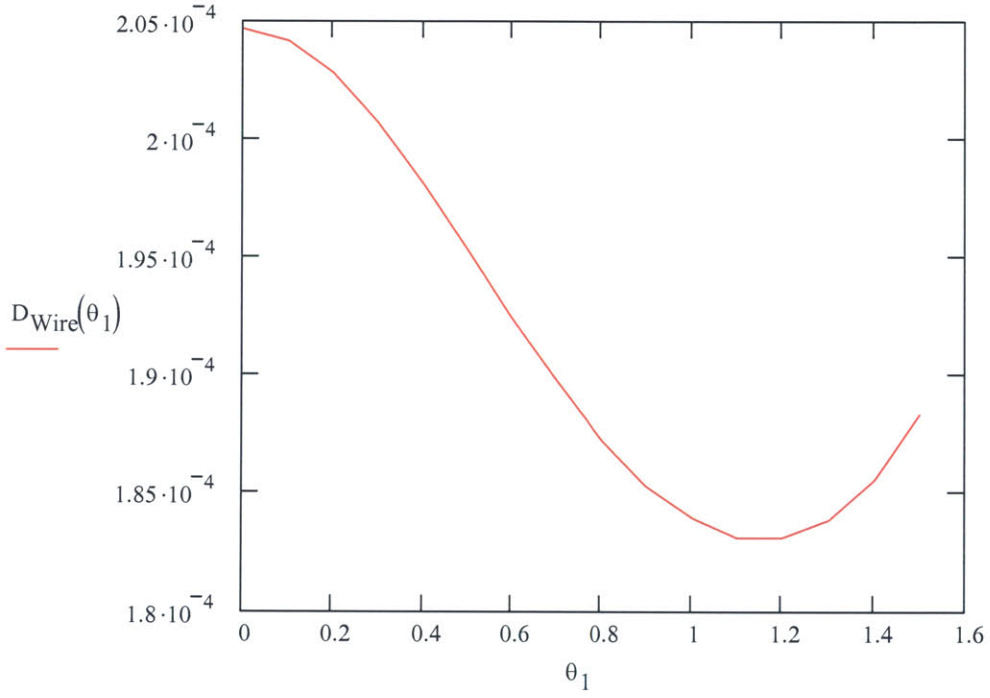

Appendix D: SMA AMP Version 1 Energy Requirement Calculation

SMA Wire Length $L := 350 \cdot mm$

Contraction Length $\Delta L := L \cdot 4\%$ $\Delta L = 0.014m$

SMA Wire Cross Section:

Wire Diameter $D := 254 \cdot 10^{-6} m$

Area $A := \pi \cdot \left(\frac{D}{2}\right)^2$ $A = 5.067 \times 10^{-8} m^2$

Force output of SMA Wire:

SMA Wire Presure Output $P := 200 \cdot 10^6 Pa$

$F_{SMA} := P \cdot A$ $F_{SMA} = 10.134N$

Work Performed by SMA Wire:

$W := F_{SMA} \cdot \Delta L$ $W = 0.142J$

Electrical to Mechanical Work Efficiency = 3%

Therefore the energy required to actuate the wire $E := \frac{W}{0.03}$ $E = 4.729J$

Energy of a Capacitor:

$E := \frac{1}{2} \cdot C \cdot V^2$

For $C := 33 \cdot 10^{-3} F$

$V_{CAP} := \sqrt{2 \cdot \frac{E}{C}}$ $V_{CAP} := 16.9v$